

Roles of OXA Proteins in Plant Mitochondrial Biogenesis

Dissertation
der Fakultät für Biologie
der Ludwig-Maximilians-Universität München

vorgelegt von

Renuka Kolli

München
20 Januar 2020

Erstgutachter: Prof. Dr. Jürgen Soll

Zweitgutachter: PD Dr. Kai Hell

Tag der Abgabe: 20.01.2020

Tag der mündlichen Prüfung: 03.03.2020

Printed with the support of the German Academic Exchange Service

Eidesstattliche Erklärung

Ich versichere hiermit an Eides statt, dass die vorgelegte Dissertation von mir selbständig und ohne unerlaubte Hilfe angefertigt ist.

München, den 05.03.2020

.....
(Renuka Kolli)

Erklärung

Hiermit erkläre ich, dass ich zuvor nicht versucht habe, anderweitig eine Dissertation einzureichen oder mich einer Doktorprüfung zu unterziehen. Die vorliegende Dissertation wurde keiner weiteren Prüfungskommission weder in Teilen noch als Ganzes vorgelegt.

München, den 05.03.2020

.....
(Renuka Kolli)

Contents

1. Abbreviations	1
2. Summary	3
3. Zusammenfassung	4
4. Introduction	5
4.1. Distinct features of plant mitochondria	5
4.2. Respiratory complex assembly	6
4.3. Mitochondrial protein import	7
4.4. The Oxa1 protein superfamily	10
4.5. The Arabidopsis OXA proteins and the TPR domain	14
5. Aims of the thesis	16
6. Materials and Methods	17
6.1. Materials	17
6.1.1. Chemicals and enzymes	17
6.1.2. Kits	17
6.1.3. DNA and protein size markers	18
6.1.4. Membranes and column materials	18
6.1.5. Oligonucleotides and vectors	18
6.1.6. Bacterial strains	18
6.1.7. Plant seeds	19
6.1.8. Antibodies, accession numbers and software	19
6.2. Methods	20
6.2.1. Molecular biological methods	20
6.2.2. Plant biological methods	22
6.2.3. Biochemical methods	26
6.2.4. Methods concerning mitochondria	29
7. Results	34
7.1. Phylogenetic and structural analyses of plant OXA proteins	34
7.1.1. OXA gene duplication must have occurred before speciation	34
7.1.2. Plant OXA2 proteins are unique	35
7.1.3. Functional specialization of OXA2 in the Brassicaceae family	36

7.1.4. Arabidopsis OXA proteins are likely to contain five TMHs.....	36
7.2. Role of OXA2b and significance of its TPR domain	39
7.2.1. Functional complementation rescued <i>OXA2b</i> knockout embryo-lethality	39
7.2.2. Severe growth retardation of <i>35S:OXA2bΔ235</i> plants.....	42
7.2.3. Severe loss of complex IV in <i>35S:OXA2bΔ235</i> plant mitochondria.....	44
7.2.4. Complex IV subunits are reduced in <i>35S:OXA2bΔ235</i> mitochondria.....	46
7.2.5. COX2 membrane insertion is affected in <i>35S:OXA2bΔ235</i> mitochondria	48
7.2.6. OXA2b TPR domain directly binds the nascent COX2 C-terminus.....	52
7.3. Role of OXA2a and significance its TPR domain.....	54
7.3.1. Partial complementation rescued <i>OXA2a</i> knockout embryo-lethality	54
7.3.2. Growth retardation of <i>ABI3p:OXA2a</i> plants	56
7.3.3. Complex III is reduced in <i>ABI3p:OXA2a</i> plants.....	59
7.3.4. Specific complex III subunits are reduced in <i>ABI3p:OXA2a</i> plants	62
7.3.5. Complex III is assembled slower in <i>ABI3p:OXA2a</i> plants	64
7.3.6. The CCM process is affected in <i>ABI3p:OXA2a</i> plants	67
7.4. Roles of OXA1b and OXA1a.....	71
7.4.1. Faster germination of <i>oxa1b</i> seeds.....	71
7.4.2. The respiratory complexes are unaffected in <i>oxa1b</i> mitochondria.....	72
7.4.3. Certain mitochondrial protein levels are altered in <i>oxa1b</i> plants	73
7.4.4. TIM22 appears to assemble faster in <i>oxa1b</i> mitochondria.....	74
7.4.5. RNA silencing of <i>OXA1a</i> does not alter the plant phenotype.....	75
7.4.6. Generation of <i>OXA1a-RNAi oxa1b</i> double mutants.....	77
8. Discussion	80
8.1. OXA2b is required for complex IV biogenesis	80
8.2. OXA2a appears to be involved in cytochrome <i>c</i> maturation	83
8.3. Roles of OXA1a and OXA1b	86
9. Supplemental Figures	89
10. Supplemental Tables.....	94
11. Appendix	103
12. References	108
13. Acknowledgements.....	115
14. Publications.....	116

1. Abbreviations

ALB	ALBino
AOX	Alternative OXidase
Bcs1	cytochrome <i>b_{c1}</i> synthesis
BN-PAGE	Blue Native PolyAcrylamide Gel Electrophoresis
CCM	Cytochrome <i>c</i> Maturation
COB	Cytochrome <i>b</i>
Cor	Core subunit of the ubiquinol-cytochrome <i>c</i> reductase complex
COX	Cytochrome <i>c</i> Oxidase
CYC	Cytochrome <i>c</i>
CYC1	Cytochrome <i>c₁</i>
CyoA	Cytochrome <i>bo₃</i> oxidase subunit 2
EMC3	Endoplasmic reticulum Membrane Complex 3
ERV1	Essential for Respiration and Vegetative growth protein 1
Get1	Guided entry of tail-anchored protein 1
GST	Glutathione S-transferase
GUS	β -Glucuronidase
IM	Inner Membrane
IMS	InterMembrane Space
IPTG	IsoPropyl β -D-1-ThioGalactopyranoside
LacY	Lactose Permease
LHCP	Light-Harvesting Chlorophyll-binding Protein
MalF	Maltose transporter
Mba1	Multi-copy bypass of AFG3 protein 1
MPP	Mitochondrial Processing Peptidase
MS	Murashige and Skoog

OM	Outer Membrane
OXA	cytochrome <i>c</i> Oxidase Assembly factor
P _i C	inorganic Phosphate Carrier
PK	Proteinase K
PRAT	PREprotein and Amino acid Transporter
PMSF	PhenylMethylSulfonyl Fluoride
PVP	PolyVinylPyrrolidone
QCR7	ubiQuinol Cytochrome <i>c</i> Reductase subunit 7
RISP	Rieske Fe/S Protein
Sec	Secretory translocase
SRP	Signal Recognition Particle
TAT	Twin Arginine Translocase
TIM	Translocase of the Inner Membrane
TMCO1	TransMembrane and COiled-coil domain-containing protein 1
TMH	TransMembrane Helix
TOM	Translocase of the Outer Membrane
TPR	TetratricoPeptide Repeat
TssL	A Tail-anchored protein/ Type VI secretion protein

2. Summary

Proteins of the Oxa1 superfamily are involved in the membrane insertion, folding and assembly of crucial proteins into the inner membrane (IM) of bacteria and mitochondria, thylakoid membrane of chloroplasts and the endoplasmic reticulum. Oxa1 and Cox18/Oxa2 are the mitochondrial homologs of this family in yeast and mammals. While Oxa1 plays a major role in the biogenesis innumerable IM proteins, Cox18 is specialized in the translocation of the second transmembrane helix of Cox2 during the biogenesis of complex IV. Due to a second gene duplication, there are four OXA proteins in plants. OXA1a, OXA2a and OXA2b were previously found to be independently essential for embryogenesis, but not OXA1b. The plant OXA2 proteins are unique in possessing a TPR domain at the C-terminus. This study sought to identify their exact roles in mitochondrial biogenesis. It was found that OXA2b is required for complex IV biogenesis by aiding in the proper membrane insertion of the COX2 subunit. The TPR domain of OXA2b was found to be very important for Cox2 biogenesis such that plant OXA2b alone could play the roles of both Cox18 and Mss2 in yeast. On the other hand, OXA2a appears to be indirectly required for complex III biogenesis by participating in the cytochrome *c* maturation pathway. In contrast to the crucial role played by the TPR domain of OXA2b, the TPR domain of OXA2a does not appear to important for its functionality. Phylogenetic analysis of all the plants whose genomic data is available revealed that the subfunctionalization of OXA2a and OXA2b is restricted to Brassicaceae. OXA1a and OXA1b appear to have some level of overlapping functionality, although only OXA1a is essential for embryogenesis. OXA1a might be the general membrane insertase in Arabidopsis, like yeast Oxa1. TIM22 is likely to be one of its substrates.

3. Zusammenfassung

Proteine der Oxa1-Superfamilie sind an der Insertion, Faltung und Assemblierung von entscheidenden Proteinen in die Innenmembran (IM) von Bakterien und Mitochondrien, die Thylakoidmembran von Chloroplasten und das endoplasmatische Retikulum beteiligt. Oxa1 und Cox18/Oxa2 sind die mitochondrialen Homologen dieser Familie in Hefe und Säugetieren. Während Oxa1 eine wichtige Rolle bei der Biogenese unzähliger IM-Proteine spielt, ist Cox18 auf die Translokation der zweiten Transmembranhelix von Cox2 während der Biogenese von Komplex IV spezialisiert. Aufgrund einer zweiten Genduplikation gibt es vier OXA-Proteine in Pflanzen. OXA1a, OXA2a und OXA2b erwiesen sich zuvor als unabhängig voneinander essentiell für die Embryogenese, nicht jedoch OXA1b. Die pflanzlichen OXA2-Proteine besitzen eine einzigartige TPR-Domäne am C-Terminus. Diese Studie versuchte, ihre genauen Rollen in der mitochondrialen Biogenese zu identifizieren. Es wurde festgestellt, dass OXA2b für die Komplex-IV-Biogenese erforderlich ist, indem die ordnungsgemäße Membraninsertion der COX2-Untereinheit unterstützt wird. Es wurde festgestellt, dass die TPR-Domäne von OXA2b für die Cox2-Biogenese sehr wichtig ist, so dass pflanzliches OXA2b allein die Rolle von Cox18 und Mss2 in Hefe spielen kann. Andererseits scheint OXA2a indirekt für die Komplex-III-Biogenese erforderlich zu sein, da es am Cytochrom-C-Reifungsweg beteiligt ist. Im Gegensatz zu der entscheidenden Rolle, die die TPR-Domäne von OXA2b spielt, scheint die TPR-Domäne von OXA2a für ihre Funktionalität nicht wichtig zu sein. Die phylogenetische Analyse aller Pflanzen, deren Genomdaten verfügbar ist, ergab, dass die Subfunktionalisierung von OXA2a und OXA2b auf Brassicaceae beschränkt ist. OXA1a und OXA1b scheinen eine gewisse Überlappungsfunktionalität zu haben, obwohl nur OXA1a für die Embryogenese wesentlich ist. OXA1a könnte die allgemeine Membran-Insertase in Arabidopsis sein, wie Hefe Oxa1. TIM22 ist wahrscheinlich eines seiner Substrate.

4. Introduction

The primordial eukaryote most likely arose from symbiosis between a facultative anaerobic archaeon (host) and an α -proteobacterium (mitochondrial ancestor) approximately 2 billion years ago (1). It then evolved over time to form the wide range of complex multicellular life on earth. Mitochondria generate more than 90% of the cellular energy in the form of ATP and are popularly known as the “powerhouse of the cell”. Moreover, they also perform several other vital cellular functions such as synthesis of heme and iron-sulfur clusters, lipid metabolism, maintenance of calcium homeostasis, thermogenesis, innate immunity, and activation of apoptosis (2). Due to the monophyletic origin of mitochondria, the fundamental mitochondrial features and functions are conserved across eukaryotes. However, lineage-specific differences do exist (3).

4.1. Distinct features of plant mitochondria

Plant mitochondria have several unique features and co-exist with chloroplasts which were also derived endosymbiotically during the evolution of plants. Plant mitochondria are involved in photorespiration and stress perception. Plant mitochondrial genomes are comparatively larger, highly variable in size and encode for more membrane proteins than those of yeast and humans (4, 5). Yeast and human mitochondrial genomes encode seven and thirteen membrane proteins, respectively, whereas the Arabidopsis mitochondrial genome encodes for 20 putative membrane proteins displaying a wide range of membrane topologies (Figure 1).

RNA metabolism in plant mitochondria is complex compared to other eukaryotes and involves a combination of bacterial as well as novel features evolved in the host cell (6). Post-transcriptional processes such as 5' and 3' RNA processing, intron splicing, RNA editing and controlled RNA stability strenuously regulate the mRNA quantities available for translation in plant mitochondria (7). Due to the presence of the alternative oxidase (AOX) and alternative NAD(P)H dehydrogenases, the electron transport chain of plant mitochondria is branched (8-10). Although the mitochondrial respiratory complexes I to V

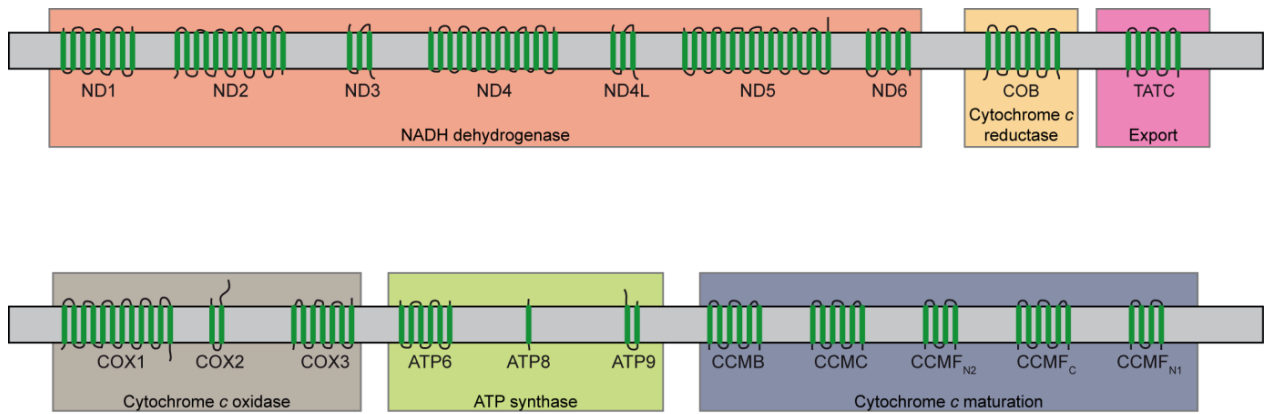


Figure 1. Transmembrane topologies of the 20 putative IM proteins that are encoded in the mitochondrial genome of *Arabidopsis thaliana*. The proteins enclosed within a separate colored box are subunit(s) of the complex indicated. The proteins are displayed in an N- to C-terminus orientation going from left to right.

in plants resemble their counterparts in fungi and mammals based on the overall structures, they have numerous extra subunits many of whose functions are still unclear (8). For example, plant complex I has an additional spherical domain containing five carbonic anhydrase-like proteins attached to the membrane arm on the matrix side, which is not found in the complex I of bacteria or other eukaryotic lineages (11, 12). The process of cytochrome *c* maturation (CCM) in land plant mitochondria occurs by a complex bacterial-type system I whereas fungal and animal mitochondria have evolved a simpler CCM mechanism called system III (13). Besides, plant mitochondria appear to use the TAT (Twin Arginine Translocase) machinery for membrane insertion of the Rieske Fe/S (RISP) protein similar to bacteria and chloroplasts, but unlike mitochondria of other eukaryotes (14).

4.2. Respiratory complex assembly

Respiratory complexes comprise 80% of the IM proteins and are preferentially located in the cristae membranes (15). The multisubunit protein complexes I to IV form the electron transport chain and generate a proton gradient across the IM that drives the production of ATP by ATP synthase (complex V). The respiratory complexes were found to associate into specific supercomplexes in many organisms (16, 17). In plant mitochondria, supercomplex I + III₂ is the most abundant supercomplex while other supercomplexes – I₂ + III₄, III₂ + IV₍₁₋₂₎, I + III₂ + IV₍₁₋₄₎, and V₂ – are found in lower abundance (18). All the respiratory complexes I to V except complex II are made up of a mosaic of both nuclear-

and mitochondrial-encoded proteins. The mitochondrial subunits nucleate assembly of complexes and form the catalytic cores.

COB (cytochrome *b*) is the only mitochondrial encoded subunit of complex III (cytochrome *bc*₁ complex or cytochrome *c* reductase), which after being synthesised in the matrix and getting inserted into the IM, nucleates the assembly of the complex (19). The remaining nine nuclear encoded subunits have to be synthesised in the cytosol and imported into mitochondria before being assembled into complex III. Interestingly, the two core subunits of complex III in yeast and human mitochondria, Cor1 and Cor2, are enzymatically inactive, whereas the corresponding homologs in plants called MPP α and MPP β are proteolytically active (20). Thus, plant complex III plays a dual role in electron transport as well as proteolytic processing of imported precursor proteins.

Cox1, Cox2, and Cox3 are the three catalytic core subunits of complex IV, which are encoded by the mitochondrial genome in most organisms (21, 22). More than 10 other subunits are nuclear-encoded, the exact number varying among organisms (23). In plants, complex IV is thought to contain upwards of 21 proteins including at least six potential plant-specific subunits (23-25). The biogenesis of human complex IV requires many more assembly factors than the actual subunits (26-28). Adding to the complexity of complex IV biogenesis, redox active metal centers must be incorporated into Cox1 and Cox2 before their assembly into a functional complex (29, 30).

4.3. Mitochondrial protein import

Most of the genes that were originally present in the genome of the α -proteobacterial endosymbiotic ancestor of mitochondria were gradually transferred to the host nucleus during the course of eukaryotic evolution (31). Therefore, all the nuclear encoded mitochondrial proteins synthesised in the cytosol had to be imported back into the organelle. The basic mitochondrial protein import machinery consisting of the core subunits had developed even before the divergence of eukaryotes into fungi, plants, and

metazoans (32). Later on, a number of lineage-specific subunits were added while others were lost. Although the majority of protein import components are conserved in plant mitochondria, the gene family members encoding the protein import components have expanded. For instance, yeast contain only a single gene encoding each of the three proteins, Tim17, Tim23, and Tim22, which belong to the preprotein and amino acid transporter (PRAT) family. On the other hand, the Arabidopsis genome contains 17 genes encoding different PRAT family members, of which ten are located in mitochondria, six in chloroplasts, and one is dual targeted (33).

At the mitochondrial outer membrane (OM), the precursor proteins interact with receptor subunits of the translocase of the outer membrane (TOM) complex (34). The TOM complex serves as an entry gate for all the nuclear-encoded mitochondrial proteins which need to cross the OM. The vast majority of mitochondrial proteins are synthesized in the cytosol and are targeted to mitochondria via N-terminal cleavable presequences (Figure 2). After emerging from the TOM complex, the presequence interacts with the TIM23 complex, which mediates the translocation of the precursor proteins across the IM into the matrix in a membrane potential- and ATP-dependent manner (35-37) (Figure 2). In the matrix, the targeting sequences are proteolytically removed by the mitochondrial processing peptidase (MPP) and the proteins are folded into their respective native structures (38). The precursor proteins with N-terminal-targeting signals that are destined to the IM are arrested at the TIM23 complex and laterally release into the membrane (Figure 2) (39). So far, all proteins identified to be using this pathway contain only a single membrane-spanning transmembrane helix (TMH) (40).

The mitochondrial carrier protein family include polytopic membrane proteins in the IM, containing multiple hydrophobic internal signals and usually lacking N-terminal cleavable targeting signals (40). The carrier proteins are transferred from TOM to the TIM22 complex via the heterohexameric chaperone complex that is composed of small Tim proteins in the intermembrane space (IMS) (Figure 2). The small Tims prevent aggregation

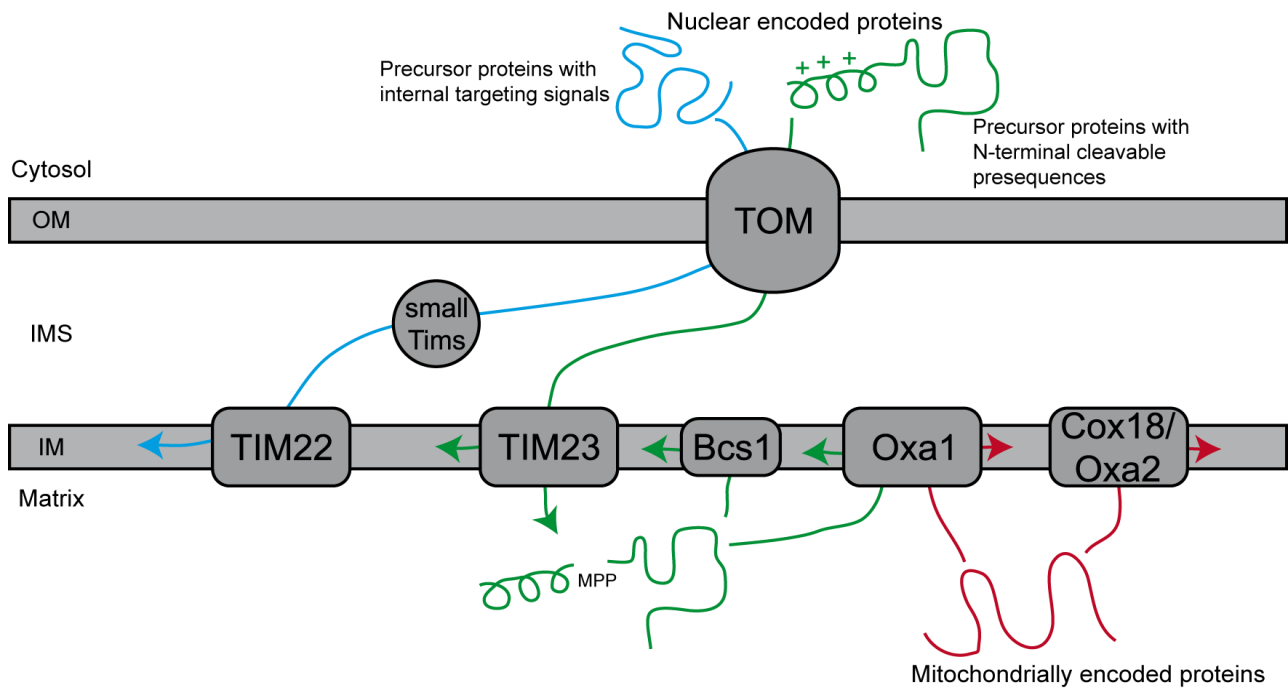


Figure 2. Mitochondrial protein transport and insertion pathways at the IM in yeast. Proteins destined to the IM can follow several routes for membrane insertion. There are the two translocase complexes in the IM, TIM22 and TIM23, which laterally insert nuclear encoded proteins into the IM. Proteins with internal targeting signals are inserted into IM by TIM22, while those with cleavable N-terminal targeting signals are inserted by TIM23. The conservatively sorted proteins are first targeted to the matrix by TIM23 and then inserted to the IM, in a manner reminiscent of bacterial IM protein insertion. These conservatively sorted and mitochondrial encoded proteins require Oxa or Cox18 for membrane insertion. The newest member for conservative sorting is the Bcs1 protein for membrane insertion of RISP.

or misfolding of the hydrophobic precursors which are then laterally released into the IM upon activation of Tim22 by the membrane potential (Figure 2) (41). Unusually, numerous carrier proteins in plant mitochondria possess a cleavable N-terminal-targeting sequence, despite displaying the typical tripartite structure and being homologous to other members of the carrier family (42). Although these extensions appear to be non-essential for correctly targeting to the mitochondria, they might be important for enhancing the import specificity and efficiency and might avoid mistargeting to chloroplasts (43). After or during import, the extension is removed in a two-step process: first processing by MPP and second processing by a putative serine protease in the IMS (44).

The Bcs1 pathway is the most recent sorting pathway to be identified in mitochondria (45, 46) (Figure 2). Bcs1 is an AAA protein with its AAA domain facing the matrix (47). In stark contrast to other translocation pathways, the Bcs1 pathway can translocate folded

proteins. Presently, the RISP subunit of complex III is the only protein known to use this unique pathway in yeast and human mitochondria. Recently, it was demonstrated that plant mitochondria most likely use the TAT pathway instead of the Bcs1 pathway (14). Bacteria and chloroplasts utilize the TAT pathway for the insertion of RISP into the cytochrome *bc₁* complex and the cytochrome *b₆f* complex, respectively (48). TAT also inserts numerous other substrate proteins, the exact number varying among different organisms (49).

4.4. The Oxa1 protein superfamily

All the mitochondrial-encoded IM proteins depend on the Oxa insertase machinery for membrane insertion (Figure 2). The Oxa protein is evolutionarily conserved for membrane protein insertion in mitochondria from the endosymbiotic bacterial ancestor. Oxa1 was first identified in 1994 in a yeast mutant that failed to assemble the COX complex, resulting in a respiration-deficient phenotype (50, 51). Oxa1 is involved in the co-translational membrane insertion of polytopic membrane proteins into the mitochondrial IM (52). In cooperation with a peripheral membrane protein, Mba1, the positively charged coiled-coil domain at the Oxa1 C-terminus interacts with the negatively charged 21S RNA of the large subunit of the ribosome, which is in proximity to the polypeptide exit tunnel (53, 54). Thus, Oxa1 is able to directly contact the nascent polypeptide very early during the translation and inserts it efficiently into the membrane. The matrix-exposed loop between the TMHs 1 and 2 may also contribute to ribosome binding.

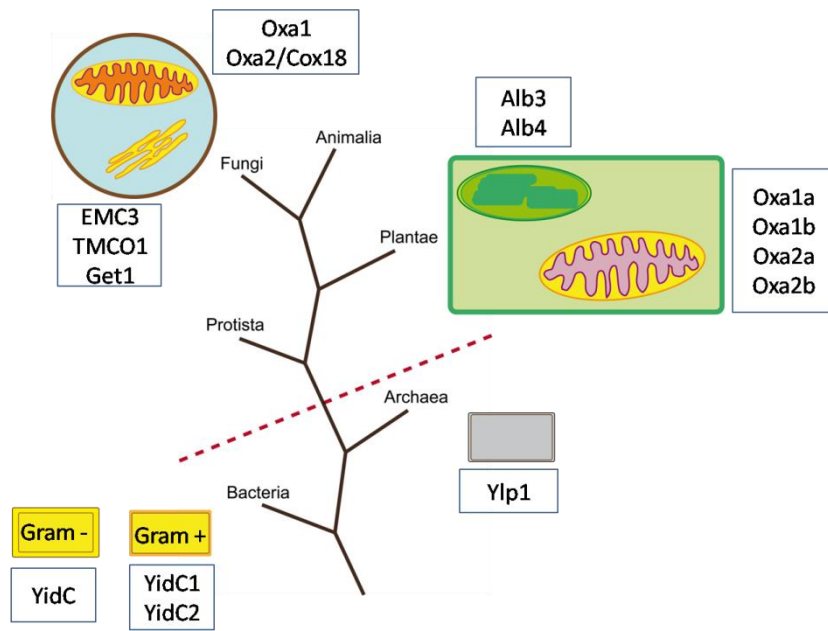
The Oxa1-ribosome interaction not only promotes co-translational insertion but is also critical for the assembly of the COX subunits (55). Similarly, during biogenesis of the Fo part of ATP synthase, although Oxa1 is not involved in the insertion of Atp9 into the IM, it is required for the assembly of Atp9 with Atp6 (56). Thus, Oxa1 can also function in a chaperone-like manner in addition to performing membrane insertion. While Oxa1 is conserved and Oxa1 proteins from different organisms are exchangeable, their specific functions can differ slightly: The yeast Oxa1 is involved in the biogenesis of complexes IV and V, whereas the human Oxa1 is required for the biogenesis of complexes I and V (57-

59). In *Neurospora crassa*, Oxa1 depletion affects the levels of complexes I and IV (60). The paralog of Oxa1, Cox18 (Oxa2), lacks the ribosome-binding coiled-coil domain. Moreover, unlike Oxa1 which acts on several known substrate proteins, Cox2 is the only known substrate of Cox18 (61). Cox18 performs a post-translational role in efficient topogenesis and stability of Cox2 during the assembly of COX.

Oxa1 is not only required for the membrane insertion of mitochondrial-encoded proteins, but also cooperates with TIM23 for the membrane insertion of certain nuclear-encoded proteins with a complex membrane topology (62) (Figure 2). After translocation into the matrix via TIM23, the substrate proteins are inserted into the IM with the help of Oxa1. Many of the proteins sorted in this manner have bacterial homologs (63, 64). Oxa1 is required for its own biogenesis based on this mechanism (65). In other cases, some TMHs of the precursor proteins are laterally sorted by TIM23 while the remaining are first translocated into the matrix and then exported into the membrane by Oxa1. For instance, during the biogenesis of Mdl1, TIM23 laterally inserts the first pair of TMHs into the IM while the subsequent pair is translocated into the matrix for insertion by Oxa1 (66). Generally, laterally inserted TMHs are more hydrophobic than those that are first translocated into the matrix. Another example is the biogenesis of Sdh4 in yeast. Sdh4 contains three TMHs, the first two are translocated through TIM23 into the matrix and exported by Oxa1, whereas the third is arrested in the TIM23 complex and laterally inserted into the IM (67). Furthermore, the two subunits of the carrier translocase, Sdh3 and Tim18 also use the TIM23-Oxa1 pathway (68). Hence, Oxa1 is also required for the biogenesis of numerous carrier proteins.

Other members of the Oxa1 superfamily are crucial for membrane protein insertion, protein folding and complex assembly in all three domains of life (69, 70) (Figure 3A). They are required for the biogenesis of the respiratory chain complexes in bacteria (YidC) and mitochondria (Oxa1) and in the assembly of photosynthetic complexes in chloroplasts (ALB3). The recently identified members of the family, Get1, EMC3, and TMCO1 insert proteins into the endoplasmic reticulum (71) (Figure 3A). The conserved hydrophobic core

A)



B)

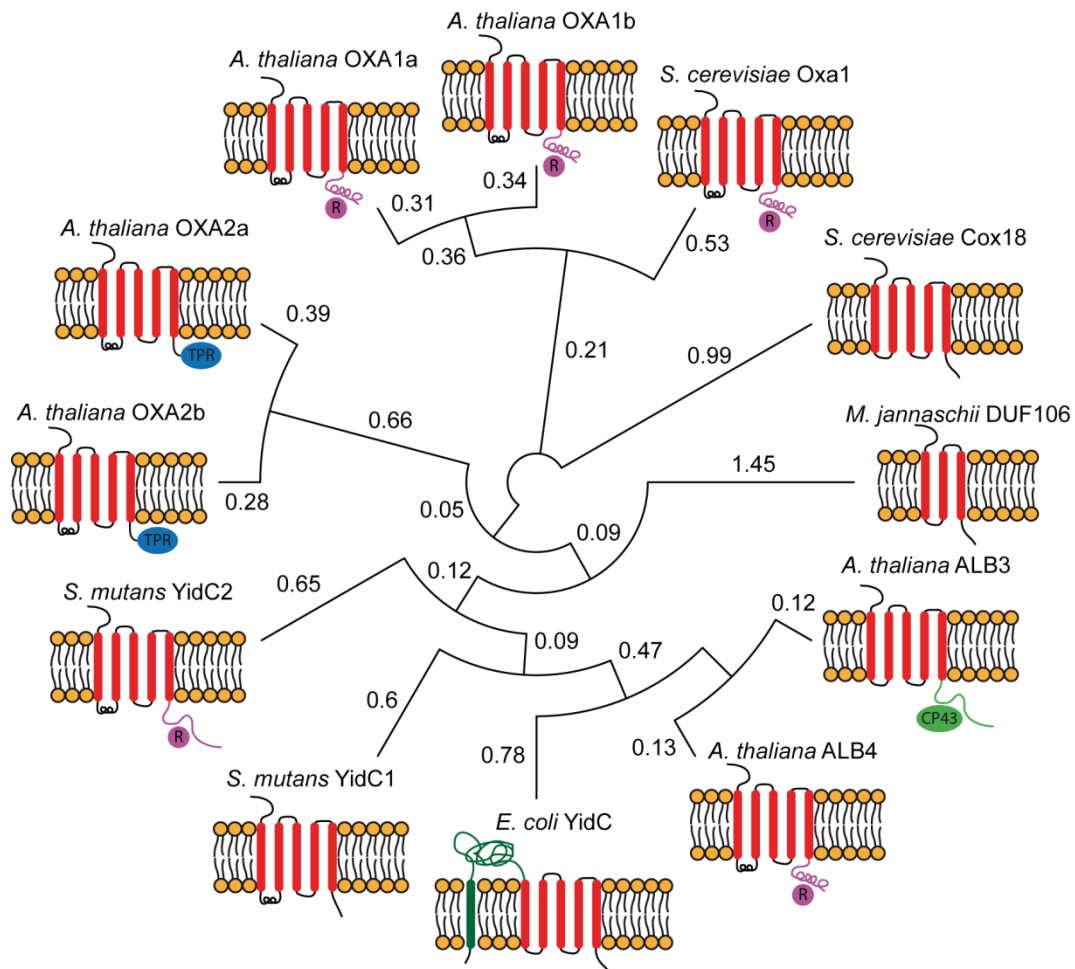


Figure 3. Phylogenetic and structural analysis of the Oxa1 protein superfamily A) A diagram depicting the existence of Oxa1 superfamily members in all three domains of life: Archaea, Bacteria, and Eukarya. The red dashed lines separate eukaryotes from prokaryotes. Simplified figures of bacteria, yeast and a plant cell are shown. Within the yeast cell, mitochondria and endoplasmic reticulum are depicted while chloroplast and mitochondria are depicted. The Oxa1 superfamily members are mentioned next to the organism or organelle in which they are found. B) The phylogenetic tree was generated based on the full-length protein sequence alignment using Clustal omega for the indicated species of the Oxa1 superfamily [60]. The phylogenetic analysis was done by Chris Carrie. The numbers next

to each node represent the measure of support for the node. The conserved five TMH secondary structure is found in all members (except archaea) of the protein family. Differences at the C-terminal ends are indicated by different colors: pink = ribosome-binding, blue = TPR domain, green = CP43-interacting.

domain consisting of three or five TMHs catalyzes membrane protein insertion (Figure 3B). This domain can be functionally exchanged among different members of the protein family (72). However, the soluble N- and C-terminal domains are variable and sometimes perform specialized functions (Figure 3B). Co-translational membrane insertion of substrate proteins is supported by the C-terminal ribosome-binding domain of the mitochondrial Oxa1 (52, 73), whereas the cpSRP43-binding region at the C-terminus of the chloroplast ALB3 is crucial for targeting LHCPs to the thylakoid membrane (74) (Figure 3B). *E. coli* YidC has an extra TMH0 near the N-terminus, an extended periplasmic loop between TMH0 and TMH1, and a unique cytoplasmic coiled-coil region between TMH1 and TMH2 (75) (Figure 3B).

The Gram-negative bacteria have only a single YidC protein whereas most Gram-positive bacteria have two YidC paralogs. In *Streptococcus mutans*, YidC2 has a ribosome-binding domain while YidC1 lacks it (76) (Figure 3B). Hence, with respect to the presence or absence of the ribosome-binding domain, the mitochondrial Oxa1 and Cox18 resemble the Gram-positive YidC2 and YidC1, respectively (Figure 3B). YidC catalyzes the membrane insertion of several substrate proteins with one or two TMHs and lacking highly charged hydrophilic domains on the periplasmic side. The substrate profile of the bacterial YidC appears to be much larger than that of its organellar counterparts, Oxa1 and ALB3. These include the subunits a, b, and c of ATP synthase, TssL, and CyoA. With LacY and MalF, YidC also functions as a chaperone to assist in the folding and stability of the nascent polypeptide (77, 78). YidC not only acts independently but also cooperates with SecYEG to facilitate the correct membrane integration and folding of membrane proteins (79).

The recent X-ray structures of YidC from *Bacillus halodurans* and *Escherichia coli* revealed a hydrophilic groove, which is open from the cytoplasm and the lipid bilayer but is closed from the periplasmic side (80, 81). Moreover, the relatively shorter TMH3, 4, and 5 cause

membrane thinning around YidC. The TMHs of the substrate slide into the lipid bilayer upon interaction with YidC in the groove region. For Sec-dependent membrane protein insertion, YidC contacts the interior of the SecY channel to form a ligand-activated and voltage-dependent complex (82). Upon substrate binding, it facilitates the partitioning of nascent membrane proteins into the lipid environment by reducing the hydrophobicity of the SecY lateral gate. (77, 78). The mechanism of protein insertion by Oxa and Alb proteins is likely to be similar to YidC since they can be modelled on the known structure of YidC. Analogous to the bacterial YidC, the chloroplast ALB3 may also cooperate with cpSecY to perform co-translational membrane insertion of proteins into the thylakoid membrane (83), in addition to its role in the post-translational insertion of LHCPs (84). ALB3 paralog, ALB4 is involved in the assembly and stability of ATP synthase (85, 86).

4.5. The Arabidopsis OXA proteins and the TPR domain

There are two additional OXA proteins in *Arabidopsis thaliana* due to independent gene duplications of OXA1 and OXA2: OXA1a, OXA1b, OXA2a, and OXA2b (Figure 3). Except OXA1b, the other three OXA proteins are essential for embryogenesis (87). This indicates that OXA1a, OXA2a, and OXA2b play vital non-redundant roles in IM protein biogenesis in all stages of plant development, while OXA1b is probably not so important for normal plant growth and physiology. Arabidopsis OXA1a and OXA1b possess a coiled-coil domain at the C-terminus, similar to yeast Oxa1 (Figure 3B). As OXA1a could functionally replace yeast Oxa1, it most likely functions similarly as a general insertase machinery for membrane proteins from the matrix side (88). Interestingly, OXA2a and OXA2b possess a tetratricopeptide repeat (TPR) domain consisting of four TPR motifs near the C-terminus, which is a plant-specific feature and is not found in any other known members of the protein family (87, 89) (Figure 3B). TPR domains are involved in protein-protein interactions in a variety of cellular proteins performing different functions. For example, the TPR domain of the TOM receptor, Tom70, interacts with the cytosolic chaperones Hsc70/Hsp70 and Hsp90, which guide precursor proteins (90). This interaction is crucial for mitochondrial precursor targeting and translocation.

Based on the available transcriptome data, all Arabidopsis OXA genes are maximally expressed in seeds (91). Among the four OXAs, OXA1a has the highest expression level while OXA2a has the lowest expression level (Appendix). Seed germination is an excellent model for studying mitochondrial biogenesis as cristae-lacking promitochondria in dry seeds are progressively transformed into fully functional mitochondria within 12 h of light exposure following stratification (92, 93). During a germination time course consisting of two days of stratification and two days of germination, OXA1a transcripts accumulated maximally during the first 6 h of germination, OXA1b and OXA2b seemed to be constitutively transcribed throughout the germination time course whereas OXA2a transcripts were abundant only during first 12 h of stratification and then decreased over time (Appendix) (94). These varied expression profiles consolidate the above statement that the Arabidopsis OXA proteins are very likely to play dissimilar roles during mitochondrial biogenesis. However, some level of overlapping functionality cannot be ruled out.

5. Aims of the thesis

As outlined in the introduction, a lot of research has been done on the roles of Oxa1 and Cox18 in yeast and humans, but very little is known about the roles of the four OXA homologs in plants. Apart from the proposal plant OXA proteins are required for mitochondrial biogenesis, their exact functions were not known. For a better characterization of the Arabidopsis OXA proteins, the following became the aims of this thesis.

1. To investigate the roles of the four Arabidopsis OXA proteins in plant mitochondrial biogenesis

Due to the problem of embryo-lethality upon knockout of OXA1a, OXA2a and OXA2b, it was first necessary to generate viable mutants. In order to accomplish this, two strategies were used: partial complementation of knockout lines using the ABI3 promoter and RNA silencing. The generated mutant plants were then analysed phenotypically and several biochemical experiments were performed with the mitochondria isolated from the plants.

2. To study the significance of the TPR domains in the two OXA2 proteins

OXA2a and OXA2b were predicted to contain a TPR domain at their C-termini, which makes them unique among known members of the Oxa1 superfamily. The TPR domain may instil in OXA2a and OXA2b some special plant-specific functions, distinct from the membrane insertion function of the conserved TMHs. In order to study the importance of the OXA2 TPR domains, mutant plants were generated by complementing knockout lines with the corresponding truncated cDNA which lacks the region coding for the TPR domain. These mutant plants and their isolated mitochondria were analysed extensively.

6. Materials and Methods

6.1. Materials

6.1.1. Chemicals and enzymes

All chemicals used were obtained from Sigma Aldrich (Taufkirchen, Germany), Roth (Karlsruhe, Germany), Merck (Darmstadt, Germany), Thermo Fisher Scientific (Braunschweig, Germany), Fluka (Buchs, Switzerland), Bio-Rad (Feldkirchen, Germany), Serva (Heidelberg, Germany) or Roche (Penzberg, Germany). ³⁵S methionine and cysteine mix (1175 Ci/mmol at 11 mCi/ml) used for radiolabelling proteins was purchased from PerkinElmer (Walluf, Germany). Pierce 1-step TMB-Blotting solution (Thermo Fisher Scientific, Rockford, USA) was used for *in gel* complex III staining. Bio-Rad protein assay dye reagent was used to estimate protein concentration. Invitrogen Gateway BP and LR Clonase II enzyme mixes were obtained from Thermo Fisher Scientific. Restriction endonucleases were purchased from either Thermo Fisher Scientific or New England BioLabs (Frankfurt am Main, Germany). Phusion DNA polymerase, T7 RNA polymerase and T4 DNA ligase were purchased from New England BioLabs and DFS-Taq DNA polymerase from Bioron (Ludwigshafen, Germany). RNasin ribonuclease inhibitor was bought from Promega (Madison, USA).

6.1.2. Kits

Macherey-Nagel's NucleoSpin Plasmid and NucleoBond Xtra Midi kits were used for plasmid DNA isolation from *E. coli* and NucleoSpin Gel and PCR Clean-up kit was used for DNA purification. DNeasy Plant Mini kit and RNeasy Plant Mini kit in combination with RNase-Free DNase Set from Qiagen (Hilden, Germany) were used for DNA and RNA isolation, respectively from Arabidopsis plants. TURBO DNA-free Kit (Thermo Fisher Scientific) was used to remove DNA contamination after total RNA isolation from Arabidopsis. cDNA was synthesised using either SuperScript III First-Strand Synthesis System (Thermo Fisher Scientific) or iScript cDNA Synthesis Kit (Bio-Rad). FastStart Essential DNA Green Master kit (Roche) was used for RT-qPCR. Rabbit reticulocyte lysate and 1 mM amino acid mixture minus methionine present in Flexi Rabbit Reticulocyte Lysate System (Promega) were used in coupled translation and translation reaction.

SuperSignal West Femto kit (Thermo Fisher Scientific) was used for heme staining.

6.1.3. DNA and protein size markers

Lambda DNA PstI Digest was used as a DNA marker for agarose gel electrophoresis. peqGOLD protein marker I (VWR, Ismaning, Germany) and PageRuler prestained protein ladder (26616, Thermo Fisher Scientific) were used as reference for proteins separated by SDS-PAGE. NativeMark unstained protein standard (LC0725, Thermo Fisher Scientific) was used for molecular weight estimation of protein complexes in BN-PAGE.

6.1.4. Membranes and column materials

Immobilon-P PVDF transfer membrane from Merck Millipore (Darmstadt, Germany) and blotting paper from Macherey-Nagel (Düren, Germany) were used for performing immunoblots. Protino Ni-NTA Agarose (Macherey-Nagel) and Glutathione Sepharose 4 Fast Flow beads (GE Healthcare) beads were used for protein purifications.

6.1.5. Oligonucleotides and vectors

DNA oligonucleotides listed in Supplemental Table 1 were ordered from Metabion (Martinsried, Germany). Cloning was performed using the Gateway system (Thermo Fisher Scientific) via pDONR207 vector. The following binary vectors were used for plant transformations: pK7GWIWG2 and pOpoff2 (Kan) for RNAi, pH2GW7 and pHABI3pGW7 for expression under the control of 35S promoter and ABI3 promoter, respectively. pDEST14 was employed for *in vitro* coupled transcription and translation. For overproduction of N-terminal His-tagged and GST-tagged proteins, pDEST17 and pGEX-6P-1 were used, respectively. All plasmids used in this study are listed in Supplemental Table 5.

6.1.6. Bacterial strains

Escherichia coli TOP10 (Thermo Fisher Scientific) was used for plasmid DNA propagation

while BL21 and BL21(DE3) (Novagen - Merck Millipore) were used for heterologous protein overproduction. *Agrobacterium tumefaciens* GV3101 (pMP90RK) was used for stable transformation of *Arabidopsis thaliana* plants (95).

6.1.7. Plant seeds

Seeds for two independent T-DNA insertions each in *OXA2b*, *OXA2a* and *OXA1b* in the *Arabidopsis thaliana* Columbia-0 background were obtained from NASC (Nottingham Arabidopsis Stock Centre). These lines, SALK_057938 (*oxa2b-1*), GABI_425B09 (*oxa2b-2*), SALK_048398 (*oxa2a-1*), GABI_492F05 (*oxa2a-2*), SALK_001468 (*oxa1b-1*) and SALK_039564 (*oxa1b-2*) were genotyped by PCR using the primers listed in Supplemental Table 1 and the insertion sites were confirmed by sequencing. Homozygous seeds of *oxa1b* isolated after selection and genotyping were used for further experiments. No homozygous line could be isolated for *oxa2b* and *oxa2a* due to their essential role during embryogenesis (87).

6.1.8. Antibodies, accession numbers and software

All the antibodies used in this study are listed in Supplemental Table 2. The gene accession numbers of proteins involved in this work can be found in Supplemental Table 6. Vector NTI (Life Technologies) was used to design cloning experiments and align DNA sequences. Plant sequences were obtained from TAIR (<https://www.arabidopsis.org>) or Aramemnon (<http://aramemnon.uni-koeln.de>) or Phytozome 12 (<https://phytozome.jgi.doe.gov/pz/portal.html>). TPRpred was used for TPR domain prediction (96). NCBI Blast server (<https://blast.ncbi.nlm.nih.gov>) was used to match DNA or protein sequences. ClustalW (<https://www.genome.jp/tools-bin/clustalw>) and SIAS tool (<http://imed.med.ucm.es/Tools/sias.html>) were employed to calculate protein sequence identity and similarity. CATMA (<http://www.catma.org>) was used to obtain gene-specific sequence tags for cloning into RNAi constructs (97). Gelmap (https://www.gelmap.de/arabidopsis_mito) was used for identifying mitochondrial proteins and complexes found in Arabidopsis (98). Graphs and statistical analyses were performed in Microsoft Excel. Images processing was done using ImageJ and figures were made using Adobe Photoshop and Illustrator (99).

6.2. Methods

General methods not listed below were performed according to (100). Methods concerning plant mitochondria were adapted from (101).

6.2.1. Molecular biological methods

6.2.1.1. DNA cloning

Competent cells for DNA transformation were prepared according to (102). gDNA from *Arabidopsis* was isolated using DNeasy Plant Mini kit (Qiagen) by following the manufacturer's instructions. PCR was performed with gDNA, cDNA or plasmid DNA as template using proof-reading Phusion polymerase (103). Primer annealing temperature and elongation time for the PCR were adapted based on oligonucleotide sequence and length of the construct. PCR products were mixed with DNA loading buffer (0.04% bromophenol blue, 0.02% xylene cyanol, 20 mM EDTA, 10% glycerol) and loaded on 1% agarose gel containing 0.5 µg/ml ethidium bromide run in TAE buffer (40 mM Tris-acetate, 2.54 mM EDTA) at 100 V for 30 min. For cloning, bands were excised from the gel and purified using NucleoSpin Gel and PCR Clean-up kit (Macherey-Nagel). Gateway system (Thermo Fisher Scientific) was used to clone constructs by homologous recombination via pDONR207 into suitable destination vectors listed in Supplemental Table 5 according to the manufacturer's instructions. pHABI3pGW7 was constructed by replacing the 35S promoter of pH2GW7 with the *ABI3* promoter to serve as a vector for partial complementation. OXAp-GUS plasmids were constructed by Golden Gate cloning (104, 105). For the construction of recombinant pGEX-6p-1 plasmid, the vector and the PCR product created with primers containing an appropriate restriction site were double digested with EcoRI and NotI and gel extracted, followed by ligation using T4 DNA ligase.

6.2.1.2. Plasmid DNA isolation and sequencing

Plasmid DNA was isolated from 2 ml overnight culture of *E. coli* using NucleoSpin Plasmid kit (Macherey-Nagel) by following the manufacturer's instructions. All plasmids in Supplemental Table 5 were confirmed by sequencing with appropriate primer(s) based

on Cycle, Clean and Run protocol performed by Sequencing Service - Faculty of Biology at Ludwig Maximilians University of Munich, Germany.

6.2.1.3. Transformation of *Agrobacterium tumefaciens*

Stable transformation into *Arabidopsis* plants were performed using *Agrobacterium tumefaciens* strain GV3101. For *Agrobacterium* transformation, 1 µg plasmid was added to 50 µl competent cells and incubated 5 min on ice, 5 min in liquid nitrogen and heat shocked at 37°C for 5 min. Then 800 µl LB medium (1% tryptone, 0.5% yeast extract, 0.5% NaCl) was added and the cells were incubated with shaking at 28°C for 4 h. Then the cells were spread onto LB plates with appropriate antibiotics and grown for 3 days at 28°C. Transformants were verified by checking the sequence of the isolated plasmid DNA.

6.2.1.4. RT-PCR and RT-qPCR

Total RNA was isolated from rosette leaves of *Arabidopsis* using the RNeasy Plant mini kit and RNase-Free DNase Set (Qiagen). The eluted RNA was further purified using TURBO DNA-free Kit (Thermo Scientific Fisher). The quality of RNA was checked by loading 2 µl onto an agarose gel and the concentration was determined using Nanophotometer (Implen). *OXA2b* cDNA was synthesised using SuperScript III First-Strand Synthesis System (Thermo Scientific Fisher) with a gene-specific reverse primer (Supplemental Table 1). To detect the presence of *OXA2b* full-length or truncated transcripts, PCR was performed using the same forward primer and different reverse primers. For RT-qPCR, total RNA was isolated from *Arabidopsis* as mentioned above and cDNA was synthesised using the iScript cDNA Synthesis Kit (Bio-Rad). A 10-fold dilution of the cDNA was used for qPCR using FastStart Essential DNA Green Master kit on LightCycler 96 (Roche). The transcript abundance of OEP24 or actin was used as reference for calculating fold change. The sequences of the PCR primers used are listed in Supplemental Table 1.

6.2.1.5. Phylogenetic analysis

Protein sequences for Oxa1/YidC/Alb3 family proteins were obtained by performing a

BLAST search of yeast Oxa1 and Cox18 sequences against the organisms listed in Supplemental Tables 1 and 2 (106). Plant protein sequences were obtained from the Phytozome 12 website (107). All the sequences were aligned using Clustal Omega (108). Gaps in the alignment were removed using TrimAI with the gappyout algorithm (109). A maximum-likelihood phylogeny was obtained with the help of IQTREE after 1000 replicates (110). Only the branches with bootstrap values above 75 were indicated on the phylogenetic trees.

6.2.2. Plant biological methods

6.2.2.1. Growth of *Arabidopsis thaliana*

All *Arabidopsis* plants were grown under controlled long day conditions (16 h light (100 μ E, 22°C), 8 h dark (18°C), 50% relative humidity) until the first flowers appeared and then moved to greenhouse. Seeds were surface-sterilized by mixing with sterilization solution (70% ethanol, 0.05% Triton X-100) for 15 min followed by washing with 70% ethanol once and then with 100% ethanol twice. The dried seeds were sown on MS (Murashige and Skoog) agar plates (half-strength MS medium, 0.05% MES and 0.75% agar, pH 5.8) followed by stratification at 4°C in the dark while those for growth on soil were stratified directly on wet soil for three days prior to their incubation in the growth chambers. For isolating mitochondria from 2-week-old plants, surface-sterilized seeds were grown in MS liquid medium (same as for MS agar medium described above, except for the omission of agar and addition of 1% sucrose and 50 μ g/mL cefotaxime) with shaking at 80 rpm for 2–3 weeks in the growth chamber. For mitochondria isolation from 4-week-old plants, at least 140 plants were grown on soil for each genotype.

6.2.2.2. Arabidopsis genotyping

gDNA was isolated from *Arabidopsis* for genotyping analysis as follows: A single leaf from a 2- to 3-week-old *Arabidopsis* plant was taken in a 2 ml microcentrifuge tube and homogenized in 500 μ l High Purity Extraction buffer (50 mM NaCl, 50 mM EDTA, 1% PVP-40, 1 M Tris, pH 7.5) with the help of a 3 mm tungsten carbide ball for 3 min using TissueLyser (Qiagen). Afterwards, 66 μ l of 10% SDS and 166 μ l of 5 M potassium acetate

were added and mixed. Then it was centrifuged for 15 min at 16,000 g and the supernatant was mixed with 0.7 volume of isopropanol and incubated for 15 min at -20°C. The sample was then centrifuged for 15 min at 16,000 g and the supernatant was discarded. The pellet was washed by gentle mixing with 500 µl of 70% ethanol and recentrifuged at 16,000 g for 5 min. The final pellet was dried at 50°C for 10 min and resuspended in 50 µl water. Genotyping PCR was performed with 2 µl gDNA in a 20 µl reaction using DFS-Taq DNA polymerase.

6.2.2.3. Stable transformation of Arabidopsis

Heterologous DNA was transformed into appropriate lines of Arabidopsis by the floral dip method via *Agrobacterium tumefaciens* GV3101 (111). 500 ml LB medium containing 50 µg/ml rifampicin, 10 µg/ml gentamycin and 100 µg/ml spectinomycin was inoculated with an overnight grown preculture of recombinant *A. tumefaciens* and grown overnight at 28°C, 200 rpm. Cells were harvested by 20 min centrifugation at 2500 g and resuspended in Silwet medium (5% sucrose, 0.03% Silwet L-77). Six flowering Arabidopsis plants were dipped in the cell suspension for about 10 sec with gentle agitation and the tray containing dipped plants was covered with a plastic lid overnight. The dipping procedure was repeated after one week. Seeds from transformed plants were harvested and selected on MS agar plates with a suitable antibiotic.

6.2.2.4. Generation of complementation lines

The constructs cloned into pH2GW7 and pHABI3pGW7 for expression under the control of 35S promoter or ABI3 promoter respectively, were transformed into the corresponding heterozygous T-DNA insertion lines via *Agrobacterium*. Homozygous plants due to complementation were isolated by selecting the seeds of transformant plants on plates containing 20 µg/ml hygromycin (for transformation selection) and 50 µg/ml kanamycin (SALK T-DNA selection) or 7.5 µg/ml sulfadiazine (GABI T-DNA selection) and genotyped by PCR. The next generation mutants were verified for homozygosity by performing genotyping PCR before being propagated for further studies.

6.2.2.5. Generation of RNAi and OXAp-GUS lines

The gene-specific sequences of OXA1a, OXA2a and OXA2b were derived from the CATMA website and amplified using the primers specified in Supplemental Table 1 (97). Amplified target sequences were inserted into dexamethasone-inducible pOpOff2 (Kan) and constitutively expressed pK7GWIWG2 vectors by Gateway recombination cloning (Invitrogen) (112). The promoter regions of all the four Arabidopsis OXA genes were fused to the GUS reporter gene by Golden Gate assembly (104, 105). The constructs were stably introduced into wild-type Columbia-0 plants and transformants were identified by screening on MS agar plates containing 50 µg/mL kanamycin (113). The resulting T2 lines were further screened on selective medium to identify lines with a single insertion locus by checking 3:1 ratio of the number of seedlings resistant or sensitive to the antibiotic. GUS staining was also performed on the seedlings induced with 50 µM dexamethasone to verify the operation of the pOp promoter (Section 6.2.2.8). The T3 progenies of the selected lines were analyzed on the antibiotic selection medium to identify homozygous lines by checking for all resistant seedlings. Three such homozygous independent insertion lines were propagated and used for subsequent experiments. The T1 generation seeds of each of the four Arabidopsis OXA promoters fused to the GUS reporter gene are available for performing OXA expression analyses.

6.2.2.6. Generation of OXA1a-RNAi oxa1b double mutants

Two OXA1a-RNAi lines, *OXA1a-RNAi-2* and *OXA1a-RNAi-3* were crossed to *oxa1b-2* by applying the anthers of the RNAi lines over the stigmas of *oxa1b-2*. The anthers of *Control-RNAi* (male) were also crossed to *oxa1b-2* (female) to serve as a control double mutant. Since kanamycin resistance of the T-DNA insert was lost, any such resistance observed in the progeny would be due to the presence of the RNAi construct. When the T1 generation was genotyped for the presence of *OXA1b* T-DNA insert and the *OXA1a* RNAi construct, only heterozygosity of the T-DNA insert was observed for all the 10 plants tested. The T2 generation was screened on kanamycin selection plates and the plants homozygous for the T-DNA insert were selected by genotyping. The T3 generation was further verified for the homozygosity of the T-DNA insert as well as for the presence of the RNAi construct by genotyping after selection on kanamycin plates. The T4 progenies of the selected lines

were analyzed on the antibiotic selection medium for all resistant seedlings to identify homozygous lines. The available T5 generation double mutant lines have to be verified for homozygosity of both the *OXA1b* T-DNA insert and the corresponding RNAi construct before further experimental analyses.

6.2.2.7. Arabidopsis phenotyping

Growth-stage-based phenotypic analysis was performed as described in (114). Root lengths were measured from 14-day-old seedlings grown on vertically placed agar plates. Data for growth progression analysis of *oxa2b* complementation lines was collected from 100 plants for the plate-based method, 24 plants for the soil-based method and 20 plants for root growth measurement while that of *oxa2a* complementation lines was collected from 60 plants for the plate-based method, 24 plants for the soil-based method and at least 30 plants for root growth measurement. For *oxa1b* germination assay, the seeds incubated at 15 °C were stratified at 1°C. To inhibit germination, 1 µM abscissic acid was used in the growth medium. Growth progress of embryos and green siliques dissected and opened using a needle were visualized using a binocular microscope (Zeiss Stemi 2000-C). Weights of seeds harvested from three different plants of each *oxa2b* complementation genotype were measured and their averages calculated except for *oxa2b-1+35S:OXA2b*, for which the seed weight was calculated based on the total weight of seeds harvested from 24 plants.

6.2.2.8. GUS Staining

The plant material was incubated in fixation solution (2% p-formaldehyde, 0.1% glutaraldehyde, 50 mM sodium phosphate, pH 7.0) for 5 min and washed with phosphate buffer (50 mM sodium phosphate, pH 7.0). Then vacuum infiltration was performed in X-Gluc staining solution (1 mM X-Gluc, 10 mM EDTA, 0.5 mM potassium ferrocyanide 0.5 mM potassium ferricyanide, 0.1% Triton X-100, 50 mM sodium phosphate, pH 7.0) at 1000-800 mbar for 5 min followed by overnight incubation in dark at 37°C. Subsequently destaining with 70% ethanol was done.

6.2.3. Biochemical methods

6.2.3.1. SDS-PAGE

SDS-PAGE was performed with 30 µg mitochondrial protein per lane. 100 µg mitochondrial protein was used for immunodetection of OXA2b due to its very low abundance. 100% sample in *oxa1b* SDS-PAGE analyses corresponds to 40 µg mitochondrial protein. Samples were denatured in SDS loading buffer (2% SDS, 0.04% bromophenol blue, 5% β-mercaptoethanol, 10% glycerol, 60 mM Tris, pH 6.8) by heating for 5 min at 95°C and loaded onto wells of a stacking gel (5% acrylamide) over a separating gel (10, 12.5 or 15% acrylamide). Electrophoresis was performed in SDS running buffer (25 mM Tris, 192 mM glycine, 0.1% SDS) at 25 mA for a small gel or 30 mA for a large gel. Then the gel was either stained with Coomassie staining solution (0.18% Coomassie brilliant blue R-250, 50% methanol, 7% acetic acid) followed by destaining (40% methanol, 10% acetic acid) or immunoblotted (Section 6.2.3.4).

6.2.3.2. BN-PAGE

BN-PAGE was performed with 100 µg mitochondrial protein per lane on native Bis-Tris gels consisting of gradient (4.4-16% acrylamide) separating gel and a stacking gel (4% acrylamide) (115). For sample preparation, 100 µg mitochondria were solubilized in 20 µl digitonin extraction buffer (5% digitonin, 150 mM potassium acetate, 10% glycerol, 30 mM HEPES, pH 7.4) for 20 min on ice. After 20 min centrifugation at 15000 g, 4°C, the supernatant was mixed with BN loading buffer (5% Coomassie brilliant blue G-250, 750 mM aminocaproic acid) and electrophoresis was performed using cathode buffer (0.02% Coomassie brilliant blue G-250, 50 mM Tricine, 15 mM Bis-Tris, pH 7.0) and anode buffer (50 mM Bis-Tris, pH 7.0) at 7 mA for 45 min followed by 15 mA for 5 h at 4°C. Then the BN gel was directly destained (40% methanol, 10% acetic acid) or enzyme activity assays were performed (Section 6.2.4.2). For immunoblotting of protein complexes (Section 6.2.3.4), BN-PAGE was performed similarly except that the cathode buffer was exchanged with the one lacking Coomassie after 2 h of electrophoresis at 15 mA and then continued for an additional 2.5 h.

6.2.3.3. 2D-BN/SDS-PAGE

2D-BN/SDS-PAGE was performed with 250 µg and 500 µg of mitochondria for immunoblotting and colloidal Coomassie staining respectively. A lane from the first dimension BN-PAGE performed as described above was incubated in SDS equilibration solution (1% β-mercaptoethanol, 1% SDS) for 30 min and washed briefly in water before placing it in a slightly angled position with the low molecular weight region higher, on a gel plate for casting the second dimension SDS gel containing 4 M urea. Electrophoresis was performed at 20 mA. Proteins were visualised by colloidal Coomassie staining (Section 6.2.3.5) or immunoblotting (Section 6.2.3.4) was performed.

6.2.3.4. Immunoblotting

Proteins were electrotransferred out of an SDS gel using a semi-dry blotting apparatus while protein complexes were electrotransferred out of a BN gel using a wet blotting apparatus. For semi-dry blotting, four blotting papers, activated PVDF membrane, gel and four blotting papers, all soaked in transfer buffer (48 mM Tris, 39 mM glycine, 1.3 mM SDS, 20% methanol) were assembled and blotted at 0.8 mA/cm² for 1 h. Blotted proteins were stained with Ponceau solution (0.1% Ponceau S, 5% acetic acid) to mark the protein marker bands and washed briefly with water and TBST (150 mM NaCl, 10 mM Tris pH 7.4, 0.1% Tween-20). For wet blotting, a sponge, one blotting paper, activated PVDF membrane, gel, a blotting paper and a sponge, all soaked in transfer buffer were assembled on the anode cassette and covered tightly with cathode cassette. Electroblotting was performed at 50 mA for 18 h. Then the major respiratory complexes were marked on the membrane using a destaining solution (30% methanol, 7% acetic acid) before washing away all the blue using methanol followed by a brief rinse with TBST.

The SDS gel blotted membrane was blocked for at least 30 min with 2% skimmed milk in TBST while the membrane for BN blots was blocked for at least 1 h with 5% skimmed milk in TBST. Incubation with primary antibody was performed overnight at 4°C (Supplemental Table 2). After three 10 min washes in TBST, the membrane was incubated for 1 h at room temperature with horse radish peroxidase conjugated secondary antibody. After another three 10 min washes in TBST, substrate solution (equal volumes of

development solutions I (2.5 mM luminol, 0.4 mM p-coumaric acid, 100 mM Tris pH 8.5) and II (0.018% H₂O₂, 100 mM Tris pH 8.5)) was added and chemiluminescence was detected on ImageQuant LAS 4000 (GE Healthcare).

6.2.3.5. Colloidal Coomassie staining

The gel was incubated in fixing solution (40% methanol, 10% acetic acid) for at least 1 h and then incubated in 100 ml of staining solution (0.08% Coomassie Brilliant Blue G-250, 1.57% o-phosphoric acid, 7.84% ammonium sulfate, 20% methanol) for about 24 h. Destaining was done several times in water before scanning.

6.2.3.6. Autoradiography

Radiolabelled proteins or complexes were detected by exposing the corresponding dried gel to a storage phosphor screen in a cassette for at least 48 h followed by visualization using Typhoon Trio scanner (GE healthcare) at high sensitivity.

6.2.3.7. Production of antibodies

For generating antibodies against all the four Arabidopsis OXA proteins, the cDNAs corresponding to the first matrix-exposed loop regions were cloned into pDEST17 and over expressed using 1 mM isopropyl β -D-1-thiogalactopyranoside (IPTG) in BL21 (DE3) cells grown in 2 l LB medium containing 100 μ g/ml Ampicillin at 37°C. After disruption of the cells using French press (SLM Aminco FA-078), the proteins were purified by IMAC using Protino Ni-NTA Agarose beads (Macherey-Nagel) by following Gravity-flow purification protocol of the user manual. The elutions were further purified by electro-elution, concentrated using Amicon Ultra centrifugal filters (Millipore) and sent to Pineda antikorper service at 2 mg/ml final concentration for injections into New Zealand white rabbits.

6.2.4. Methods concerning mitochondria

6.2.4.1. Isolation of mitochondria

Mitochondria were isolated from 10 to 14-day-old plants (wild-type and full-length *oxa2b*-complemented plants), 17 to 21-day-old plants (C-terminally truncated-*oxa2b*-complemented plants) and 2 weeks various *oxa2a*-complemented plants grown in liquid medium. Approximately 50 g of Arabidopsis plant tissue was pounded in a mortar with 150 ml of grinding buffer (0.3 M sucrose, 25 mM Na₄P₂O₇, 2 mM EDTA, 10 mM KH₂PO₄, 1% PVP-40, 1% BSA, 20 mM ascorbic acid, pH 7.5). The filtrated lysate was centrifuged for 5 min at 2,500 g, 4°C and the supernatant was centrifuged for 20 min at 17,400 g, 4°C. The pellet was resuspended in the residual buffer and washed in wash buffer (0.3 M sucrose, 0.1% BSA, 10 mM TES, pH 7.5) by repeating the above two centrifugation steps. Then the crude mitochondrial pellet was loaded over two 0-4.4% PVP-40 gradients containing 28% percoll (GE Healthcare) in wash buffer and centrifuged for 40 min at 40,000 g, 4°C with the brakes off. Mitochondria found as a light-yellow cloudy band near the bottom of the tube was collected and mixed with wash buffer without BSA for washing twice at 31,000 g, 4°C for 15 min with slow deceleration. The mitochondria in the form of a loose pellet was collected and protein content was quantified by Bradford assay of 1 µl mitochondria in five replicates using Bio-Rad protein assay dye reagent and the samples were then used directly for analyses or frozen at -80°C for further analyses.

Mitochondria were similarly isolated from the various *oxa2a*-complemented plants grown for 2 weeks. For mitochondria isolation from 4-week-old *oxa2a*-complemented plants grown on soil, above ground plant material was ground in grinding buffer B (0.3 M sucrose, 60 mM TES, 2 mM EDTA, 25 mM Na₄P₂O₇, 10 mM KH₂PO₄, 1 mM glycine, 1% PVP-40, 1% BSA, 50 mM sodium ascorbate, 20 mM cysteine, pH 8.0) instead of the grinding buffer mentioned above and the rest of the protocol performed similarly (116, 117).

6.2.4.2. *In gel* enzyme activity assays

Enzyme assays for the respiratory complexes I (118), III (119) and IV (120) were performed

after BN-PAGE by incubating the gel in 50 ml of the respective freshly prepared staining solution at RT. Complex I was visible in 20 min of incubation in its staining solution (0.14 mM NADH, 0.1% nitroblue tetrazolium, 0.1 M Tris, pH 7.4). Complex III was stained after 6 h using Pierce 1-step TMB-Blotting solution (Thermo Scientific, Rockford, USA). Complex IV was detected after incubation in its staining solution (1 mg/ml cytochrome *c*, 0.1% 3,3'-diaminobenzidine, 10 mM potassium phosphate, pH 7.4) for 80 min. The gels were transferred into fixing solution (40% methanol, 10% acetic acid) to stop the reactions and decrease Coomassie blue background before scanning. In order to distinguish the blue coloured band corresponding to complex III catalytic activity from the blue color of Coomassie coupled to proteins, digital processing of the image was performed in RGB working space of Adobe Photoshop resulting in green-yellow color of the complex III band (119).

6.2.4.3. Heme staining

Heme staining was performed on mitochondrial sample transferred to PVDF membrane (Millipore Immobilon-P) after its separation by BN-PAGE (100 µg) or SDS-PAGE (50 µg). The blot was washed twice in TBS without Tween and incubated for 5 min in 1:1 mixture of the solutions in SuperSignal West Femto kit (Thermo Scientific) for chemiluminescence detection on ImageQuant LAS 4000 (121).

6.2.4.4. *In organello* protein synthesis

For performing *in organello* mitochondrial translation, 200 µg of freshly isolated mitochondria were resuspended in 100 µl of master mix (300 mM mannitol, 60 mM KCl, 50 mM HEPES, 10 mM MgCl₂, 10 mM sodium malate, 10 mM sodium pyruvate, 20 mM GTP, 10 mM DTT, 20 mM ADP, 5 mM KH₂PO₄, pH 7.0) and placed on ice for 3 min. Then 4 µl of 1 mM amino acid mixture minus methionine and 22 µCi ³⁵S-methionine were added. The reactions were performed by incubation at 25°C with shaking at 350 rpm for 10, 30, and 60 min and stopped by addition of 1 ml mitochondria wash buffer containing 10 mM methionine. In control experiments, 25 mM sodium acetate was used instead of sodium malate and sodium pyruvate. Radiolabeled proteins were separated by SDS-PAGE and complexes by BN-PAGE before visualization by autoradiography (Sections 6.2.3.1, 6.2.3.2

and 6.2.3.6). The protein bands were identified by aligning immunoblot analyses of certain mitochondrially translated proteins using wild-type mitochondria run on the same gel (Supplemental Figure 4).

6.2.4.5. Preparation of mitoplasts

For preparing mitoplasts, the mitochondrial OM was disrupted by osmotic swelling. Mitochondrial pellet corresponding to 100 μg was resuspended in 10 μl of SEH buffer (250 mM sucrose, 1 mM EDTA, 10 mM HEPES, pH 7.4). Then 155 μl of 20 mM HEPES, pH 7.4 was added and incubated on ice for 15 min. Subsequently 25 μl of 2 M sucrose and 10 μl of 3 M KCl were added and mixed. Then the sample was typically aliquoted into two, one of which was treated with Proteinase K (PK) and the other mock-treated as described below (Section 6.2.4.6).

6.2.4.6. Proteinase K treatment

For PK digestion of mitochondria and mitoplasts, the enzyme was added to a final concentration of 32 $\mu\text{g}/\text{ml}$ and 60 $\mu\text{g}/\text{ml}$ respectively. In case of a mock treatment, another corresponding sample was taken without the addition of PK. All the samples were incubated on ice for 30 min. The proteolysis was inhibited using 1 mM phenylmethylsulfonyl fluoride (PMSF) and mitochondria or mitoplasts were collected by centrifugation at 16,000 g for 5 min at 4°C. The pellet was resuspended in 2X SDS loading buffer and analysed by SDS-PAGE followed by autoradiography (Sections 6.2.3.1 and 6.2.3.6).

6.2.4.7. *In vitro* mitochondrial protein import

^{35}S labelled precursor proteins were synthesised in a coupled transcription-translation reaction (50% rabbit reticulocyte lysate, 1.75 μg plasmid, 13.75 μCi ^{35}S methionine and cysteine mix, 50 mM Tris pH 8, 1.5 μM MgCl_2 , 100 μM rNTPs, 62.5 U T7 RNA polymerase, 20 μM amino acid mixture minus methionine, 64 U RNasin ribonuclease inhibitor, made up to a final volume of 50 μl with nuclease-free water) at 30°C for 90 min.

In vitro imports of the precursor proteins were performed into mitochondria isolated from 2-week-old plants. Mitochondria of 250 µg were added to 450 µL of ice-cold import master mix (0.3 M sucrose, 50 mM KCl, 10 mM MOPS, 5 mM KH₂PO₄, 0.1% BSA, 1 mM MgCl₂, 1 mM methionine, 0.2 mM ADP, 0.75 mM ATP, 5 mM succinate, 5 mM DTT, 5 mM NADH, 1 mM GTP, pH 7.5) and incubated on ice for 3 min. After adding 25 µl of radiolabeled precursor protein, the import reaction was performed for the indicated times at 26°C with gentle rocking at 350 rpm. Then 100 µl containing 50 µg mitochondrial protein was removed and treated with PK (Section 6.2.4.6). For the nine-lane import experiment of Arabidopsis OXA proteins with AOX and TIM23 as positive controls (Figure 7), an appropriate amount of the import master mix was divided into two tubes and valinomycin was added into one of them to a final concentration of 1 µM before proceeding for the import reaction as described above as well as mitoplast preparation and PK treatment protocols (Sections 6.2.4.5 and 6.2.4.6). For analysing radiolabelled protein complexes, 100 µg mitochondria after the import reaction were pelleted and prepared for BN-PAGE followed by autoradiography (Sections 6.2.3.2 and 6.2.3.6).

6.2.4.8. Mitochondrial protein pull-down assays

The recombinant pGEX-6P-1 plasmid containing the TPR domain of OXA2b (GST-OXA2bTPR) and the empty vector (GST) were transformed into BL21 *E. coli* cells. After induction with 1 mM IPTG, the cells were grown overnight in 1 l LB medium containing 100 µg/ml ampicillin at 12°C. The harvested cells were resuspended in PBS buffer and homogenized using French press (SLM Aminco FA-078) at 12,000 psi cell pressure. The cell lysate was centrifuged (10,000 g, 20 min, 4°C) and the supernatant was incubated with 1 ml Glutathione Sepharose 4 Fast Flow beads (GE Healthcare) that were washed and resuspended in PBS (140 mM NaCl, 2.7 mM KCl, 10 mM Na₂HPO₄, 1.8 mM KH₂PO₄, pH 7.3), for 1 h at RT on a roller. After collecting the flow-through followed by three washes, the bound proteins were eluted in 2.5 ml GST elution buffer (10 mM reduced glutathione, 50 mM Tris-HCl, pH 8.0). Purified GST and GST-OXA2bTPR were dialyzed overnight using standard RC tubing (Spectra/Por, MWCO: 3.5 kD) in PBS at 4°C to remove bound glutathione and protein concentrations were measured using Bio-Rad protein assay dye reagent.

In organello translation of mitochondrial-encoded proteins was performed with Col-0 mitochondria (Section 6.2.4.4). Then the mitochondria were lysed in mitochondrial lysis buffer (1% Triton X-100, 140 mM NaCl, 2.7 mM KCl, 10 mM Na₂HPO₄, 1.8 mM KH₂PO₄, 1mM PMSF, pH 7.4) for 20 min on ice and centrifuged at 15,000 g for 20 min at 4°C. The clarified lysate was applied to 25 µl of Glutathione Sepharose 4 Fast Flow beads (GE Healthcare) that were loaded with 2.4 nmol of GST (control) or GST-OXA2bTPR and blocked with 3% BSA in PBS buffer supplemented with 1mM PMSF, and incubated for 3 h at 4°C. After collecting the flow-through and washing, the bound proteins were eluted in 25 µl GST elution buffer after which SDS-PAGE was performed followed by autoradiography (Sections 6.2.3.1 and 6.2.3.6). For pull-down assays with *in vitro* synthesized proteins, 20 µl of the beads loaded with 100 µg of GST (control) or GST-OXA2bTPR were incubated with the translation reaction for 1 h at RT. After washing, the bound proteins were eluted and detected similarly as described above.

7. Results

7.1. Phylogenetic and structural analyses of plant OXA proteins

7.1.1. OXA gene duplication must have occurred before speciation

The Oxa1 superfamily is well conserved from a structural and mechanistic standpoint, although the protein sequences are diverse (71). Previous attempts to determine whether OXA2b is more closely related to yeast or mammalian Oxa1 or Cox18 were limited to small data sets (87). To overcome this limitation, Oxa1-like proteins of all plant species found in the Phytozome database were used to create an unrooted phylogenetic tree (Figure 4; Supplemental Table 3). For comparison, a selection of bacterial YidC and chloroplast Alb3/Alb4 sequences were also included in the phylogenetic analysis. As observed in (87), YidC and Alb3/Alb4 proteins were more closely related and clustered together on one side (Figure 4). All the Oxa proteins were found on the other side of the

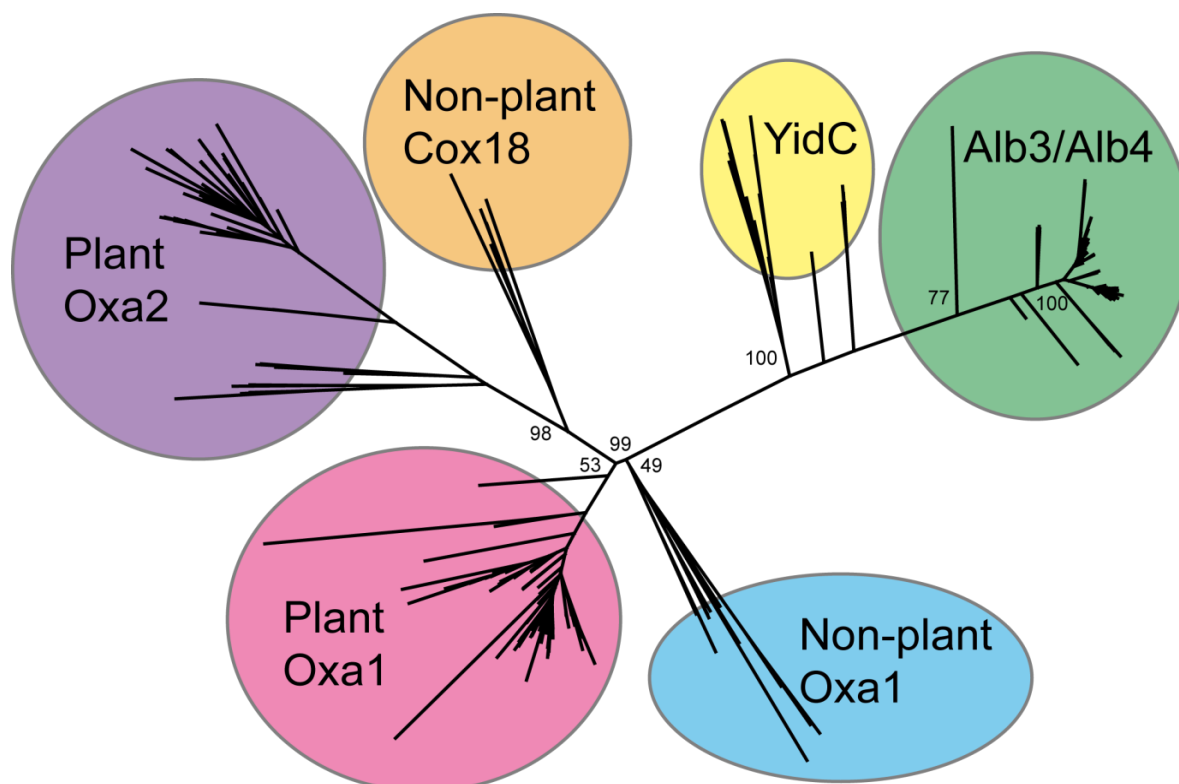


Figure 4. Phylogeny of plant Oxa proteins. A maximum-likelihood phylogenetic tree of Oxa1/YidC/Alb3 proteins is shown. Numbers represent ultrafast bootstrap values from IQTREE. Only the main branches bootstrap values are shown for better visibility. The organisms included in the analysis can be found in Supplemental Table 3. The phylogenetic analysis was performed by Dr. Chris Carrie.



tree. The non-plant Oxa1 and the plant Oxa1 proteins, including both the Arabidopsis homologs, OXA1a and OXA1b grouped together, while Cox18 and plant Oxa2 sequences, including the Arabidopsis proteins, OXA2a and OXA2b formed another group (Figure 4). Moreover, the plant Oxa2 proteins were clearly distinct and formed their own group (Figure 4). Only the plant Oxa2 group proteins have a predicted TPR domain when TPRpred program was used (108).

7.1.2. Plant OXA2 proteins are unique

Based on the identity and similarity profiles of the two OXA1 and the two OXA2 proteins present in Arabidopsis, they appear to have arisen from two independent gene duplications (Figure 5A). Only low scores of percentage similarity of approximately 26-27% was found between AtOXA1 and ScOxa1. This score is even lower between AtOXA1 and ScCox18/Oxa2 at approximately 17-18%. However, this is not surprising because all known members of the Oxa1 superfamily are conserved structurally on the basis of a

A)

	AtOXA1a	AtOXA1b	AtOXA2a	AtOXA2b	ScOxa1	ScCox18	EcYidC
AtOXA1a		41.95	10.95	9.32	17.16	7.59	9.32
AtOXA1b	52.91		11.83	9.97	16.41	8.86	8.12
AtOXA2a	17.94	21.80		45.33	11.94	9.49	8.19
AtOXA2b	18.41	20.64	57.90		9.45	8.54	8.39
ScOxa1	27.86	26.36	22.38	16.41		10.44	7.21
ScCox18	14.24	16.77	18.03	17.72	18.98		7.27
EcYidC	17.01	16.47	17.14	14.23	13.93	16.45	

 %identity
 %similarity

B)

Protein Name	Systematic Name	Protein Precursor			Transit Peptide	Mature Protein			C-terminus		
		Length (amino acids)	MW (kD)	pI	Length (amino acids)	Length (amino acids)	MW (kD)	pI	Length (amino acids)	MW (kD)	pI
AtOXA1a	At5g62050	429	47.9	9.6	82	347	38.3	9.4	89	10.0	11.0
AtOXA1b	At2g46470	431	47.9	9.3	82	349	38.7	8.6	88	10.0	11.2
AtOXA2a	At1g65080	525	58.3	5.9	56	469	52.0	5.2	245	27.2	5.0
AtOXA2b	At3g44370	566	62.8	6.4	43	523	57.9	5.8	235	25.7	5.6
ScOxa1	YER154W	402	44.8	10.8	42	360	40.0	9.7	86	10.1	10.7
ScCox18	YGR062C	316	35.7	11.8	50	266	30.1	11.2	7	1.0	8.6
EcYidC	b3705	548	61.5	7.7	24	548	61.5	7.7	16	1.9	11.1

Figure 5. A Comparison of Oxa homologs. **A)** Identity and Similarity of Oxa proteins. Protein sequence identity and similarity of Oxa1 homologs in Arabidopsis, yeast and bacteria were calculated with SIAS tool after aligning the sequences using ClustalW. **B)** The length, molecular weight (MW) and pI of the various protein segments of Oxa proteins are tabulated. In case of EcYidC, it refers to signal peptide instead of transit peptide. At – *Arabidopsis thaliana*, Sc – *Saccharomyces cerevisiae* and Ec - *Escherichia coli*.

hydrophobic core domain rather than by sequence conservation (69, 71, 72). Oxa homologs can be divided into two groups based on the C-terminal extension. An elongated and highly positively charged C-terminus is a characteristic feature of Oxa1 in yeast (Figure 5B). On the other hand, yeast Cox18 has a very short C-terminus with a relatively lower positive charge. Both OXA1a and OXA1b proteins of Arabidopsis have the length and charge of their C-termini close to the corresponding values of yeast Oxa1 (Figure 5B). Thus, they are very likely to be functionally similar as well. However, OXA2a and OXA2b proteins of Arabidopsis appear to be very different from yeast Cox18. They have an unusually long C-terminus which is negatively charged and was predicted to form a TPR domain as mentioned above (Figure 5B) (87, 108). Thus, the Arabidopsis OXA2 proteins are structurally unique among members of the Oxa1 superfamily and might perform certain plant-specific roles.

7.1.3. Functional specialization of OXA2 in the Brassicaceae family

When the distribution of OXA2 proteins in plants was studied, it was found that the majority of plant species contain only one OXA2-like protein (Figure 6). However, in the Brassicaceae family, a clear split into OXA2a and OXA2b groups was observed (Figure 6). Since the knockout of OXA2a and OXA2b is independently embryo lethal, they perform non-overlapping essential roles in Arabidopsis (87). Therefore, it can be hypothesized that the OXA2 gene duplication in the Brassicaceae family was followed by subfunctionalization. This means that it is likely that in other plant species, the sole OXA2 protein can either perform the roles of both OXA2a and OXA2b from Arabidopsis or does not require the extra function of one of the Arabidopsis OXA2s.

7.1.4. Arabidopsis OXA proteins are likely to contain five TMHs

It was previously shown that all the four Arabidopsis OXA proteins get imported into mitochondria (87). Here, in order to confirm the intra-mitochondrial localization in the IM and study the membrane topology, the mitochondrial OM was osmotically ruptured following import of the radioactive protein to generate mitoplasts (MP) and treated with

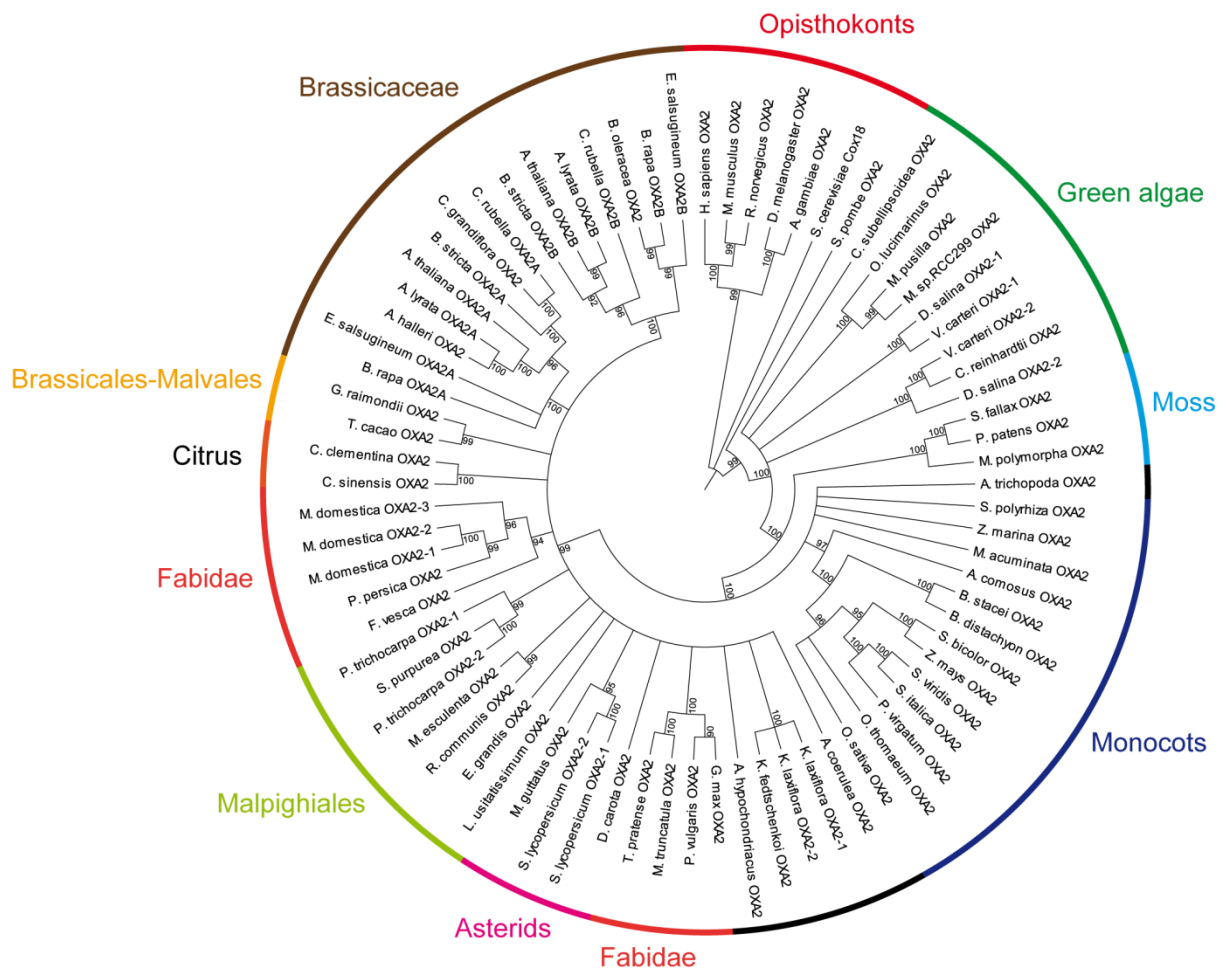


Figure 6. Phylogeny of Oxa2 proteins. A maximum-likelihood phylogenetic tree of OXA2 proteins with numbers representing ultrafast bootstrap values from IQTREE after 1000 replicates. Only the branches with bootstrap values above 75 are shown for better visibility. Species included in the analysis can be found in Supplemental Table 4. The phylogenetic analysis was performed by Dr. Chris Carrie.

Proteinase K (PK). In addition to the four OXA proteins, imports of AOX and TIM23 were performed as controls. As expected, AOX is imported and processed to its mature form. Since no part of AOX is exposed to the intermembrane space (IMS), there is no change upon PK treatment of MPs (Figure 7). As for TIM23, it does not have a cleavable presequence. Since its N-terminus is exposed to the IMS, it was cleaved upon generating MPs and subsequent PK treatment (Figure 7). All the four Arabidopsis OXA proteins were imported and processed to their mature forms (Figure 7). OXA1a and OXA1b mature proteins were further cleaved upon PK treatment of MPs (Figure 7). Based on the apparent molecular weight of the peptide cleaved, they appear to have their substantially long N-terminus exposed to the IMS and the alternative possibility of C-terminus being exposed to the IMS is ruled out. Interestingly, while only a single fragment of OXA1a was detected,

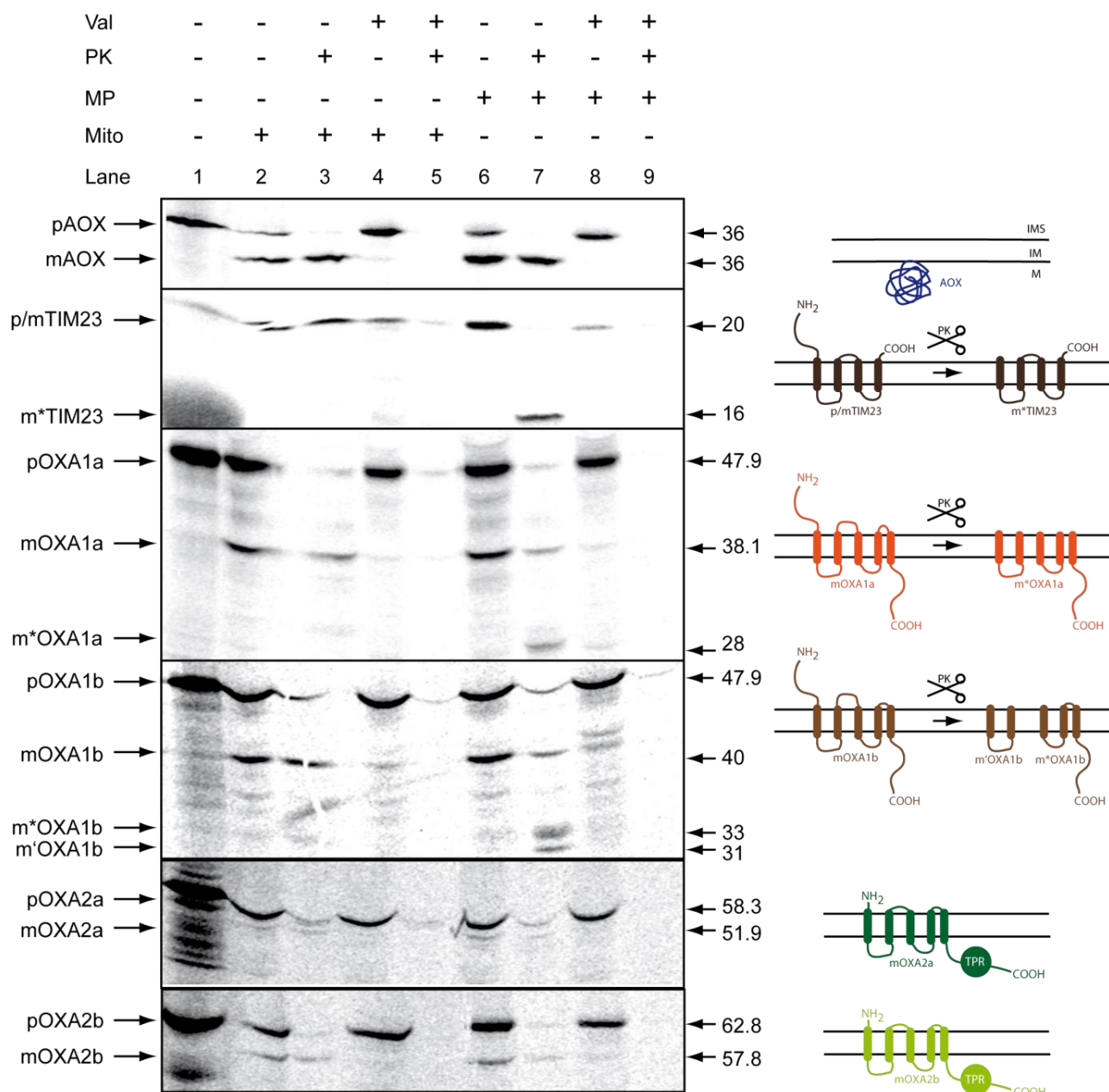


Figure 7. Import of OXA proteins into mitochondria. A typical nine-lane import used to determine the ability of a protein to be imported into isolated mitochondria and study its membrane topology. Lane 1: Radiolabelled precursor protein only, which represents 40% of that used in the import reactions of AOX, TIM23, OXA1a and OXA1b and 20% of that used in the import reactions of OXA2a and OXA2b. Lane 2: the precursor protein was incubated with isolated Col-0 wild-type mitochondria (Mito) under conditions supporting mitochondrial protein import. Lane 3: As in Lane 2, but PK was added after the import reaction. Lanes 4 and 5: As in lanes 2 and 3 respectively, but with the addition of valinomycin (Val) to the import reaction. Val dissipates the membrane potential and prevents import into or across the IM. Lanes 6 to 9: As in lanes 2 to 5 respectively, but the OM was osmotically ruptured to generate mitoplasts (MP) following the import reaction. PK digestion was performed subsequently. The prefixes p, m and m* before the OXA protein name indicate the precursor, mature and the remainder of mature protein after PK digestion respectively. PK digestion of OXA1b cleaved the protein into two parts that were named with prefixes m* and m'. The molecular masses of the protein bands in kD are specified on the right side. The predicted membrane topology of proteins is depicted in the form of cartoons. The outcomes of PK digestion of the proteins that have IMS-exposed regions are also shown.

two fragments of OXA1b were detected (Figure 7). Hence the IMS-exposed loops of OXA1a and OXA1b are very likely to differ in length and/or accessibility of PK. On the other hand, as OXA2a and OXA2b were not cleaved upon PK treatment of MPs, they do not appear to have any considerable IMS-exposed regions. Based on the apparent molecular masses of the protein cleavage fragments observed in this import experiment combined with structural alignments with bacterial homologs, all the four OXA proteins are likely to contain five TMHs with the N-terminus in the IMS and the C-terminus in the matrix (Figure 7).

7.2. Role of OXA2b and significance of its TPR domain

7.2.1. Functional complementation rescued OXA2b knockout embryo-lethality

It has been reported previously that *OXA2b* is an essential gene in Arabidopsis (87). To confirm this, two independent T-DNA insertion lines, *oxa2b-1* (SALK_057938) and *oxa2b-2* (GABI_425B09) were genotyped. T-DNA insertions in *oxa2b-1* and *oxa2b-2* were found in intron 11 and intron 12, respectively and were confirmed by sequencing (Figure. 8A). In agreement with previous results, only heterozygous but no homozygous plant could be identified, corroborating the essential nature of *OXA2b* (87). As no homozygous line could be isolated upon partial complementation of T-DNA insertion lines using the *ABI3* promoter, the embryo-lethality of *OXA2b* could not be rescued by this strategy (122). This indicates that *OXA2b* is essential also during the later developmental stages beyond embryogenesis.

In order to study the functional role of *OXA2b*, *oxa2b-1* and *oxa2b-2* were complemented with the conserved *OXA2b* insertase domain, but lacking the C-terminal TPR region. The *35S:OXA2b Δ 235* construct had a *35S* promoter-controlled truncated *OXA2b* cDNA, which encodes only the first 331 amino acids (Figure. 8B). The *35S:OXA2b* construct with the *35S* promoter-controlled full-length cDNA of *OXA2b* which encodes all 566 amino acids was used as a control for complementation (Figure. 8B). Both the constructs were transformed into *oxa2b-1* and *oxa2b-2* heterozygous mutants to create the following four

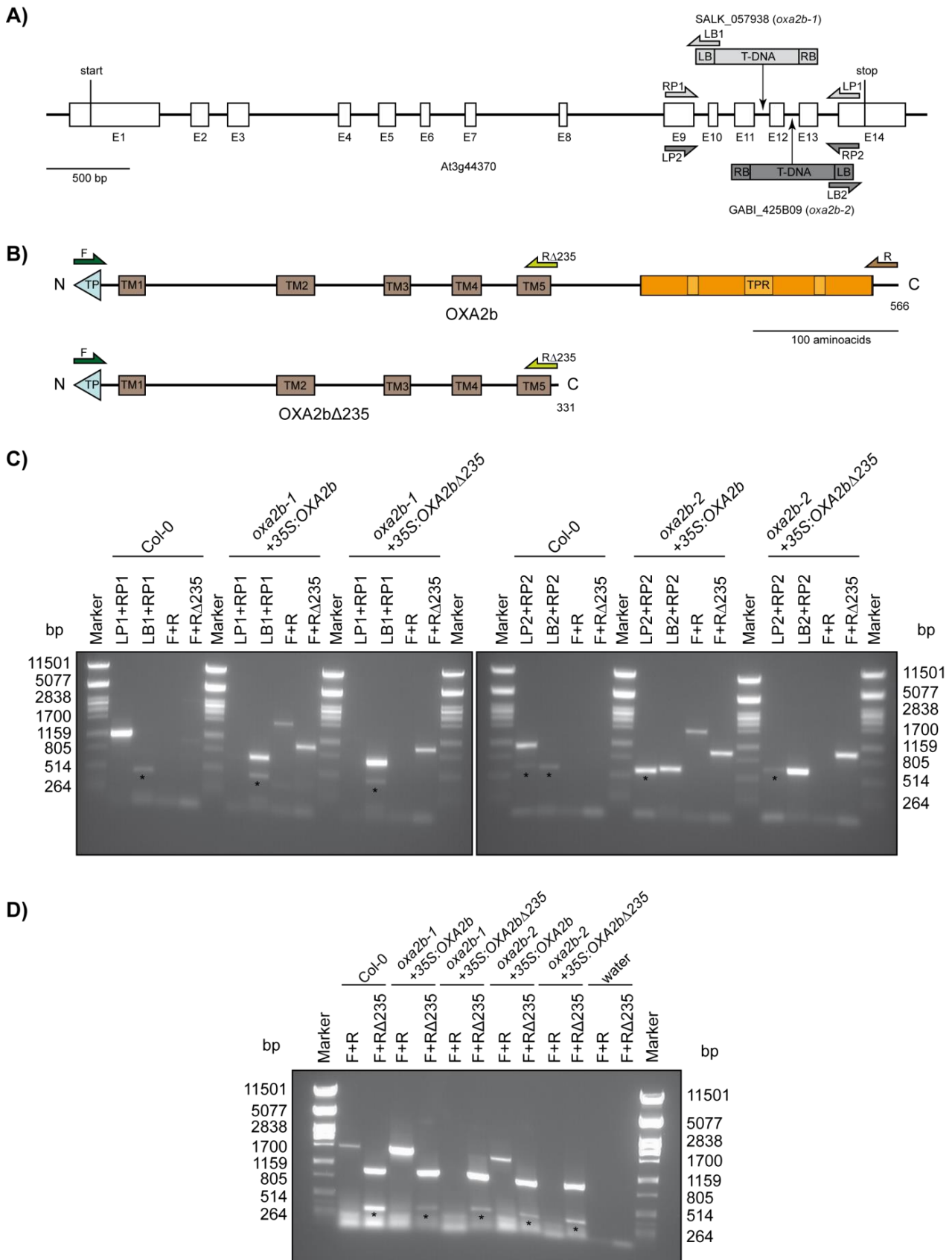


Figure 8. DNA and RNA analysis of *oxa2b* complementation mutants. **A)** Diagram of the genomic region encoding *OXA2b*, drawn to scale. The locations of T-DNA insertions and primer binding sites are indicated. Boxes labelled E1 to E14 signify exons. Spaces between adjacent exons correspond to introns. **B)** Diagram depicting the predicted secondary structure of full length and C-terminally truncated versions of *OXA2b* proteins drawn to scale. The total number of amino acid residues is indicated near the C-terminus. The corresponding cDNA of each version was inserted into the genome for complementing *oxa2b-1* and *oxa2b-2*. The primers used to confirm the cDNA insertion, F, RA235 and R,

are shown. TP: Targeting peptide; TPR: TPR domain consisting of four TPR motifs; TM1 to TM5: Transmembrane helices 1 to 5 forming the conserved core domain. N: N-terminus; C: C terminus. **C)** Genotyping PCR analysis. All lines were genotyped first for the correct T-DNA insertion and then for the presence of the inserted *OXA2b* cDNA. The primer binding positions are indicated in **A** and **B**. The sizes of the PCR products are as follows: (LP1-RP1) = 1165 bp, (LB1-RP1) = ~700 bp, (LP2-RP2) = 1073 bp, (LB2-RP2) = ~700 bp, (F-R) = 1698 bp and (F-R235) = 993 bp. * indicates non-specific PCR products. **D)** RT-PCR analysis for full length and truncated *OXA2b* transcripts. Primers are the same as in **C** and binding positions are indicated in **B**. * indicates non-specific PCR products.

complementation lines: *oxa2b-1+35S:OXA2b*, *oxa2b-1+35S:OXA2bΔ235*, *oxa2b-2+35S:OXA2b*, and *oxa2b-2+35S:OXA2bΔ235*. For the sake of simplicity, they are hereafter referred to as *35S:OXA2b-1*, *35S:OXA2bΔ235-1*, *35S:OXA2b-2* and *35S:OXA2bΔ235-2* respectively.

All the complementation plants were genotyped for the original T-DNA insertion in *OXA2b* and for the presence of the correct complementation construct (Figure. 8C). All the complementation lines were homozygous for the original T-DNA insertion as evidenced by a PCR product using the corresponding LB and RP primers, while a product for the wild-type genomic DNA (LP+RP) was not amplified (Figure. 8C). To confirm the presence of the two complementation constructs, different reverse primers were used: F+R can only amplify the full-length cDNA while F+RΔ235 can amplify the truncated as well as the full-length cDNA. All the four lines resulted in a PCR product using the F+RΔ235 primers (Figure. 8C). Using the primer set, F+R, the full-length cDNA present only in *35S:OXA2b* lines was amplified (Figure. 8C). Therefore, the endogenous *OXA2b* gene was knocked out successfully in both *oxa2b-1* and *-2* due to complementation by both *OXA2b* and *OXA2bΔ235*.

To confirm the presence of the correct transcript in the complementation plants, RT-PCR was performed using the same F+R and F+RΔ235 primer pairs mentioned above. The PCR products corresponding to both the primer pairs were found with wild-type (Col-0) control and with the *35S:OXA2b* plants (Figure. 8D). In comparison to the abundance of the wild-type transcript, the transcript of *35S:OXA2b-1* was much more abundant, while the transcript of *35S:OXA2b-2* was only slightly more abundant. RT-PCR with *35S:OXA2bΔ235-1* and *35S:OXA2bΔ235-2* resulted in an amplification product using the

F+R Δ 235 primer pair only. This clearly indicated that these plants no longer expressed a full-length *OXA2b* transcript and only expressed the truncated form.

To confirm the expression levels, RT-qPCR was carried out and expression levels of *OXA2b* as well as *OXA2a* were calculated with reference to wild-type (Supplemental Figure 1). While the transcript levels of endogenous *OXA2a* remained unchanged, the corresponding transcript levels of *OXA2b* in the different complementation lines were significantly different due to their expression using the 35S promoter, which is also influenced by the region of integration in the chromosome. Overall, both the genotyping and transcript analyses strongly indicated the successful knockout of genomic *OXA2b* by complementation with *OXA2b* and *OXA2b* Δ 235.

7.2.2. Severe growth retardation of 35S:*OXA2b* Δ 235 plants

After confirming homozygous complementation in 35S:*OXA2b* and 35S:*OXA2b* Δ 235 plants, quantitative phenotyping was performed using the method outlined in (114). It was already evident from plate-based phenotyping that the C-terminal deletion mutants grew at a noticeably slower rate (Figure 9A). Fourteen-day-old 35S:*OXA2b* Δ 235 plants failed to reach stage 1.02 (two rosette leaves > 1 mm in length) whereas wild-type and 35S:*OXA2b* plants had already reached stage 1.04 (four rosette leaves > 1 mm in length; Figure 9A). Growth on vertical MS plates showed that the roots of 35S:*OXA2b* Δ 235 plants grew very slowly compared to wild-type or 35S:*OXA2b* plants (Figure 9B). Slower root growth has been observed in several other *Arabidopsis* mutants with altered mitochondrial biogenesis (123, 124). Based on soil-based phenotyping, the slow growth phenotype of 35S:*OXA2b* Δ 235 plants was even more pronounced at later developmental stages (Figure 9, C-E). They were slower to reach all major growth milestones and on average took an extra month to complete a full life cycle (Figure 9C).

35S:*OXA2b* Δ 235 plants also displayed a smaller overall leaf area and the leaves were crumpled (Figure 9D). They also failed to reach the height attained by wild-type and

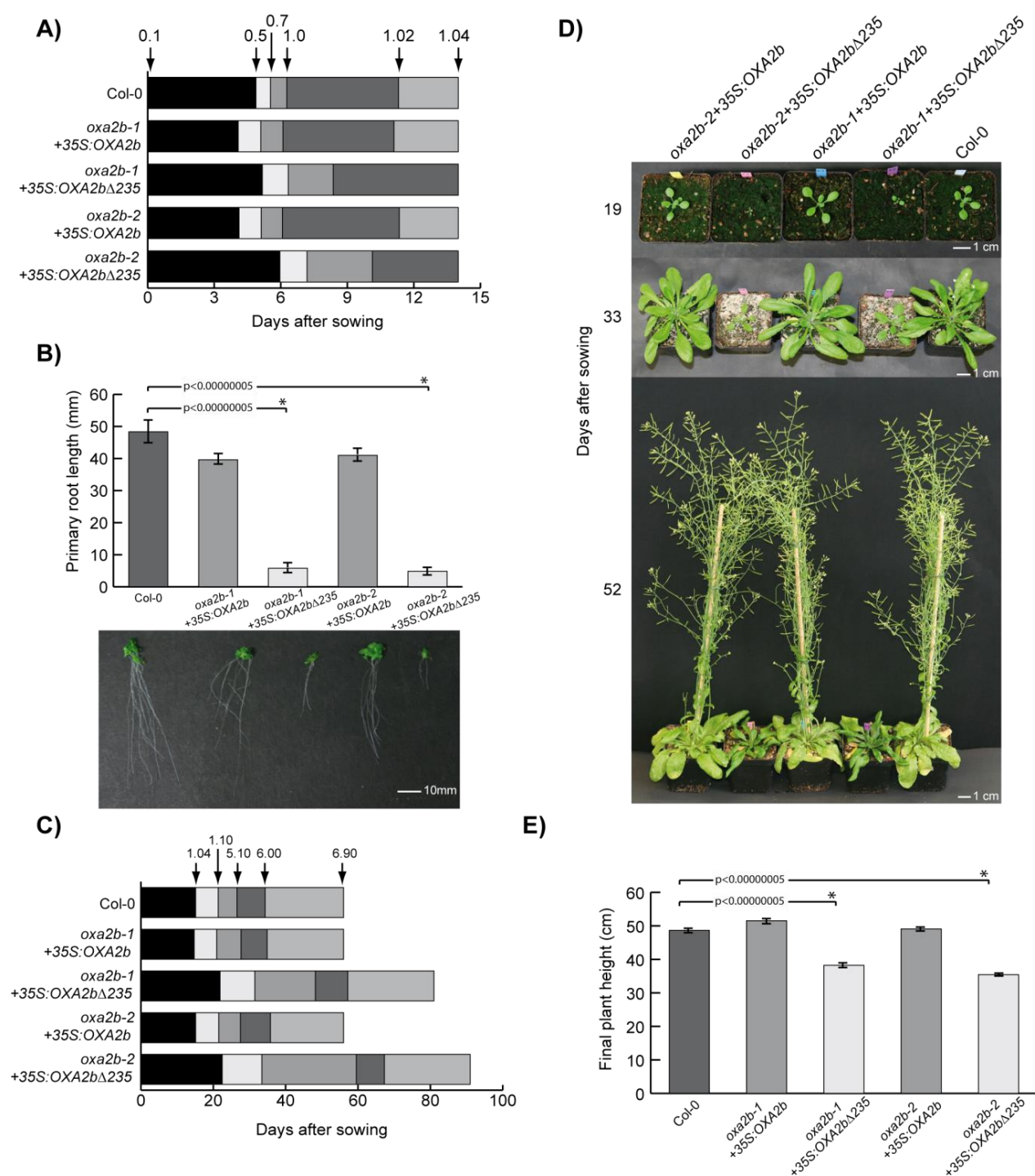


Figure 9. Phenotypes of *oxa2b* complementation plants. **A)** Plate-based growth progression analysis. Arrows indicate the time taken by wild-type plants to reach the developmental stages: 0.1: Imbibition; 0.5: Radicle emergence; 0.7: Hypocotyl and cotyledon emergence; 1.0: Cotyledons fully open; 1.02: two rosette leaves > 1 mm in length; 1.04: four rosette leaves > 1 mm in length. The boxes represent the time between the growth stages. Data are given as averages for 100 plants. **B)** Primary root length of plants grown vertically for 14 d. Data are given as averages \pm SE. n = 12, 20, 16, 17, and 9 for Col-0, *oxa2b-1*+35S:OXA2b, *oxa2b-1*+35S:OXA2b Δ 235, *oxa2b-2*+35S:OXA2b and *oxa2b-2*+35S:OXA2b Δ 235, respectively. Statistical significance based on Student's *t* test is indicated by * with a specified *p* value. **C)** Soil-based growth progression analysis. Developmental stages: 1.10: 10 rosette leaves > 1 mm in length; 5.10: First flower buds visible; 6.00: First flower open; 6.90: Flowering complete. Data are given as averages for 24 plants. **D)** Representative pictures of plants grown for the soil-based phenotyping. Pictures were taken after the indicated days of growth. **E)** Plant height measured at stage 6.90. Data are given as averages \pm SE for 24 plants. Statistical significance based on Student's *t* test is indicated by * with a specified *p* value.

35S:OXA2b plants (Figure 9E). Further phenotyping also demonstrated that the *35S:OXA2bΔ235* plants produced fewer seeds and did not germinate as efficiently as wild-type and *35S:OXA2b* plants (Supplemental Figure 2). As *OXA2b* has been shown to be essential for embryogenesis (87), the siliques of all the genotypes were also analyzed. The siliques of *35S:OXA2bΔ235* plants were consistently shorter and contained fewer embryos than wild-type siliques (Supplemental Figure 3). They also displayed a large number of aborted embryos, similar to the original findings for the T-DNA insertional lines (87), indicating that the complementation at an embryo level is incomplete. All the above phenotyping data indicated that *35S:OXA2bΔ235* plants displayed a severe growth retardation in comparison to those *35S:OXA2b* and wild-type plants.

7.2.3. Severe loss of complex IV in *35S:OXA2bΔ235* plant mitochondria

To determine the underlying cause for the slow growth phenotype in *35S:OXA2bΔ235* plants, mitochondria were isolated from all the lines and BN-PAGE was performed. With Coomassie staining, the supercomplex composed of complexes I and III, complex I, complex V, and the complex III dimer were visible in wild-type, as well as in all four complementation lines (Figure 10A). As Coomassie staining showed no obvious differences, *in gel* enzyme activity stains were performed. All the lines showed very similar complex I activities, but the supercomplex consisting of complexes I, III, and IV was missing in *35S:OXA2bΔ235* lines (Figure 10A). Upon staining for complex IV enzyme activity, the activity was barely detectable in the *35S:OXA2bΔ235* mitochondria while it was similar to the wild-type level in the *35S:OXA2b* mitochondria (Figure 10A).

In order to examine the abundance of the respiratory complexes, the mitochondrial complexes separated by BN-PAGE were used for immunoblot assays. Complex I, III, and V blots displayed no major difference in all four complementation lines with reference to wild-type (Figure 10B). Interestingly, there was more complex II in *35S:OXA2bΔ235* mitochondria compared with that in wild-type mitochondria (Figure 10B). For a more detailed analysis of complex IV abundance, immunoblotting for all three mitochondrial-encoded subunits of complex IV (COX1, 2, and 3) was performed. None of the blots

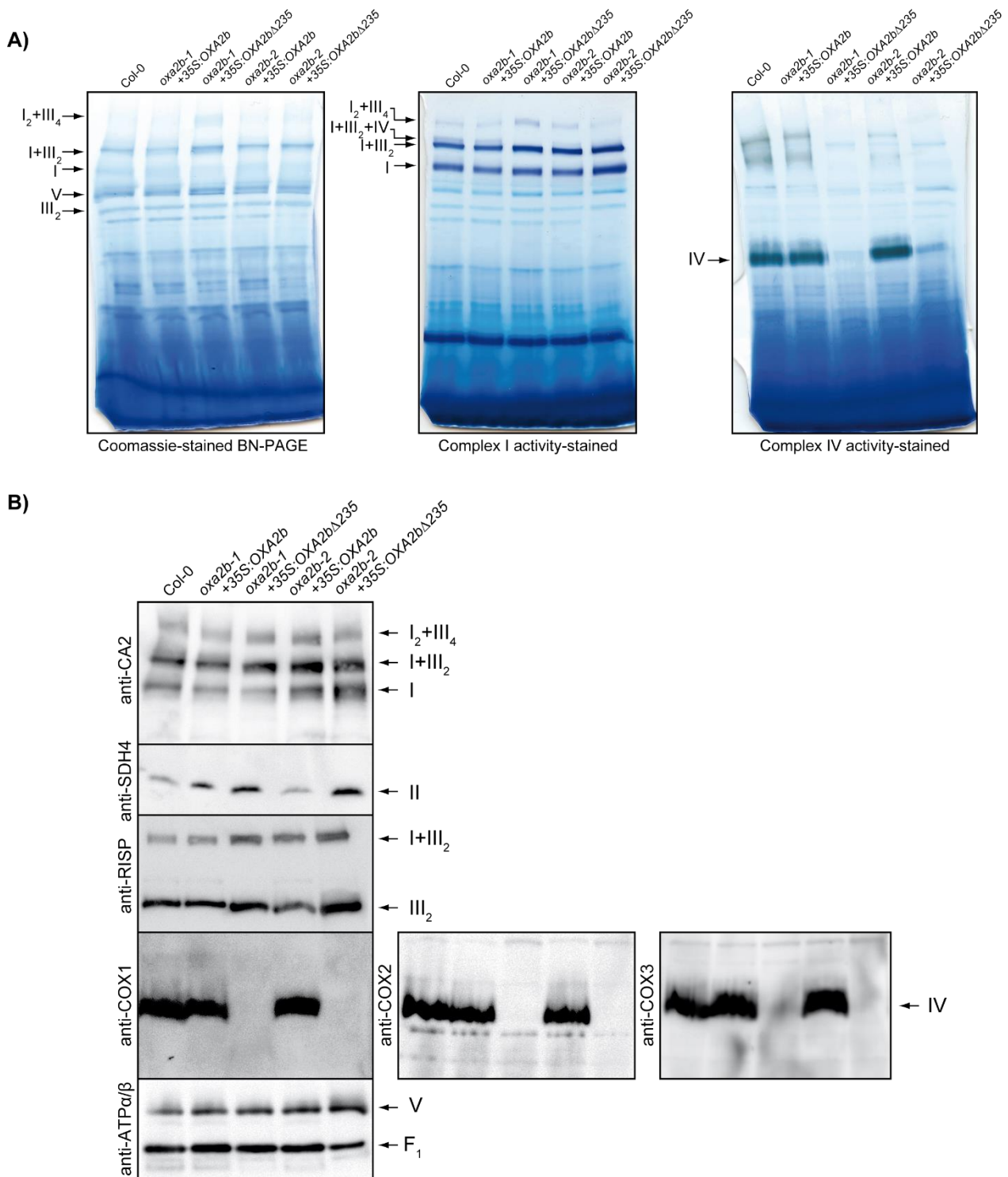


Figure 10. Analysis of mitochondrial complexes in *oxa2b* complementation plants. **A)** BN-PAGE analysis of mitochondrial complexes. The gel on the left was Coomassie-stained, the gel in the middle was stained for NADH dehydrogenase activity (Complex I), and the gel on the right was stained for cytochrome *c* oxidase activity (complex IV). Complexes and supercomplexes are indicated where appropriate. **B)** Immunoblot analysis of mitochondrial complexes after BN-PAGE with the following antibodies: carbonic anhydrase 2 (complex I), succinate dehydrogenase subunit 4 (complex II), RISP subunit of cytochrome *c* reductase (complex III), complex IV subunits 1, 2, and 3 (COX1, 2 and 3, complex IV), and subunits alpha and beta of ATP synthase (complex V). I, complex I; V, complex V; III₂, dimeric complex III; F₁, F₁ part of complex V; I+III₂, supercomplex composed of complex I and dimeric complex III; I₂+III₄, supercomplex composed of two complex I monomers and two copies of dimeric complex III; I+III₂+IV, super complex composed of complex I, dimeric complex III, and complex IV. CA2, carbonic anhydrase 2; SDH₄, succinate dehydrogenase subunit 4; RISP, a subunit of cytochrome *c* reductase; ATPα/β, subunits alpha and beta of ATP synthase.

detected complex IV in *35S:OXA2bΔ235* mitochondria, while the level of complex IV in *35S:OXA2b* mitochondria appeared to be identical to wild-type levels (Figure 10B). It is highly likely that severe complex IV deficiency resulted in the slow growth phenotype of *35S:OXA2bΔ235* plants (Figure 9).

7.2.4. Complex IV subunits are reduced in *35S:OXA2bΔ235* mitochondria

To further analyze the complex IV defect, mitochondrial proteins separated by SDS-PAGE were subjected to immunoblot analysis. Among the several electron transport chain proteins analyzed, the proteins from complexes I (CA2), III (RISP, QCR7, and CYC1), and V (ATP α/β) displayed no obvious differences between wild-type and all the four complementation lines (Figure 11A), in agreement with the complex activity and abundance results (Figure 10). An increase in the abundance of a complex II subunit, SDH4, was observed in *35S:OXA2bΔ235* mitochondria (Figure 11A), supporting increased complex II abundance (Figure 10B). Importantly, a complete absence of COX1 and COX3 and a severe reduction in the abundance of COX2 were observed in the mitochondria from *35S:OXA2bΔ235* plants (Figure 11A). The absence of complex IV and its catalytic core subunits was accompanied by a large increase in the abundance of AOX (Figures 10 and 11A), which is not surprising because AOX is generally up-regulated upon respiratory chain disruption in plants (125). Interestingly, no change in cytochrome *c* abundance was observed, although complex IV was barely detectable in *35S:OXA2bΔ235* mitochondria (Figures 10 and 11A).

Probing with antibodies against mitochondrial protein import components produced some interesting results. Although no obvious changes were observed for the proteins present in OM and IMS (Figure 11B), certain IM import components were up-regulated in *35S:OXA2bΔ235* mitochondria, namely TIM21, TIM50, TIM23, TIM22, and HSP70 (Figure 11B). This is most likely due to a general up-regulation of mitochondrial biogenesis similar to that observed with other respiratory chain mutants (126). In relation to other processes, the only other proteins to change in abundance were the S10 ribosomal protein and LETM1, both of which were upregulated in *35S:OXA2bΔ235* mitochondria (Figure 11C).

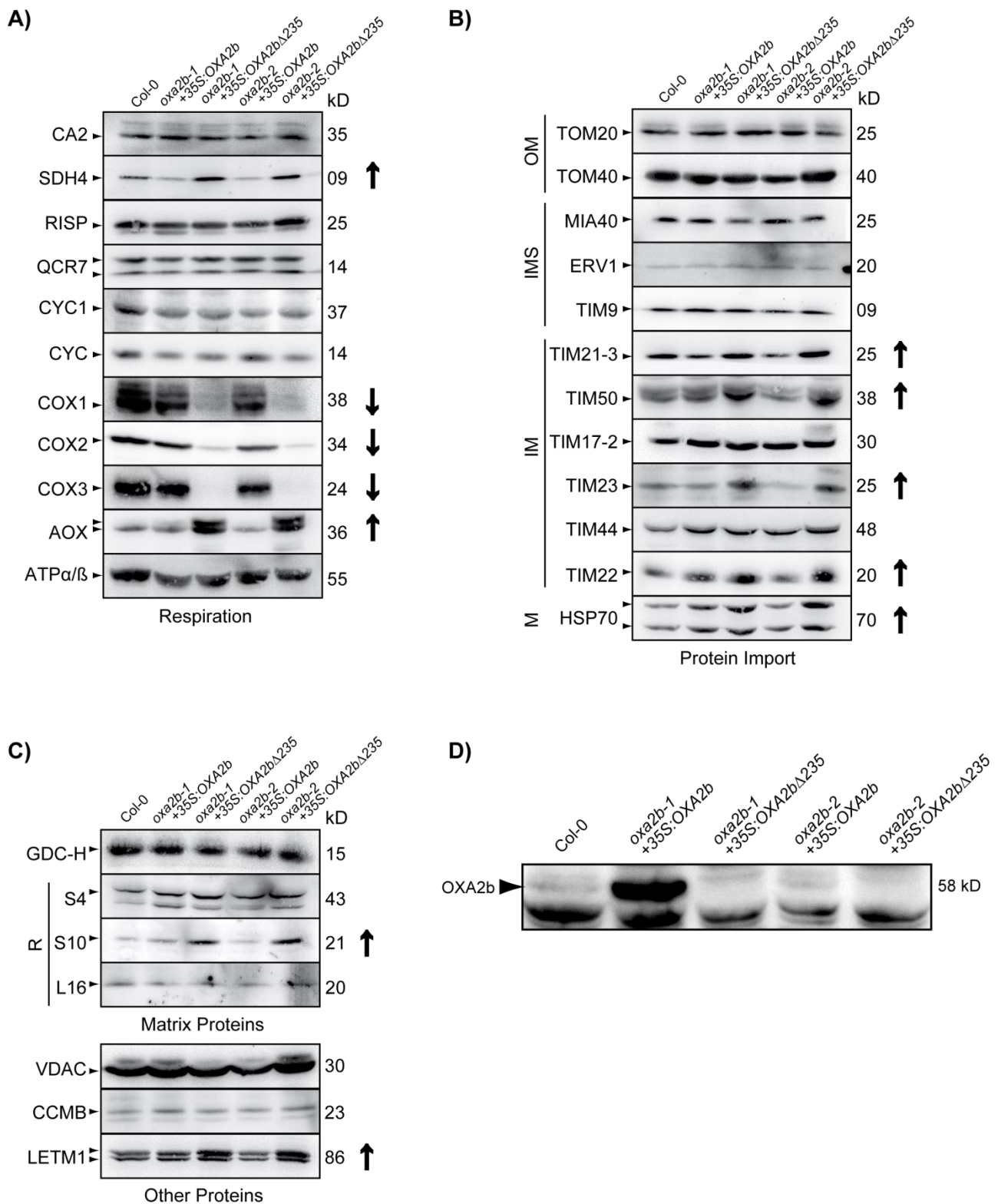


Figure 11. Analysis of mitochondrial proteins in *oxa2b* complementation plants. **A)** Immunoblot analysis of the indicated proteins involved in the respiratory chain. **B)** Immunoblot analysis of the indicated proteins involved in the import of proteins into mitochondria. **C)** Immunoblot analysis of a selection of other mitochondrial proteins. **D)** Immunoblot for OXA2b. As OXA2b is a low abundance protein, 100 mg mitochondrial protein was loaded per lane, instead of 30 mg. In all panels, the antibody used is on the left of the gel and the molecular mass in kD is located on the right. The correct band is indicated with a small arrow head on the left-hand side. In some cases, more than one isoform is detected. Bands not indicated are nonspecific reactions of the antibody. Where protein abundance is notably different, it is indicated on the right side by either an up (up-regulated) or a down (down-regulated) arrow. For full list of antibodies, see Supplemental Table 2. M, matrix; IM, inner membrane; R, ribosomal proteins.

As with the import components, these are most likely indirect effects due to increased mitochondrial biogenesis in response to a strong reduction in complex IV.

Immunoblots for OXA2b were performed using an antibody generated against the loop region between TMHs 1 and 2 (Figure 11D). Full-length OXA2b (58 kD) was readily visible in *35S:OXA2b* mitochondria, but hardly noticeable in wild-type and *35S:OXA2bΔ235* mitochondria, even when using more than 3-fold mitochondrial protein than was generally used for all other blots. OXA2b in wild-type plants appeared to be a very low abundant protein. The protein levels of OXA2b are in agreement with the corresponding transcript levels (Figures 11D and 8; Supplemental Figure. 1). The truncated version of OXA2b, which has a predicted molecular mass of 32 kD, was not found in either *35S:OXA2bΔ235-1* or *35S:OXA2bΔ235-2* mitochondria. However, this does not indicate their absence due to instability or degradation. As mentioned previously, OXA2b is essential for embryogenesis (87), and without complementation with at least the conserved insertase domain of OXA2b (*OXA2bΔ235*), it is not possible to obtain viable mutants. Moreover, the truncated version of OXA2b at the DNA and transcript level was clearly detected in the previous results (Figure 8, C and D). It is most likely that *35S:OXA2bΔ235* mitochondria had very low amounts of truncated OXA2b, probably much less than the amount of full-length protein found in wild-type and *35S:OXA2b* mitochondria.

7.2.5. COX2 membrane insertion is affected in *35S:OXA2bΔ235* mitochondria

To check the synthesis and assembly of mitochondrial-encoded proteins, *in organello* translation reactions were carried out using isolated mitochondria. Since the corresponding *35S:OXA2b* and *35S:OXA2bΔ235* lines of *oxa2b-1* and *oxa2b-2* behaved similarly in all the previous experiments and difficult nature of the mitochondrial experiments, only with the complementation lines of *oxa2b-1* and wild-type were chosen. Radiolabelled mitochondrial translation products were observed after 10, 30, and 60 min of translation. For wild-type and the *35S:OXA2b* plants, the mitochondrial translation rates were identical as determined by similar intensities of the translated protein bands (Figure 12A). Although the translation rates of mitochondrial proteins were reduced in

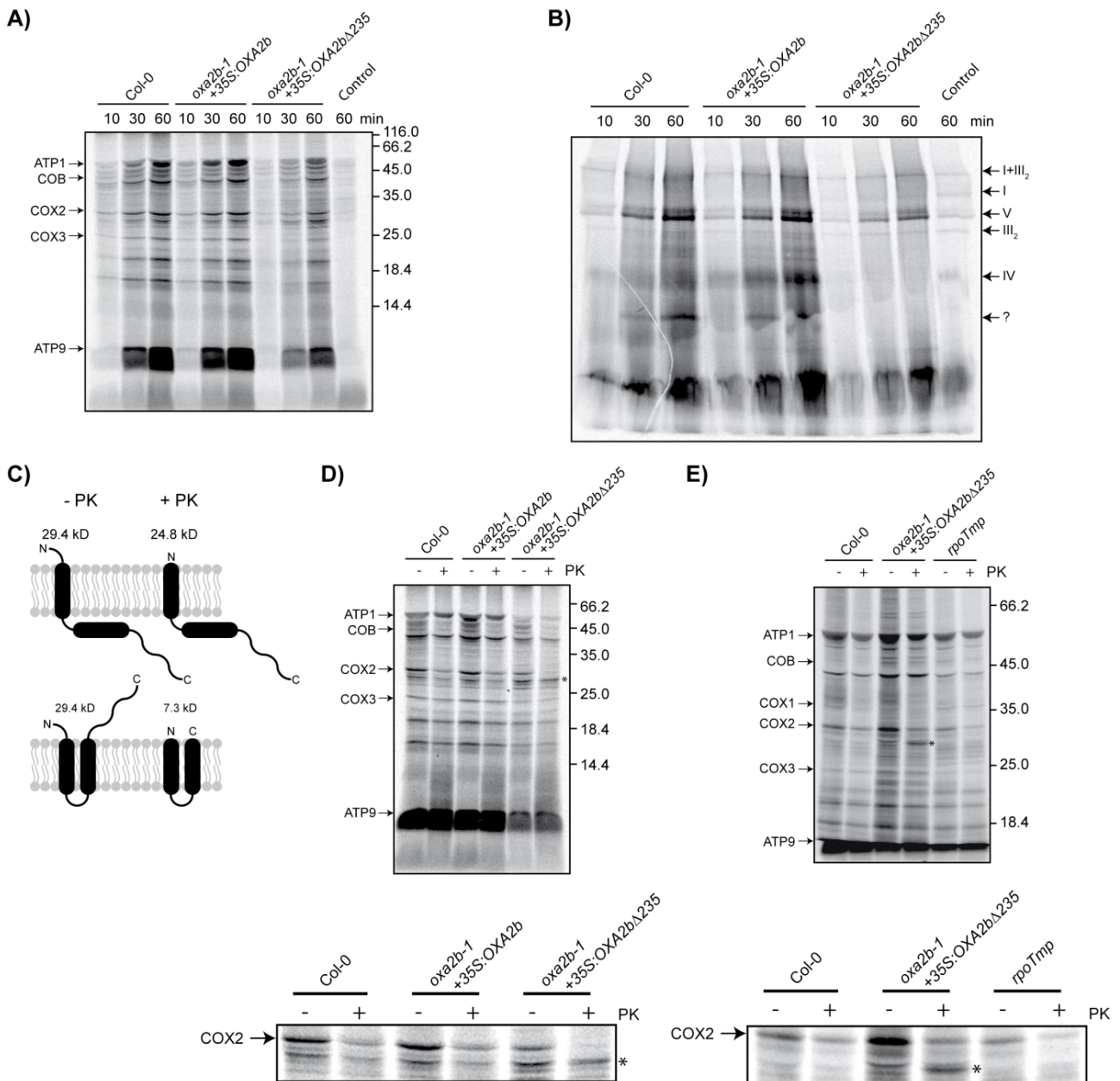


Figure 12. Translation and assembly of mitochondrial-encoded proteins in *oxa2b-1* complementation plants. **A)** Autoradiogram of proteins synthesized *in organello* for 10, 30, and 60 min in the mitochondria isolated from the indicated plants after separation by SDS-PAGE. The proteins identified in Supplemental Figure 4 are indicated on the left. The lane labeled “control” is a bacterial contamination control where sodium acetate was used as an energy source. The large smear at the bottom of the gel is ATP9. Due to its high hydrophobicity, ATP9 runs aberrantly on SDS gels. The molecular weights of protein marker in kD are shown on the right. **B)** The same treatment as in (A), but separated by BN-PAGE to show the incorporation of newly translated proteins into complexes. The respective respiratory complexes are indicated on the right. The question mark indicates a complex of unknown origin. **C)** Potential topologies of COX2 in mitoplasts before and after PK treatment. Before PK treatment, both forms of COX2 would have identical sizes. After PK treatment, if COX2 is partially inserted and only the N-terminus is in the IMS, it has a predicted size of 24.8 kD, whereas if COX2 is fully inserted and has both the N- and C- termini in the IMS, it has a predicted size of 7.3 kD. **D)** Autoradiogram of a 60 min *in organello* translation reaction that was split in half, with one half mock-treated (-) and the other half PK-treated (+) after preparing mitoplasts. The major proteins are indicated on the left. The asterisk indicates a band that is produced only with PK-treated mitoplasts of 35S:OXA2bΔ235. The full gel is shown on the top and the region containing COX2 is enlarged below it. **E)** The same treatments as in (D), except that another complex IV mutant (*rpoTmp*) was included for comparison. Again, the full gel is shown on the top and the region containing COX2 is enlarged below it.

35S:*OXA2b*Δ235 mitochondria, all the major mitochondrial translation products that we identified in wild-type (Figure 12A; Supplemental Figure 4) were still detected. This means that the 35S:*OXA2b*Δ235 mitochondria were still able to synthesize all the three mitochondrial-encoded COX proteins, although at a slower rate. Moreover, all the other respiratory complexes accumulate at wild-type levels despite the observed reduction in the rate of protein synthesis (Figures 10B and 12A). Hence, complex IV deficiency in 35S:*OXA2b*Δ235 plants may not be due to a problem in mitochondrial protein synthesis.

Can the 35S:*OXA2b*Δ235 plants assemble the mitochondrial-encoded complex IV subunits after their synthesis? To answer this question, the same *in organello* translation reactions from above were separated by BN-PAGE. For wild-type and 35S:*OXA2b* mitochondria, the radiolabeled proteins were efficiently assembled into respiratory complexes (Figure 12B). Although complex V was assembled at the highest rate in both wild-type and 35S:*OXA2b* mitochondria, the 35S:*OXA2b* mitochondria assembled complex IV faster than wild-type mitochondria (Figure 12B). This could be due to over-expression of *OXA2b* in the 35S:*OXA2b*Δ235 in comparison to the wild-type level (Figure 8D; Supplemental Figure 1). As for the 35S:*OXA2b*Δ235 mitochondria, the overall signal was less, most likely due to a reduced translation rate (Figure 12, A and B). Nevertheless, the assembly of complexes I, V, and III as well as the supercomplex I+III₂ was observed whereas complex IV assembly was not detected (Figure 12B). An unknown complex labelled with a question mark also failed to accumulate in the 35S:*OXA2b*Δ235 mitochondria (Figure 12B). It is possibly either a subcomplex or assembly intermediate of complex IV. The contents of this complex could not be determined, despite several attempts. However, the above results clearly indicated that the mitochondrial-encoded subunits of complex IV can be synthesised, but not assembled into a complex, in the 35S:*OXA2b*Δ235 plant mitochondria.

In yeast and human mitochondria, Cox18 inserts the second TMH of Cox2 into the IM and translocates the soluble C-terminus into the IMS (29, 61). As *OXA2b* is closely related to Cox18, COX2 is its most likely substrate (Figure 4). To confirm this, mitochondrial translation reactions were performed for 60 min, after which the mitochondrial OM was ruptured by osmotic shock to generate mitoplasts. Then the reactions were split in half

and one half was treated with PK. The rationale here is that if COX2 is fully inserted with its C-terminus in the IMS, PK treatment should produce a 7.3-kD protein (Figure 12C). But if only the first TMH is inserted and the C-terminus remains in the matrix, then after PK treatment, a 24.8-kD band should be produced (Fig. 12C). When wild-type and the *35S:OXA2b* plant mitochondrial translations were treated with PK, no obvious differences were observed (Figure 12D). In fact, most of the COX2 band was degraded, indicating correct insertion across the IM, while the remaining COX2 was most likely located within complex IV and thus protected from protease treatment (Figure 12D). The predicted 7.3-kD band, however, is not visible, presumably due to the presence of the large band representing ATP9 near the bottom of the gel (Figure 12D). With the *35S:OXA2bΔ235* plant mitochondria, after PK treatment, no protected COX2 was visible (Figure 12D). This again suggests that complex IV was not assembled in *35S:OXA2bΔ235* mitochondria.

Interestingly, after PK treatment of *35S:OXA2bΔ235* plant mitoplasts, a band appeared, below where COX2 normally runs, with an intensity similar to PK-untreated COX2 band (Figure 12D). This band was not found with PK-treated wild-type and *35S:OXA2b* plant mitoplasts. It is very likely that this band, with an apparent molecular mass slightly higher than the predicted value of 24.8 kD, represented a partially membrane-inserted COX2 with the C-terminus located in the matrix. All other proteins were ruled out based on the following reasons: First, proteins belonging to other respiratory complexes are unlikely because only complex IV is affected. Second, COX1 is not translated at a very high level and in most cases, it cannot be readily identified; therefore, it is unlikely to produce a strong band after PK treatment. Third, since COX3 full-length protein was already found lower than the PK-generated band, it cannot be COX3. Therefore, the extra band generated upon PK treatment of *35S:OXA2bΔ235* plant mitoplasts is most likely a partially inserted COX2 whose N-terminus, exposed in the IMS, was digested.

To check if this partially inserted COX2 band is not observed generally in other complex-IV deficiencies, PK digestions of *in organello* translation reactions were also performed on a previously characterized complex IV mutant, *rpoTmp*, which is missing the Phage type RNA polymerase specifically required for COX1 transcription (127). Lack of COX1

transcript leads to a reduction in complex IV and these mutants have a phenotype similar to that observed with *35S:OXA2bΔ235* plants (127) (Figure 9D). However, the smaller COX2 band was not observed when *in organello* translation reactions of *rpoTmp* mutant mitochondria were treated with PK (Figure 12E). This means that COX2 was inserted into the IM in the correct orientation in the *rpoTmp* mutant, with its C-terminus in the IMS and was not causing the complex IV reduction. The partially inserted COX2 band appeared only with *35S:OXA2bΔ235* mitoplasts. The *35S:OXA2bΔ235* sample was overloaded in this experiment to try and reach the same band intensity as wild-type and for a better visualization of the COX2 PK band. All other bands remained unchanged upon PK treatment, indicating that they are either matrix-located or are fully inserted into the membrane without any substantial IMS-exposed regions. It can therefore be concluded that OXA2b is required for membrane insertion of the second TMH and translocation of the C-terminus of COX2 into the IMS.

7.2.6. OXA2b TPR domain directly binds the nascent COX2 C-terminus

To confirm that the TPR domain of OXA2b is required for the correct membrane topology of COX2, pull-down assays were performed using recombinant expressed and purified OXA2b TPR domain fused to GST (GST-OXA2bTPR). Isolated wild-type mitochondria were *in organello* translated to generate newly synthesized mitochondrial-encoded proteins, lysed using Triton X-100 and incubated with either GST-OXA2bTPR or GST control, that were prebound to glutathione beads. After elution, COX2 was found to be pulled-down by GST-OXA2bTPR (Figure 13A). The slight shift in its running behavior, as compared to the control lysate where mitochondria were directly lysed in SDS-PAGE loading buffer, is believed to be due to the presence of Triton X-100. As expected, GST alone does not appear to interact with any of the known mitochondrial translations. The bait proteins, GST (26 kD) and GST-OXA2bTPR (53 kD), have non-specifically bound to some radioactive species in the extract that appear as curved bands in the corresponding lanes. The other two mitochondrial-encoded complex IV subunits, COX1 or COX3, whose steady-state levels were severely reduced (Figure 11A), could not be detected in the

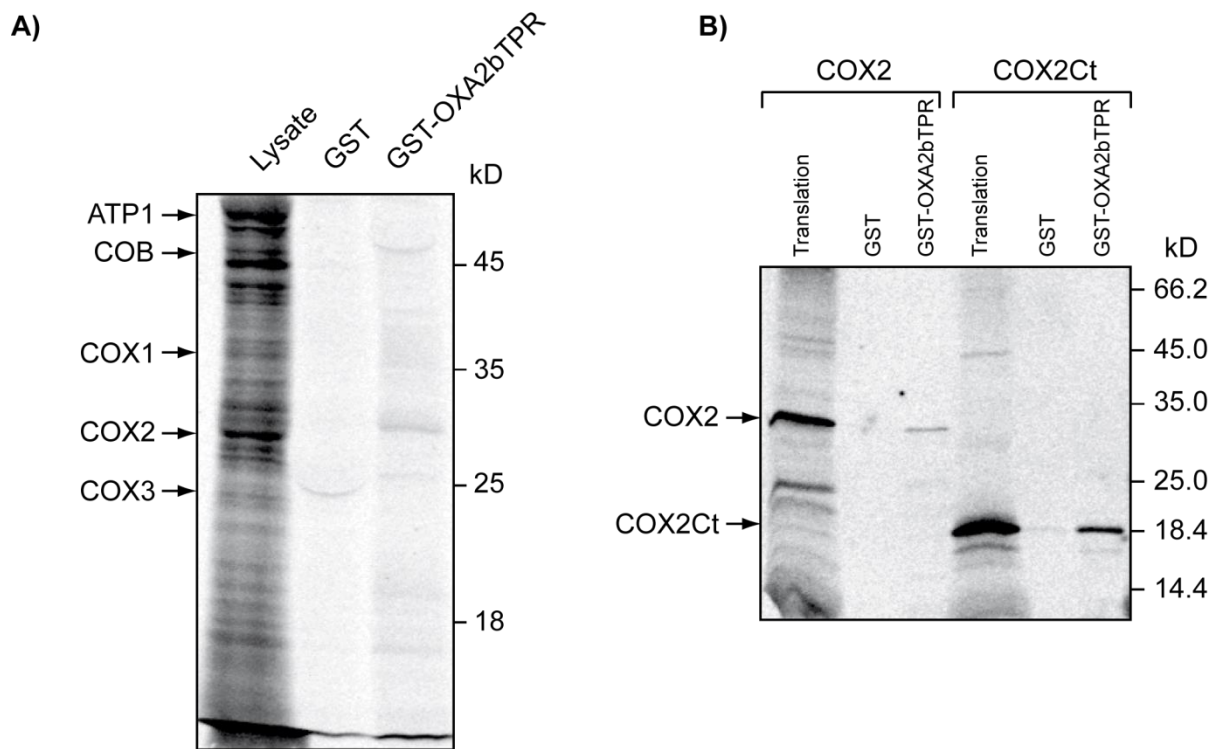


Figure 13. The TPR domain of OXA2b interacts with newly synthesized COX2. **A)** Mitochondria isolated from Col-0 plants were used for *in organello* translation reactions, lysed with Triton X-100 and incubated with recombinant GST or GST fused to OXA2bTPR, prebound to glutathione beads. After washing, the bound material was eluted and proteins were analyzed by SDS-PAGE and autoradiography was recorded. Lysate (8.3% of mitochondrial lysate) was used for binding. Mitochondrial translation products are shown with arrows on the left and molecular weight markers are indicated on the right. **B)** *In vitro* translated COX2 (34 kD) and its C-terminus alone, COX2Ct (17 kD), were incubated with recombinant GST or GST fused to OXA2bTPR, prebound to glutathione beads. After washing, the bound material was eluted, proteins were analyzed by SDS-PAGE, and autoradiography was recorded. In the lane labelled as 'Translation', 20% of the translation reaction used for binding was loaded for reference.

GST-OXA2bTPR pull-down fraction (Figure 13A). Hence the TPR domain of OXA2b specifically interacts with nascent COX2.

Because the TPR domain of OXA2b appeared to be involved in the insertion of the COX2 C-terminus (Figure 12) and also interacted with nascent COX2 (Figure 13A), it was also tested if it interacted specifically with the C-terminus of COX2. For this purpose, GST-OXA2bTPR and GST control were used to pull-down *in vitro* synthesized COX2 and COX2 C-terminus. Even though OXA2bTPR was found to interact with both COX2 and COX2 C-terminus, the interaction with COX2 C-terminus appeared to be more prominent (Figure 13B).

7.3. Role of OXA2a and significance its TPR domain

7.3.1. Partial complementation rescued OXA2a knockout embryo-lethality

Two independent T-DNA insertion lines, *oxa2a-1* (SALK_048398) and *oxa2a-2* (GABI_492F05) whose *OXA2a* genomic sequence was disrupted in intron 8 and intron 1, respectively were used to study the role of OXA2a in plant mitochondrial biogenesis (Figure 14A). Due to essential nature of the gene (87), genotyping results of both the lines displayed heterozygosity but no homozygosity of the T-DNA insert. Therefore, two strategies were used to generate viable mutants. In the first strategy, *OXA2a* was placed under the control of the *ABI3* promoter so that homozygous mutant embryos can be produced due to the complementation construct being expressed during embryogenesis. Thereafter, during seedling development, the *ABI3* promoter becomes inactive and *OXA2a* should no longer be expressed (128). *oxa2a-1* was complemented with *OXA2a* cDNA under the control of *ABI3* promoter (*ABI3p:OXA2a*) (Figure 14B). In order to rule out random non-specific effects, two such independent complementation lines were used for further experimental analyses. In the second strategy, *oxa2a-2* was complemented with the conserved OXA2a insertase domain, but lacking the C-terminal TPR region. The construct contained truncated *OXA2a* cDNA, which encodes only the first 280 amino acids under the control of 35S promoter (*35Sp:OXA2aΔ245*) (Figure 14B). As a positive control for this complementation, another construct containing the full-length *OXA2a* cDNA encoding all 525 amino acids (*35Sp:OXA2a*), was employed (Figure 14B). Thus, four different complementation plant lines were generated: *oxa2a-1+ABI3p:OXA2a-1*, *oxa2a-1+ABI3p:OXA2a-2*, *oxa2a-2+35Sp:OXA2a* and *oxa2a-2+35Sp:OXA2aΔ245*. For the sake of simplicity, these lines are hereafter called as *ABI3p:OXA2a-1*, *ABI3p:OXA2a-2*, *35Sp:OXA2a* and *35Sp:OXA2aΔ245* respectively.

All the transformed plants of *OXA2a* were genotyped for the presence of the respective T-DNA insertion and the corresponding complementation construct used. They were all found to be homozygous for the specific T-DNA insertion as evidenced by the presence of a PCR product using the corresponding LB and RP primers and the absence of a PCR product meant to amplify the wild-type genomic DNA (LP+RP) (Figure 14C). To confirm the presence of the *ABI3* promoter upstream of *OXA2a*, a forward primer (ApF) that binds

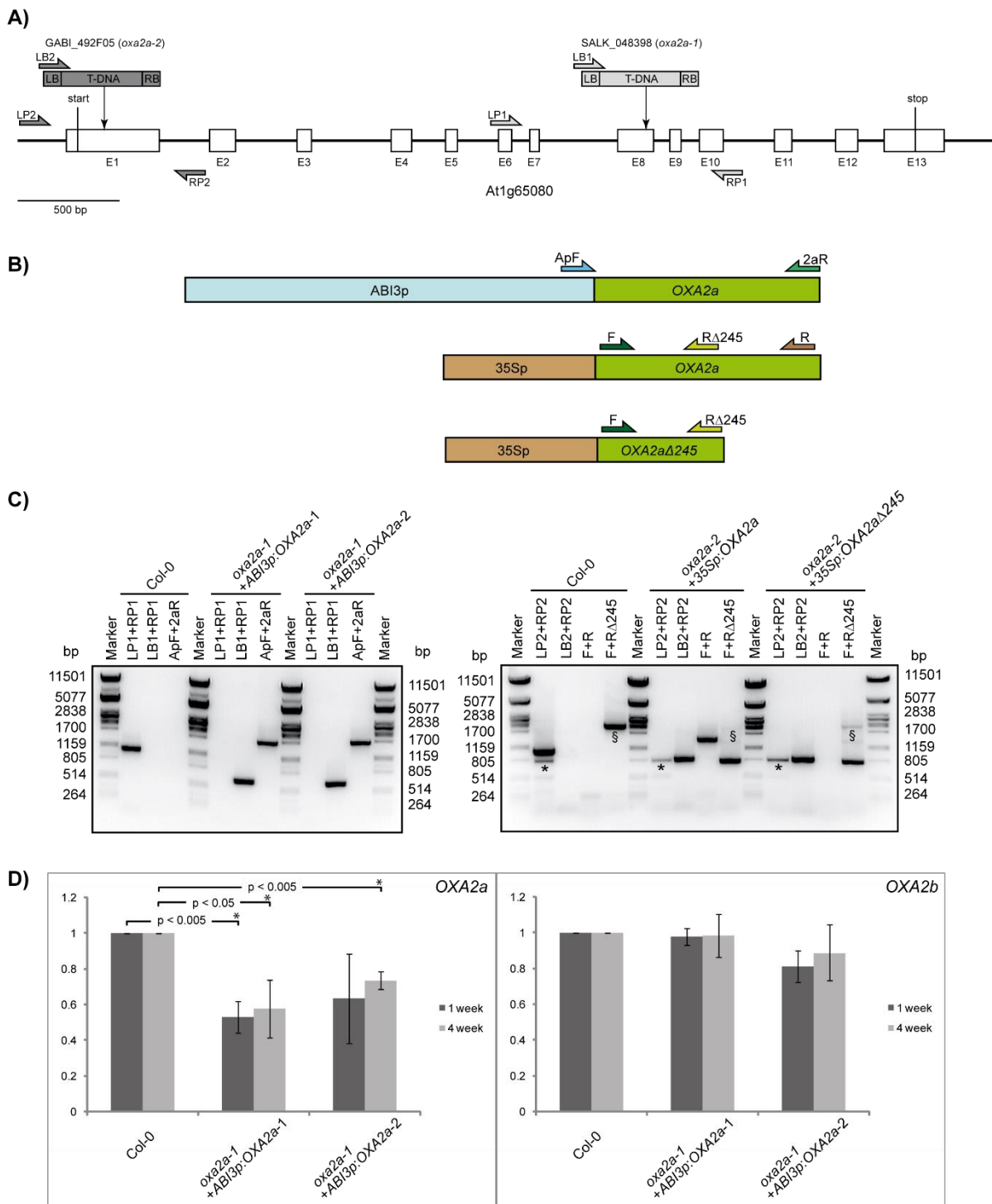


Figure 14. DNA and RNA analyses of *oxa2a* partial complementation plants. **A)** Diagram of the genomic region encoding *OXA2a*, drawn to scale. The locations of T-DNA insertions and primer binding sites are indicated. Boxes labelled E1 to E13 signify exons. Spaces between adjacent exons correspond to introns. **B)** Diagram depicting the constructs inserted into the genome for partial complementation of *oxa2a-1* and *oxa2a-2*. The primers used to confirm the insertion of the constructs: ApF, 2aR, F, RA245 and R, are shown. **C)** Genotyping PCR analysis. All lines were genotyped first for the correct T-DNA insertion and then for presence of the inserted construct. The primer binding positions are indicated in A and B. The sizes of the PCR products are as follows: (LP1-RP1) = 1077 bp, (LB1-RP1) = ~700 bp, (ApF-2aR) = 1691 bp, (LP2-RP2) = 1082 bp, (LB2-RP2) = ~800 bp, (F-R) = 1471 bp and (F-R245) = 798 bp (A PCR product of 2104 bp, indicated by §, is formed due to amplification of *OXA2a* genomic region instead of the cDNA insert). * indicates a non-specific PCR product. **D)** RT-qPCR analysis. Relative transcript abundances of *OXA2a* and *OXA2b* were calculated with reference to Actin transcript abundance. Data are presented as averages \pm SE of three independent biological replicates taken from leaves of 1- and 2-week-old plants. Statistical significance based on Student's *t* test is indicated by * with a specified *p* value.

within the *ABI3* promoter and a reverse primer (2aR) that binds *OXA2a* cDNA were used (Figure 14B). Both *ABI3p:OXA2a* lines produced the expected PCR product with these primers. To indicate the presence or absence of the *OXA2a* TPR domain, a single forward primer and different reverse primers were used: F+R can only amplify the full-length cDNA while F+R Δ 245 can amplify the truncated as well as the full-length cDNA (Figure 14B). The primer set, F+R amplified the full-length cDNA present in *35Sp:OXA2a* plants only whereas primer set, F+R Δ 245 amplified the cDNA corresponding to the insertase domain of *OXA2a*, which is present in both *35Sp:OXA2a* and *35Sp:OXA2a Δ 245* plants (Figure 14C). Therefore, the endogenous *OXA2a* gene was knocked out successfully in *oxa2a-1* and *-2* due to complementation with developmentally regulated *OXA2a* and with constitutively expressed *OXA2a* and *OXA2a Δ 245* respectively.

RT-qPCR was performed to monitor the expression levels of *OXA2a* in 1- and 4-week-old plants of *ABI3p:OXA2a* plants. *OXA2a* transcript levels of both the lines were significantly reduced as compared to the wild-type transcript levels irrespective of the plant age (Figure 14D). On the other hand, the endogenous transcript levels of the closely related homolog, *OXA2b* remained unchanged (Figure 14D). Thus, the transcript analysis further confirms the successful complementation of genomic *OXA2a* by complementation with *OXA2a* cDNA under the control of *ABI3* promoter.

7.3.2. Growth retardation of *ABI3p:OXA2a* plants

Quantitative phenotyping of all the partial complementation lines was performed based on the method of (114). Plate-based phenotyping showed that *ABI3p:OXA2a* plants grew very similar to wild-type plants until the two rosette leaves stage, but were significantly slower to reach the four rosette leaves stage (1.04) (Figure 15A). This could be attributed to the *ABI3* promoter still being active during germination (129). Growth on vertical MS plates showed that the roots of *ABI3p:OXA2a-2* plants grew significantly slower in comparison to the roots of wild-type plants (Figure 15B). Slower root growth has been observed in several other *Arabidopsis* mutants with altered mitochondrial biogenesis (123, 124).

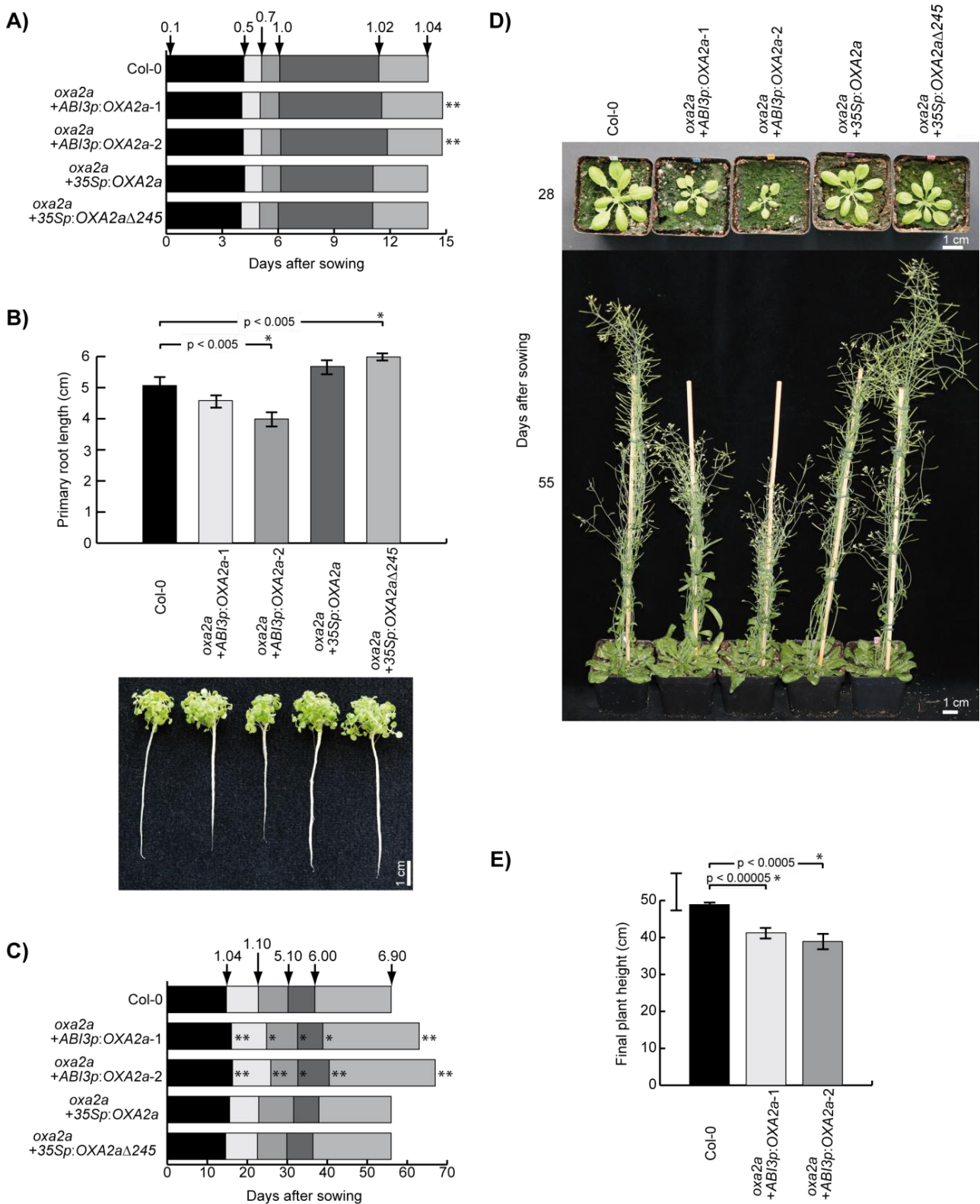


Figure 15. Phenotypes of *oxa2a* partial complementation plants. **A)** Plate-based growth progression analysis. Arrows indicate the time taken by wild-type plants to reach the developmental stages: 0.1: Imbibition; 0.5: Radicle emergence; 0.7: Hypocotyl and cotyledon emergence; 1.0: Cotyledons fully open; 1.02: two rosette leaves > 1 mm in length; 1.04: four rosette leaves > 1 mm in length. Boxes represent time between the growth stages. Data are given as averages for 60 plants. Statistical significance with a p value < 0.00005 based on Student's t test with reference to Col-0 is indicated by **. **B)** Primary root lengths of plants grown vertically for 14 days. Data are given as averages \pm SE. $n = 30, 36, 26, 34$ and 33 for Col-0, *oxa2a+ABI3p:OXA2a-1*, *oxa2a+ABI3p:OXA2a-2*, *oxa2a+35Sp:OXA2a* and *oxa2a+35Sp:OXA2a Δ 245*, respectively. Statistical significance based on Student's t test is indicated by * and a

specified *p* value. **C)** Soil-based growth progression analysis. Developmental stages: 1.10: 10 rosette leaves > 1 mm in length; 5.10: First flower buds visible; 6.00: First flower open; 6.90: Flowering complete. Data are given as averages for 24 plants. Statistical significance with a *p* value < 0.00005 or < 0.0005 based on Student's *t* test with reference to Col-0 is indicated by ** or * respectively. **D)** Representative pictures of plants grown for the soil-based phenotyping. Pictures were taken after the indicated days of growth. **E)** Plant height measured at stage 6.90. Data are given as averages ± SE for 24 plants. Statistical significance based on Student's *t* test is indicated by * and a specified *p* value.

Starting from the four rosette leaves stage (1.04), the slow growth phenotype of *ABI3p:OXA2a* plants continued on to all the later developmental stages in soil-based phenotyping (Figure 15A, C, D and E). They were slower to reach all major growth milestones and took on an average about 10 days longer to complete their life cycle (Figure 15C). The slow growth phenotype of *ABI3p:OXA2a* plants was clearly evident during phenotyping (Figure 15D). These plants also failed to reach the same height attained by wild-type plants (Figure 15E). Furthermore, the siliques of *ABI3p:OXA2a* plants were consistently shorter and contained fewer embryos than wild-type siliques (Supplemental Figure 5). A large number of aborted embryos were found similar to those found in siliques of the original T-DNA insertion lines that proved the essential nature of *OXA2a* during embryogenesis (87), which indicates that *ABI3p:OXA2a* partial complementation at the embryo level is incomplete. All the above phenotyping data collectively implies that a normal level of *OXA2a* is very important during all stages of plant growth and development.

On the other hand, the phenotypes of *35Sp:OXA2a* as well as *35Sp:OXA2aΔ245* plants were similar to wild-type plants during all the growth stages analysed (Figure 15A-D and Supplemental Figure 5). The only exception being, significantly faster root growth of *35Sp:OXA2aΔ245* plants. The roots of *35Sp:OXA2a* plants also appeared to be longer, although not statistically significant. Therefore, it is likely that the strong promoter activity of *35S* promoter caused an overexpression of *OXA2a* resulting in faster root growth in these plants. The overall normal phenotype of *35Sp:OXA2aΔ245* plants indicates that the TPR domain of *OXA2a* may not be very important for its functionality.

7.3.3. Complex III is reduced in *ABI3p:OXA2a* plants

In order to determine the underlying cause for the slow growth phenotype of *ABI3p:OXA2a* plants, mitochondria were isolated and the respiratory complexes separated by BN-PAGE were examined. In the *ABI3p:OXA2a* plants, the supercomplex composed of complexes I and III and the complex III dimer were reduced whereas complexes I and V

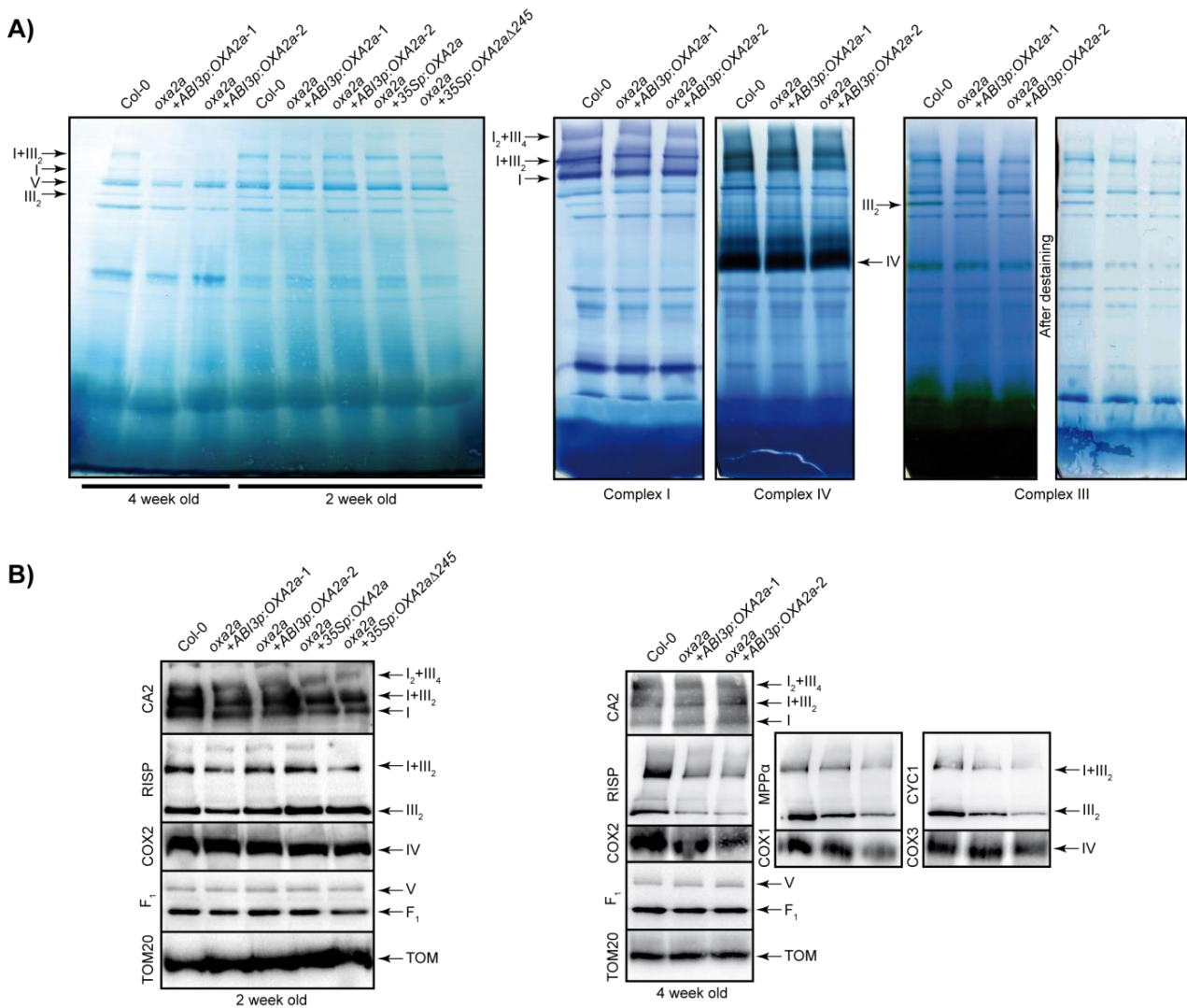


Figure 16. Analysis of mitochondrial complexes in *oxa2a* partial complementation plants. **A)** BN-PAGE analysis of mitochondrial complexes. On the left, coomassie stained complexes of mitochondria isolated from 2- and 4-week-old plants are represented on a PVDF membrane. Adjacently, gels containing 4-week-old samples were stained for NADH dehydrogenase (Complex I) activity, cytochrome *c* oxidase (complex IV) activity and ubiquinol-cytochrome *c* oxidoreductase (complex III) activity which was subsequently destained for better visibility. Complexes and supercomplexes are indicated where appropriate. **B)** Immuno-blot analysis of mitochondrial complexes of 2- and 4-week-old plants after BN-PAGE using the antibodies against: carbonic anhydrase 2 (CA2, complex I), three complex III subunits: mitochondrial-processing peptidase subunit α (MPP α), cytochrome c_1 (CYC1) and Rieske iron-sulfur protein (RISP), complex IV subunits 1, 2 and 3 (COX1, 2 and 3, complex IV), F₁ part of ATP synthase (F₁, complex V) and TOM20 (TOM complex). I – complex I, V – complex V, III₂ – dimeric complex III, I+III₂ – supercomplex composed of complex I and dimeric complex III, I₂+III₄ – supercomplex composed of two complex I monomers and two copies of dimeric complex III.

appeared similar to the wild-type levels (Figure 16A). Moreover, the reduction in complex III was noticeably more pronounced in the 4-week-old plants than that in the 2-week-old plants. In order to confirm the complex III reduction evident after BN-PAGE, in-gel enzyme activity stains were performed using 4-week-old plant mitochondria. While there was no significant difference in the enzyme activities of complexes I and IV, complex III enzyme activity was indeed severely reduced in *ABI3p:OXA2a* plants (Figure 16A). The complex III deficiency most likely accounts for the slow growth phenotype of *ABI3p:OXA2a* plants.

The abundance of the respiratory chain complexes in both 2- and 4-week-old plants was verified by immuno-blot assays of the mitochondrial complexes separated by BN-PAGE. In the 2-week-old *ABI3p:OXA2a* plants, complex III was only slightly reduced (Figure 16B). However, in the 4-week-old *ABI3p:OXA2a* plants, there was more severe reduction in complex III in all the blots probed for its different subunits, MPP α , CYC1 and RISP (Figure 16B). In both 2- and 4-week-old *ABI3p:OXA2a* plant mitochondria, the abundances of complex I and its supercomplexes, complex V and the TOM complex were very similar to the wild-type levels (Figure 16B). There was no major difference in complex IV levels of both the *ABI3p:OXA2a* lines in 2-week-old samples probed for COX2 as well as in 4-week-old samples probed for COX1, COX2 and COX3 (Figure 16B). Moreover, complex IV enzyme activity of both the *ABI3p:OXA2a* lines in 4-week-old samples was also similar to the wild-type enzyme activity, as mentioned above. On the other hand, corresponding to the lack of an obvious growth phenotype, the *35Sp:OXA2a Δ 245* plants did not display any change in the abundance of respiratory complexes (Figure 16A and B).

An immunoblot against COB after BN-PAGE not only showed reduced complex III, but also an accumulation of a lower molecular weight complex in *ABI3p:OXA2a* plants upon longer exposure (Figure 17A). It is very likely that this lower molecular weight complex is an assembly intermediate of complex III which accumulated in *ABI3p:OXA2a* plants due to slower rate of complex III biogenesis. In order to study the assembly intermediate further, immunoblots against various complex III subunits were performed following 2D

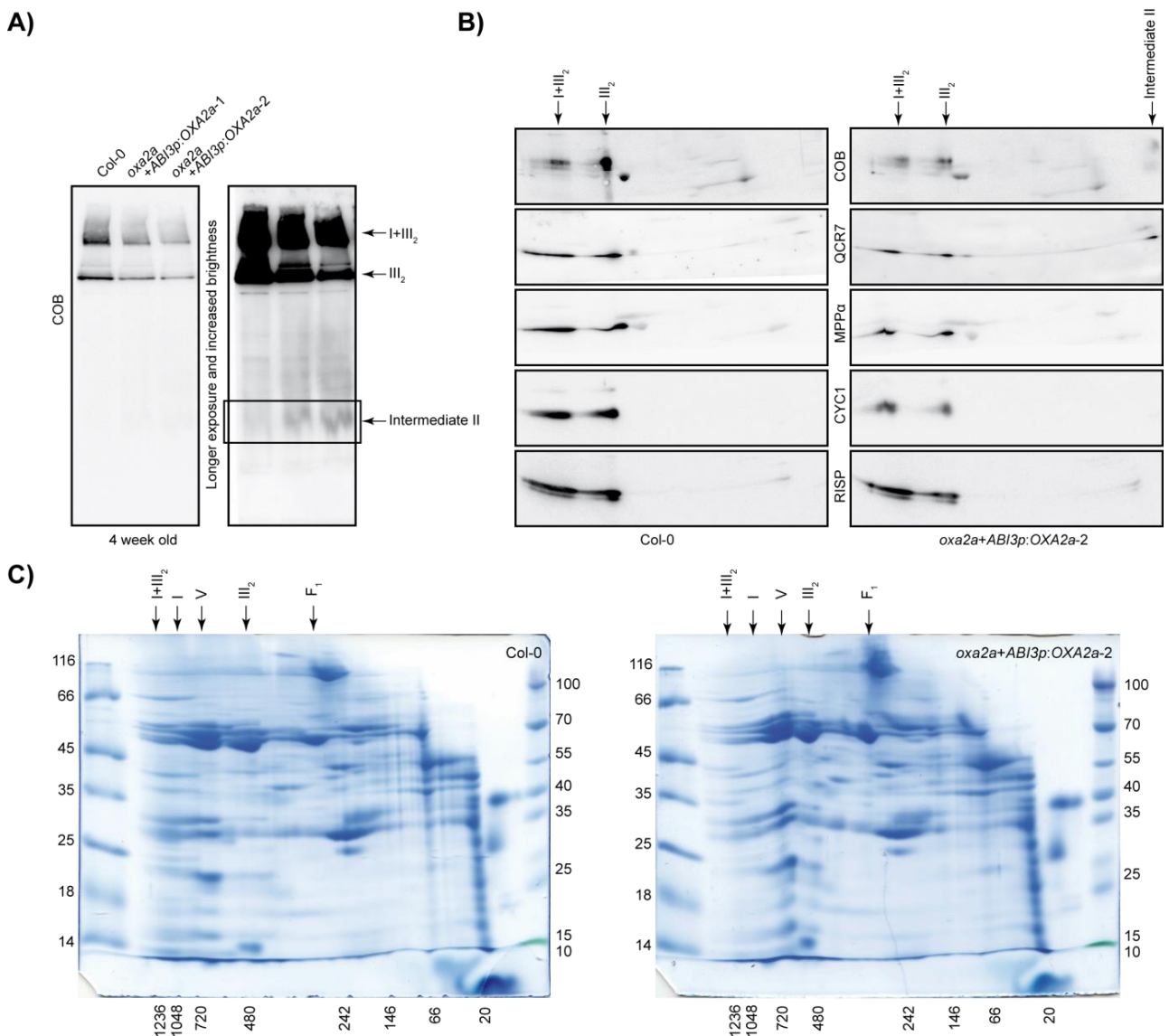


Figure 17. Analysis of complex III in *ABI3p:OXA2a* plants. **A)** Immuno-blot analysis of complex III-containing supercomplexes separated by BN-PAGE using the antibody against cytochrome *b* (COB). Upon longer exposure of the blot, a putative assembly intermediate of complex III (Intermediate II) was detected exclusively in the complementation plants. **B)** Immuno-blot analysis of the specified complex III subunits after 2D-BN/SDS-PAGE of mitochondria from 4-week-old plants. **C)** 2D-BN/SDS-PAGE of mitochondria from 4-week-old plants followed by colloidal Coomassie staining. Molecular weight markers of 1st and 2nd dimension are indicated below and on either side of gels respectively. I – complex I, V – complex V, III₂ – dimeric complex III, F₁ – F₁ part of complex V, I+III₂ – supercomplex composed of complex I and dimeric complex III, Intermediate II – an assembly intermediate of complex III.

BN/SDS-PAGE. All the subunits tested, COB, QCR7, MPP α , CYC1 and RISP were detected in complex III and the supercomplex comprising complex I and complex III (Figure 17B). Additionally, COB and QCR7 appeared to be present in the same assembly intermediate in *ABI3p:OXA2a-2* plants, but not in wild-type plants (Figure 17B). During complex III assembly in yeast, COB and QCR7 and QCR8 assemble into intermediate II, after which all the remaining subunits are recruited (19, 130). The accumulation of COB

and QCR7 in an assembly intermediate which is most likely intermediate II in *ABI3p:OXA2a-2* plants suggests that the process of complex III assembly in plants might be similar to that observed in yeast, at least during the early stages (Figure 17B). Coomassie staining of 2D BN/SDS-PAGE did not reveal any obvious deviation of the *ABI3p:OXA2a-2* plant mitochondria from wild-type plant mitochondria (Figure 17C). Hence, the stability of newly synthesised complex III subunits and/or the rate of complex III assembly could be affected in *ABI3p:OXA2a* plant mitochondria.

7.3.4. Specific complex III subunits are reduced in *ABI3p:OXA2a* plants

Next, steady state abundances of mitochondrial proteins in 2-week-old plants were analysed by immuno-blots following SDS-PAGE. In agreement with the phenotype and abundances of respiratory complexes, there was no obvious difference in any of the protein levels in *35Sp:OXA2aΔ245* plants (Figure 18A). Among the tested complex III subunits in *ABI3p:OXA2a* plants, COB levels appeared normal and QCR7 was increased whereas CYC1 (cytochrome *c*₁) and RISP levels were both decreased (Figure 18A). CYC (cytochrome *c*) is also reduced in *ABI3p:OXA2a* plants (Figure 18A). Correlating with the normal complex IV abundance, its subunits, COX2 and COX3 were also at normal levels in *ABI3p:OXA2a* plants (Figures 16 and 18A). The AOX is generally upregulated upon respiratory chain disruption in plants (125). It is interesting that even the small reduction in complex III in *ABI3p:OXA2a* plants leads to a large increase in the abundance of AOX (Figure 18A). Interestingly, the cytochrome *c* maturation protein B (CCMB) was more abundant in the *ABI3p:OXA2a* plants.

Immunoblot analyses of mitochondrial proteins were also performed using 4-week-old *ABI3p:OXA2a* plant mitochondria since complex III reduction was found to be more severe in the 4-week-old plants than the 2-week-old plants (Figures 16 and 18B). Most respiratory proteins of 4-week-old plants followed the same pattern as that of the 2-week-old plants described above (Figure 18). The complex III subunit, MPPα also remained at the normal wild-type level in *ABI3p:OXA2a* plants, similar to the pattern observed with COB and QCR7 levels (Figure 18B). However, COX3, which was at the normal level in the

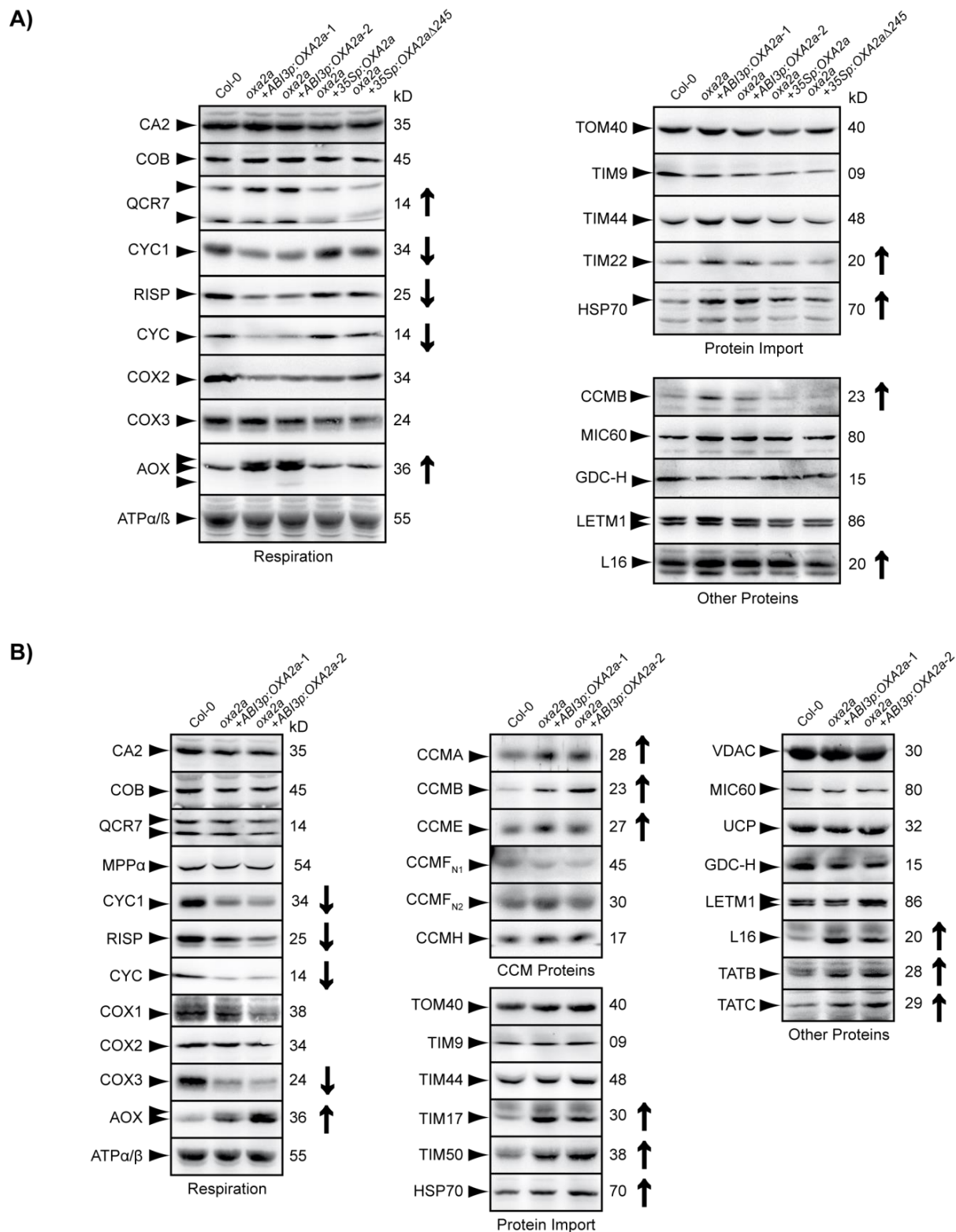


Figure 18. Analysis of mitochondrial proteins in *oxa2a* partial complementation plants. **A)** Immuno-blot analysis of the indicated proteins involved in respiration, protein import and other functions using 2-week-old plant mitochondria. **B)** Immunoblot analysis of the indicated proteins involved in respiration, cytochrome *c* maturation (CCM), protein import and other functions using mitochondria isolated from 4-week-old plants. In all panels, 30 μ g mitochondrial sample was loaded, the antibody used is mentioned on the left side and the molecular weight in kD is located on the right. The correct band is indicated with an arrow head next to the protein name. In some cases, more than one isoform was detected. Bands not indicated are non-specific reactions of the antibody. Where protein abundance is notably different, it is indicated on the right side by either an up (upregulated) or a down (downregulated) arrow. For full list of antibodies see Supplemental Table 2.

2-week-old *ABI3p:OXA2a* plants was reduced in the 4-week-old plants (Figure 18). To check whether the CCM pathway was affected, a selection of CCM components in addition to CCMB were analysed in 4-week-old *ABI3p:OXA2a* plants. Among them, CCMA, CCMB and CCME were increased in the *ABI3p:OXA2a* plants whereas CCMF_{N1}, CCMF_{N2}, and CCMH were at similar levels to those of wild-type plants (Figure 18B).

The complex I subunit, CA2, the complex IV subunit, COX2 and the complex V subunits, ATP α and $-\beta$ remained unchanged in *ABI3p:OXA2a* plants irrespective of the plant age (Figure 18). Among the proteins involved in protein import, TOM40 and TIM9 were at normal levels whereas TIM22, TIM17, TIM50 and HSP70 were increased in *ABI3p:OXA2a* plant mitochondria (Figure 18). Moreover, the mitochondrial ribosomal subunit, L16 and mitochondrial TAT subunits, TATB and TATC were also increased in *ABI3p:OXA2a* plants (Figure 18B). The increased levels of these proteins could be attributed to a general upregulation of mitochondrial biogenesis upon disruption of the respiratory chain (126). Some other mitochondrial proteins analysed, VDAC, MIC60, UCP, GDC-H and LETM1 remained at normal levels in *ABI3p:OXA2a* plants (Figure 18).

7.3.5. Complex III is assembled slower in *ABI3p:OXA2a* plants

In order to check whether mitochondrial protein synthesis and complex assembly were affected in *ABI3p:OXA2a* plants, *in organello* synthesised proteins labelled with ³⁵S methionine were analysed by SDS-PAGE and BN-PAGE. This experiment was performed using 2-week-old plants grown in sterile liquid medium, due to the technical difficulty of obtaining mitochondria free from bacterial contamination using 4-week-old soil grown plants. Although not as severe as 4-week-old plants, 2-week-old *ABI3p:OXA2a* plants still display a noticeable decrease in complex III abundance (Figure 16B). COB, which is the only mitochondrial encoded subunit of complex III, appeared to be synthesised normally (Figure 19A), but its rate of assembly into complex III could not be assessed clearly, possibly due to very low signal intensity of the whole complex (Figure 19B). The rates of synthesis of ATP1, COX1, COX2, COX3 and ATP9 as well as assembly of complexes I, V

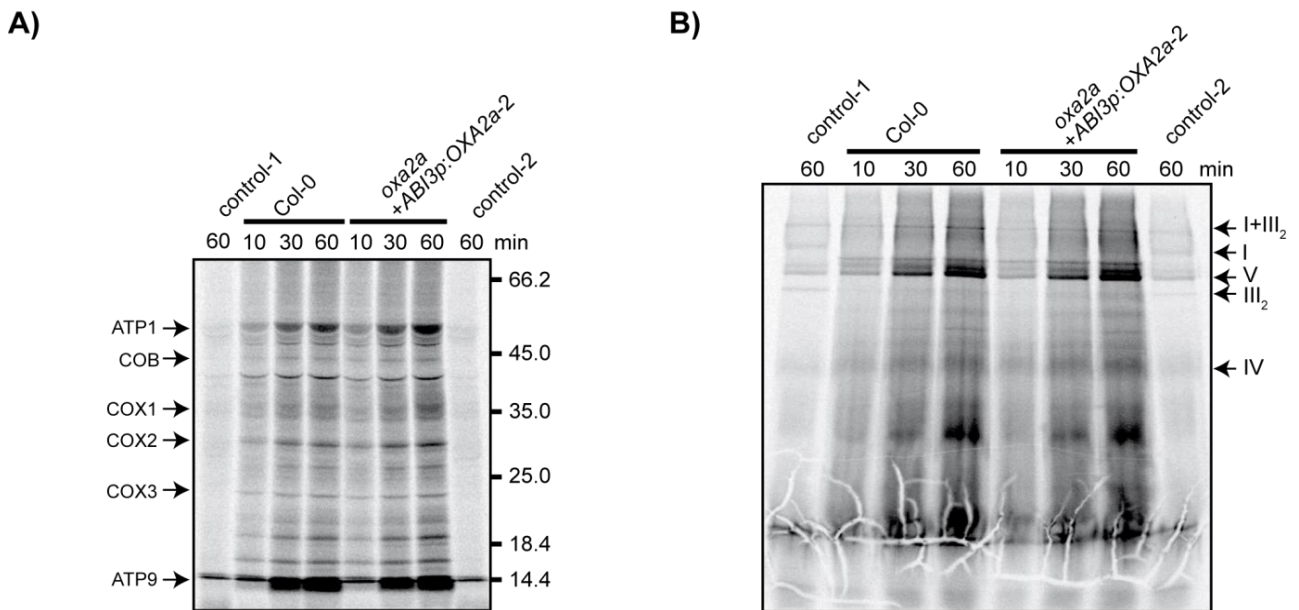


Figure 19. Translation and assembly of mitochondrial-encoded proteins in *ABI3p:OXA2a-2* plants. **A)** Autoradiogram of proteins synthesized *in organello* for 10, 30 and 60 min in the mitochondria isolated from 2-week-old plants that were separated by SDS-PAGE. The known proteins are indicated on the left and the molecular weight marker in kD is shown on the right. The lanes labelled ‘control-1’ and ‘control-2’ are bacterial contamination controls of Col-0 and *ABI3p:OXA2a-2* samples respectively where sodium acetate was used as the energy source. The large smear at the bottom of the gel is ATP9. Due to its high hydrophobicity, ATP9 runs aberrantly on SDS gels. **B)** The same reaction mix as in A was separated by BN-PAGE to show incorporation of the newly translated proteins into respiratory complexes, which are indicated on the right.

and IV and supercomplex I+III₂ in *ABI3p:OXA2a-2* plants appeared to be similar to those of wild-type mitochondria (Figure 19).

Next, mitochondrial protein import rates of the nuclear encoded subunits, QCR7 and CYC1 were studied in *ABI3p:OXA2a* plants by *in vitro* import of the radiolabelled precursor proteins. The mitochondria isolated from 2-week-old plants were used for the import experiment since the mitochondria of 4-week-old plants displayed a very low import efficiency. As QCR7 does not have a cleavable presequence, its import was monitored by treatment with PK. While the rate of QCR7 import into *ABI3p:OXA2a-2* plant mitochondria appeared similar to that of wild-type plant mitochondria (Figure 20A), the rate of CYC1 import into the mitochondria of *ABI3p:OXA2a-2* plants appeared faster (Figure 20B). This faster import rate might be due to the higher abundance of certain import components in the mitochondria of *ABI3p:OXA2a* plants (Figure 18A). Since the final membrane topology of CYC1 should be N-out C-in, it was next tested whether CYC1

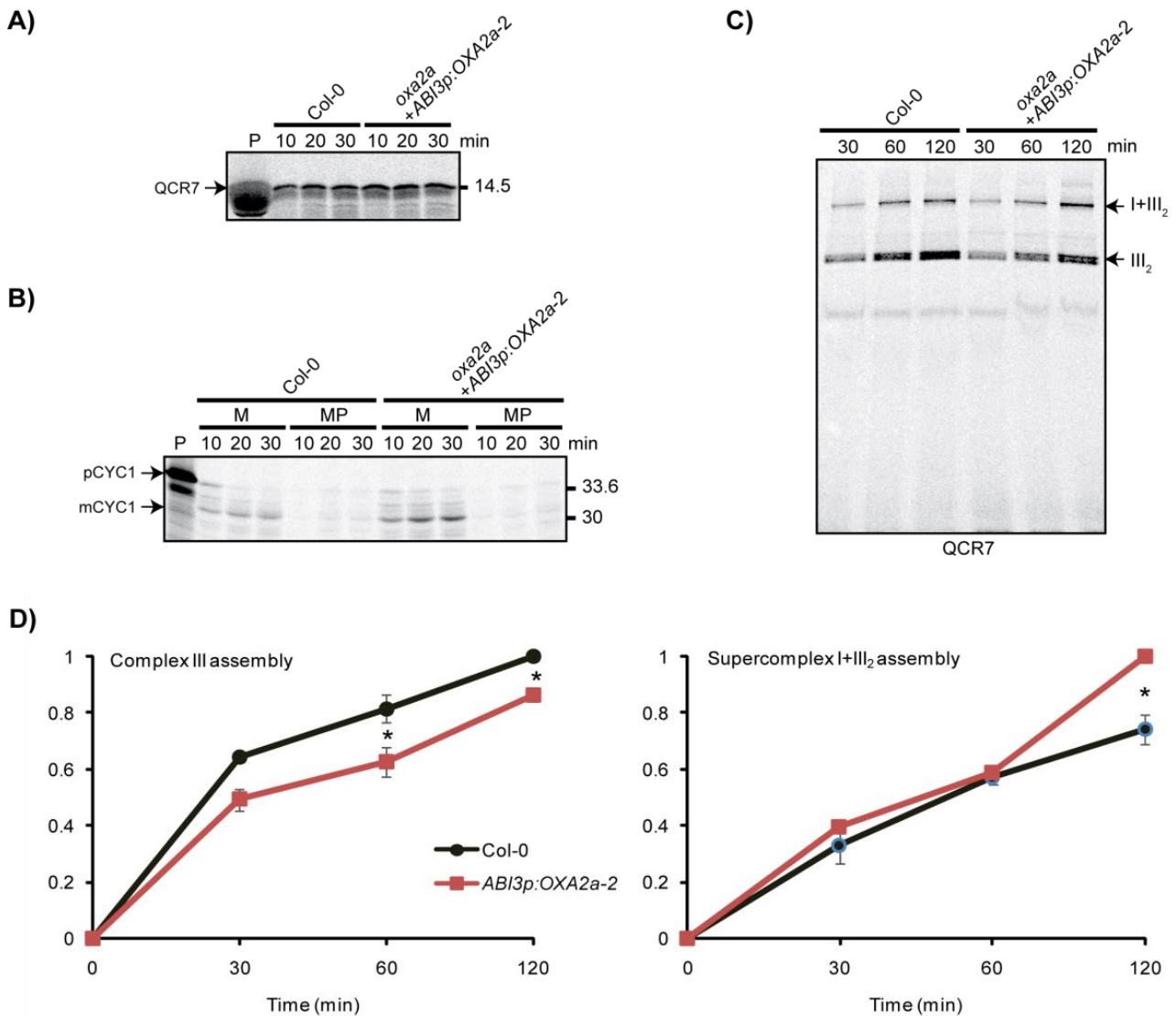


Figure 20. Import of complex III subunits into *ABI3p:OXA2a-2* mitochondria. **A)** Autoradiogram of QCR7 imported into mitochondria isolated from 2-week-old plants for 10, 20 and 30 min followed by treatment with PK and SDS-PAGE. The molecular weight marker in kD is specified on the right. **B)** The radiolabelled precursor of CYC1 was treated similarly as in A for the samples labelled as M (mitochondria). As for the samples labelled as MP (mitoplasts), after import for the indicated time point, mitochondria were subjected to osmotic shock to rupture the OM and then PK treatment and SDS-PAGE was performed. **C)** Autoradiogram of the complexes assembled after the indicated time points of importing QCR7 into mitochondria isolated from 2-week-old plants. **D)** Three independent experiments as in C were used to quantitate the assembly of imported QCR7 into complex III and supercomplex I+III₂ at each time point. Data are given as averages ± SE (n = 3) after normalization to the highest value obtained in each replicate experiment. A statistically significant difference based on Student's *t* test with a *p* value < 0.05 is indicated by *.

is able to attain the right membrane topology after its import into *ABI3p:OXA2a-2* plant mitochondria. Hence mitoplasts were generated by rupture of the OM and treated with PK after import. Since CYC1 contains a large domain exposed to the IMS, PK treatment resulted in complete digestion of CYC1 in both wild-type and *ABI3p:OXA2a-2* plant

mitochondria (Figure 20B). Therefore CYC1 apparently does achieve the correct membrane topology in *ABI3p:OXA2a-2* plants, as in wild-type plants.

Following the import of radioactive QCR7, its assembly into complex III and the supercomplex I+III₂ was studied in 2-week-old *ABI3p:OXA2a-2* plants. The overall rate of complex III assembly in *ABI3p:OXA2a-2* plants appeared to be lower than that in wild-type plants (Figure 20C). Based on the band intensities obtained in three independent experiments, the rate of QCR7 incorporation into complex III and supercomplex I+III₂ was interpreted (Figure 20D). The reduction in the rate of complex III assembly in *ABI3p:OXA2a-2* plants was calculated to be approximately 20%. Therefore, slower assembly of complex III could have caused a steady reduction in the abundance and enzyme activity of complex III in the *ABI3p:OXA2a* plants that became more prominent as the plants grew older (Figures 15, 16, 20C and 20D). Surprisingly, the overall rate of formation of the supercomplex I+III₂ was found to be 12% faster in *ABI3p:OXA2a-2* plants (Figures 20C and 20D). Since supercomplex formation is believed to enhance the stability of individual complexes and the efficiency of electron transfer, increased biogenesis of the supercomplex I+III₂ could be a measure to compensate for the decrease in biogenesis of complex III (131-133). However, the abundance of the supercomplex I+III₂ was reduced in *ABI3p:OXA2a-2* plants, indicating that it is probably not as stable as in wild-type plants (Figure 16B). The assembly of radioactive CYC1 into complex III could not be examined following its import, possibly because the heme binding process is not supported in isolated mitochondria.

7.3.6. The CCM process is affected in *ABI3p:OXA2a* plants

Since both the mitochondrial *c*-type cytochromes, CYC1 and CYC were reduced and the CCM proteins, CCMA, CCMB and CCME were upregulated in *ABI3p:OXA2a* plants (Figure 18B). Furthermore, heme staining corroborated that the *c*-type cytochromes, CYC and CYC1 were reduced in 4-week-old *ABI3p:OXA2a* plant mitochondria (Figure 21A), which correlates with their reduced protein abundances (Figure 18B). Therefore, it was sought to investigate whether the CCM process might have been disrupted. Interestingly,

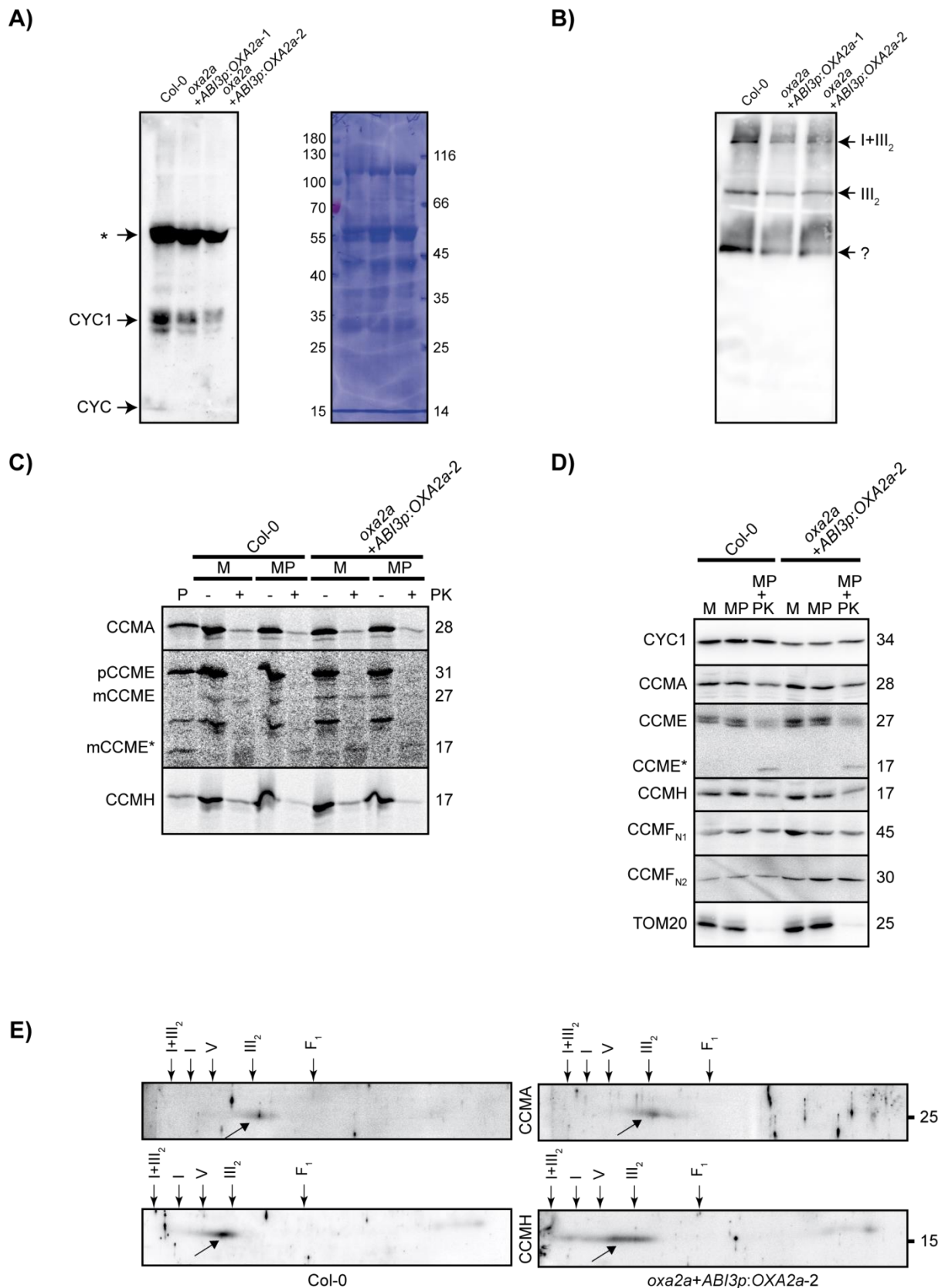


Figure 21. Analyses of the CCM process in *ABI3p:OXA2a* plants. A) Mitochondrial proteins of 4-week-old *ABI3p:OXA2a* plants separated by SDS-PAGE were subjected to heme staining. The stained proteins are indicated and * denotes a non-specific band. Adjacently, the Coomassie-stained membrane is shown along with molecular weight markers in kD. B) Mitochondrial complexes of 4-week-old *ABI3p:OXA2a* plants separated by BN-PAGE were subjected to heme staining. The stained complexes are indicated. '?' indicates an unknown complex. C) Autoradiogram of the indicated CCM proteins imported into mitochondria isolated from 2-week-old plants followed by treatment with

PK and SDS-PAGE. The molecular weight marker in kD is specified on the right. For the samples labelled as MP (mitoplasts), M (mitochondria) were subjected to osmotic shock in order to rupture the OM. **D**) Immunoblot analysis of the specified proteins present in mitochondria (M), mitoplasts (MP) made by osmotic rupture of the OM and PK treated mitoplasts (MP+PK) performed using mitochondria isolated from 2-week-old plants. The molecular weight marker in kD is shown on the right. **E**) Immuno-blot analysis of the specified CCM proteins after 2D-BN/SDS-PAGE of mitochondria from 4-week-old plants. I – complex I, V – complex V, III₂ – dimeric complex III, F₁ – F₁ part of complex V, I+III₂ – supercomplex composed of complex I and dimeric complex III.

heme staining performed on mitochondrial complexes displayed a reduction in complex III and the supercomplex containing complex III (Figure 21B), which also correlates with the reduction in their respective abundances (Figure 16B). Additionally, an unknown complex was also reduced in the heme stain of *ABI3p:OXA2a* plants (Figure 21B). When import rates and membrane topologies of all the three nuclear encoded CCM proteins, CCMA, CCME and CCMH were analysed using the mitochondria isolated from 2-week-old *ABI3p:OXA2a-2* plants, no significant difference was found (Figure 21C). This indicates that their import and topogenesis does not require OXA2a.

CCMA and CCMB function as an ABC transporter in the CCM pathway (134). In *ABI3p:OXA2a-2* plants, besides an increase in the protein levels of CCMA and the mitochondrial encoded CCMB, more CCMA was found to accumulate in a mitochondrial complex, which is likely to be the ABC transporter (Figure 21E). Among the mitochondrial encoded CCM proteins, CCMF_{N1} and CCMF_{N2} were not affected in their membrane topology based on PK treatment following rupture of the mitochondrial OM (Figure 21D). Since CCMF_{N1}, CCMF_{N2} and CCMF_C together form a complex that interacts with CCMH in *Arabidopsis* mitochondria, it is very likely that CCMF_C is also not affected in *ABI3p:OXA2a* plants (135). Besides, more CCMH was found to accumulate in a mitochondrial complex in *ABI3p:OXA2a-2* plants (Figure 21E).

The remaining known CCM protein is CCMC, which is mitochondrial encoded. CCMC most likely has six TMHs and three IMS-exposed loops, based on the structure of *E. coli* CcmC (135, 136) (Figure 22A). The WWD motif of *E. coli* CcmC, which is exposed to the periplasm, has the ability to bind heme and transfer it to CCME (137) (Figure 22A).

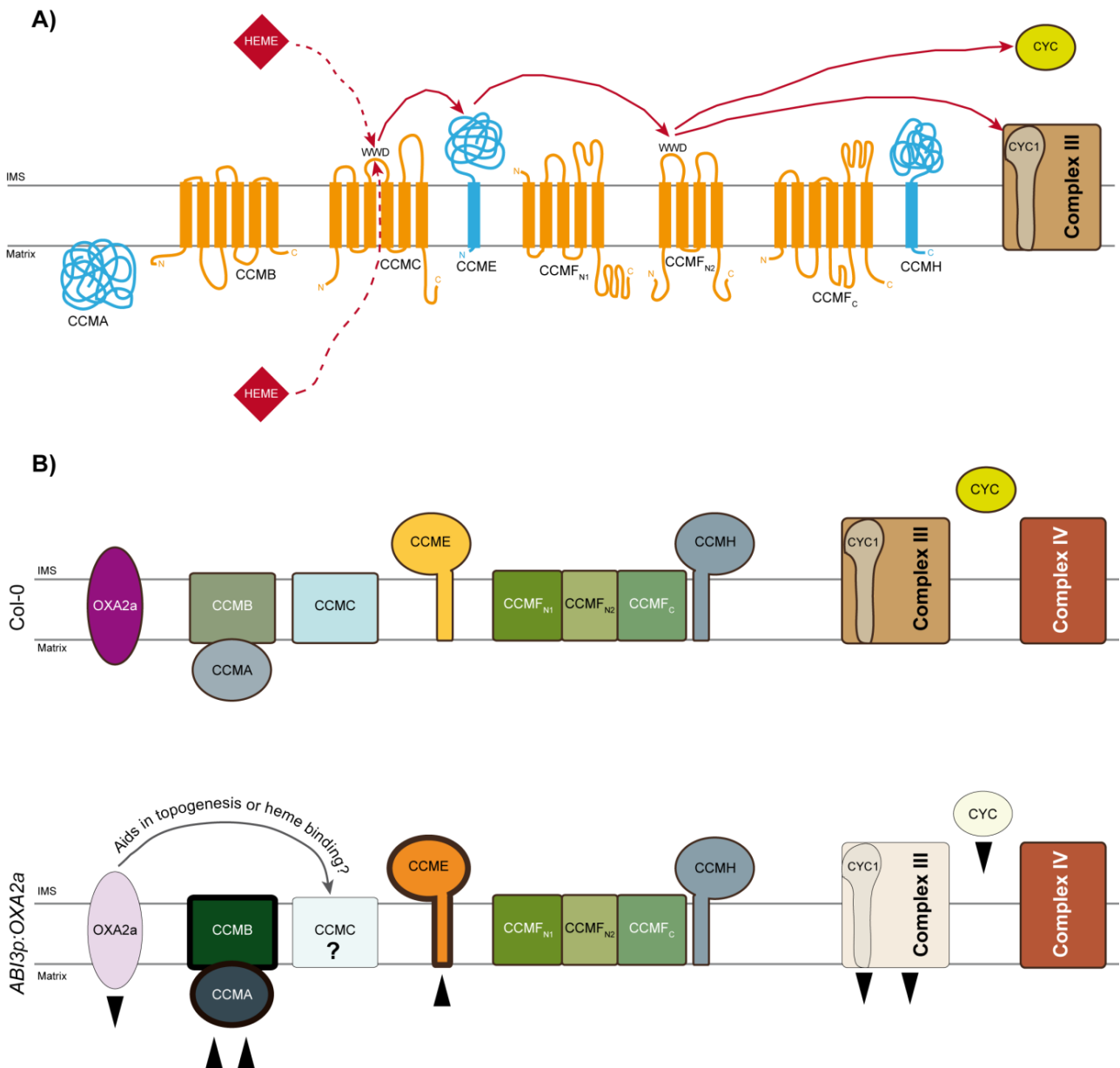


Figure 22. The CCM pathway is affected in *ABI3p:OXA2a* plants. **A)** An illustration of the predicted topology of the CCM proteins in Arabidopsis. The mitochondrial encoded CCM proteins are colored in orange and the nuclear encoded ones in blue. Heme trafficking during CCM process is shown with arrows. Dashed lines indicate that the origin of heme is not clear. **B)** *OXA2a* reduction in *ABI3p:OXA2a* plants results in reduction of the *c*-type cytochromes, CYC and CYC1 leading to complex III reduction. Changes in steady state levels are shown with a corresponding arrow head and altered color intensity. The steady-state levels of certain CCM proteins are increased, possibly to compensate for a defect in CCMC. Thus, CCMC could be a potential substrate of *OXA2a*.

Although CCMF_{N2} also has an IMS exposed WWD motif, it does not appear to be affected in *ABI3p:OXA2a-2* plants, as mentioned above. Hence it is likely that the unknown heme stained complex that was reduced in *ABI3p:OXA2a-2* plants could contain CCMC and CCME. It has to be noted that in a previous study on plant mitochondrial complexes, both CCMC and CCME were found to accumulate in a complex of similar size to this unknown

heme stained complex (25). Therefore, it is very likely that OXA2a might aid in the export of one or more IMS-exposed loops and/or in heme binding of CCMC during its biogenesis (Figure 22B).

7.4. Roles of OXA1b and OXA1a

7.4.1. Faster germination of *oxa1b* seeds

In collaboration with Prof. James Whelan (La Trobe University, Melbourne), it was observed that the *oxa1b* seeds germinate significantly faster than the wild-type seeds under normal growth conditions (Figure 23A). Non-optimal growth conditions such as low

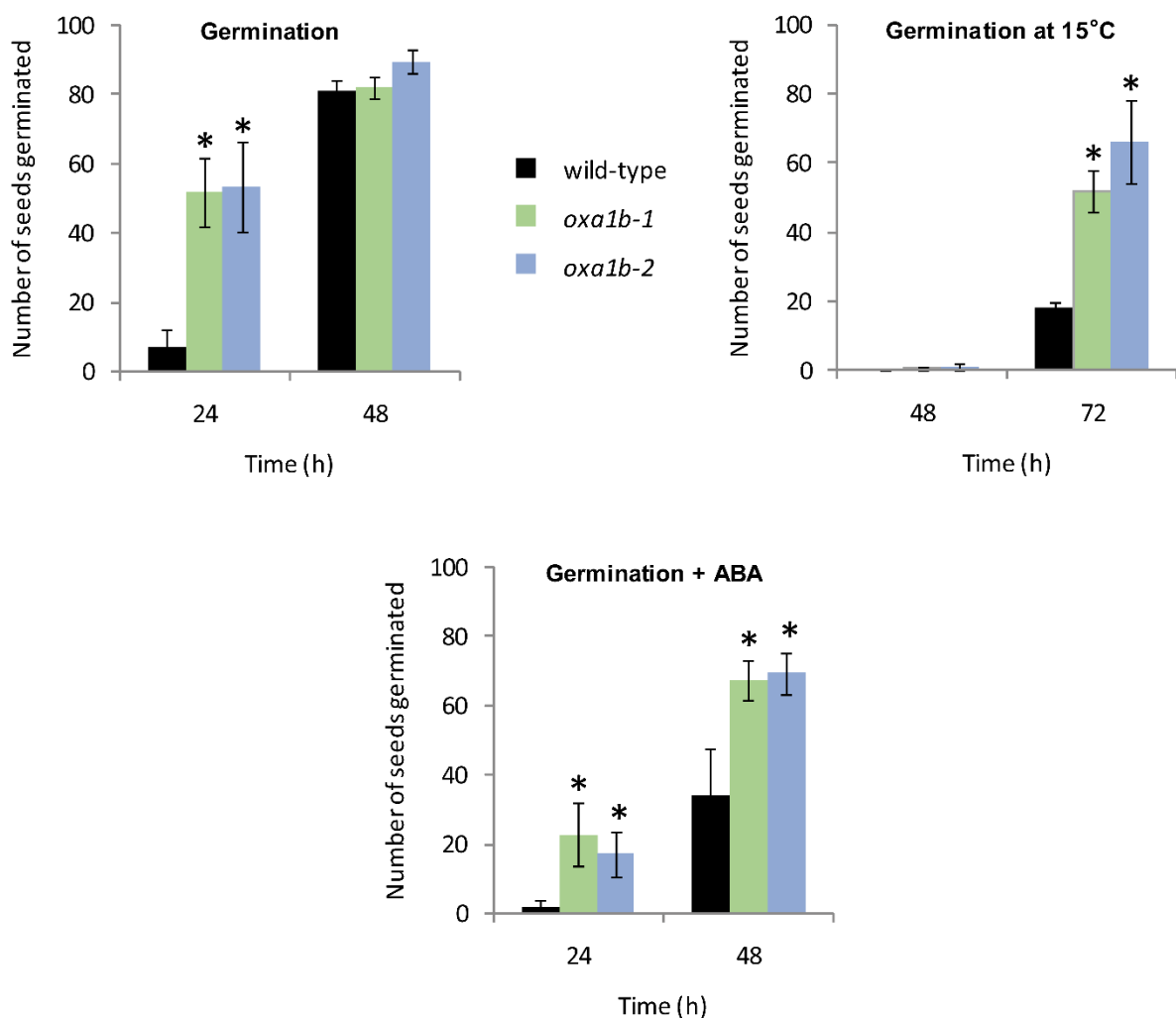


Figure 23. Germination of *oxa1b* seeds. **A)** Seeds were allowed to germinate under optimal growth conditions at 21°C for the indicated time after stratification in dark at 4°C for 3 days. **B)** Seeds were allowed to germinate at 15°C for the indicated time after stratification in dark at 1°C for 3 days. **C)** Seeds were allowed to germinate in the presence of abscisic acid (ABA) which inhibits germination. All other growth conditions were the same as mentioned for A. Data are given as averages \pm SE. Statistical significance with a p value < 0.05 based on Student's t test with reference to Col-0 is indicated by *.

temperature inhibit seed germination (138, 139). Based on the external environmental stimuli, seed dormancy and germination are regulated by the antagonistic action of two plant hormones, abscisic acid (ABA) and gibberellin (GA) (140, 141). ABA is required to establish dormancy during seed maturation, maintains dormancy in mature seeds, and can inhibit germination when externally applied to seeds, whereas GA stimulates seed germination (142). Faster germination of the *oxa1b* seeds was consistent even under the germination suppressing conditions, at low temperature of 15°C as well as in the presence of abscisic acid (Figures 23B and 23C). However, in all the later growth stages, the *oxa1b* plants did not display any significant phenotypic variation (Figure 24). Faster germination and normal phenotype of the *oxa1b* mutants suggest that the loss of OXA1b might either have a direct positive effect on the plant metabolism or a negative effect which might have been compensated by any of the other three OXA protein present, most likely OXA1a.

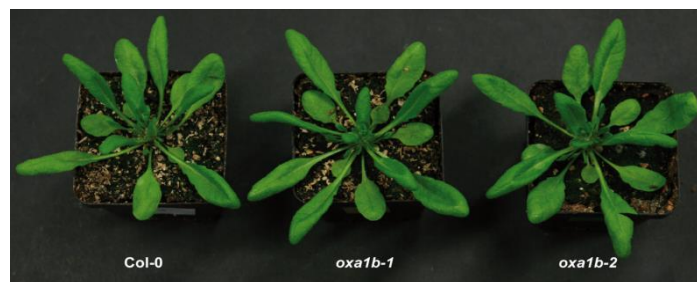


Figure 24. Phenotype of *oxa1b* plants. A representative picture of 4-week-old plants. The *oxa1b* plants appeared similar to Col-0 plants. Twelve plants of each genotype were examined.

7.4.2. The respiratory complexes are unaffected in *oxa1b* mitochondria

In order to check whether OXA1b depletion affects mitochondrial respiratory complexes, mitochondria were isolated and the respiratory complexes separated by BN-PAGE were examined. The levels of supercomplexes composed of complexes I and III, complex V and the complex III dimer in *oxa1b* mitochondria appeared similar to those in wild-type mitochondria (Figure 25A). Then, *in gel* enzyme activity stains were performed to test the levels of complexes I and IV (Figures 25B and 25C). There was no significant difference in the enzyme activities of either of these complexes in *oxa1b* mitochondria as compared to wild-type mitochondria. Moreover, the levels of complexes III and V were also unaffected in *oxa1b* mitochondria based on immunoblot analyses (Figure 25D).

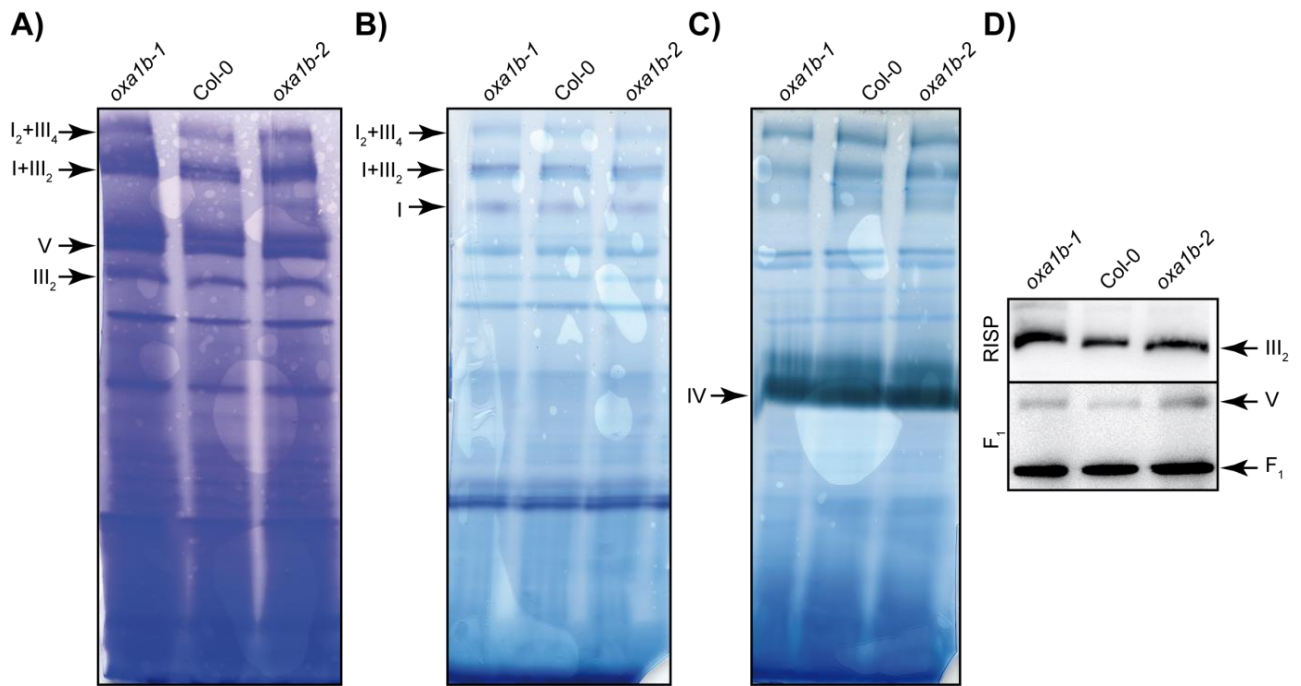


Figure 25. Respiratory complexes in *oxa1b* mitochondria. A) Respiratory complexes stained with Coomassie upon BN-PAGE. B) In gel NADH dehydrogenase (Complex I) activity staining following BN-PAGE. C) In gel cytochrome c oxidase (complex IV) activity staining following BN-PAGE. D) Immuno-blot analysis of the mitochondrial complexes using the antibodies against: RISP (complex III) and F₁ part of ATP synthase (complex V). Complexes and supercomplexes are indicated where appropriate. I – complex I, III₂ – dimeric complex III, I+III₂ – supercomplex composed of complex I and dimeric complex III, I₂+III₄ – supercomplex composed of two complex I monomers and two copies of dimeric complex III, IV – complex IV and V – complex V.

7.4.3. Certain mitochondrial protein levels are altered in *oxa1b* plants

Next, steady state abundances of several mitochondrial proteins were analysed by immunoblots following SDS-PAGE. Confirming *OXA1b* gene knockout, the *OXA1b* protein was not found in *oxa1b* plant mitochondria (Figure 26). Additionally, considerable difference was observed in the levels of *OXA1a*, *S10* and *ERV1*. The levels of *OXA1a* appeared increased in *oxa1b* mitochondria (Figure 26). This indicates that *OXA1a* and *OXA1b* might have some overlapping functionality and more *OXA1a* could be compensating for the loss of *OXA1b*. A reduction in the levels of *S10* and *ERV1* was found in *oxa1b* mitochondria (Figure 26). *S10* is a nuclear-encoded mitoribosomal subunit whose silencing was found to affect the ratio of the small and large subunits of mitoribosomes (143). *ERV1* is a sulfhydryl oxidase which promotes protein import and oxidative protein folding in the IMS (144, 145). Based on the immunoblot analyses, *OXA1b* influences *S10* and *ERV1* levels either directly or indirectly (Figure 26).

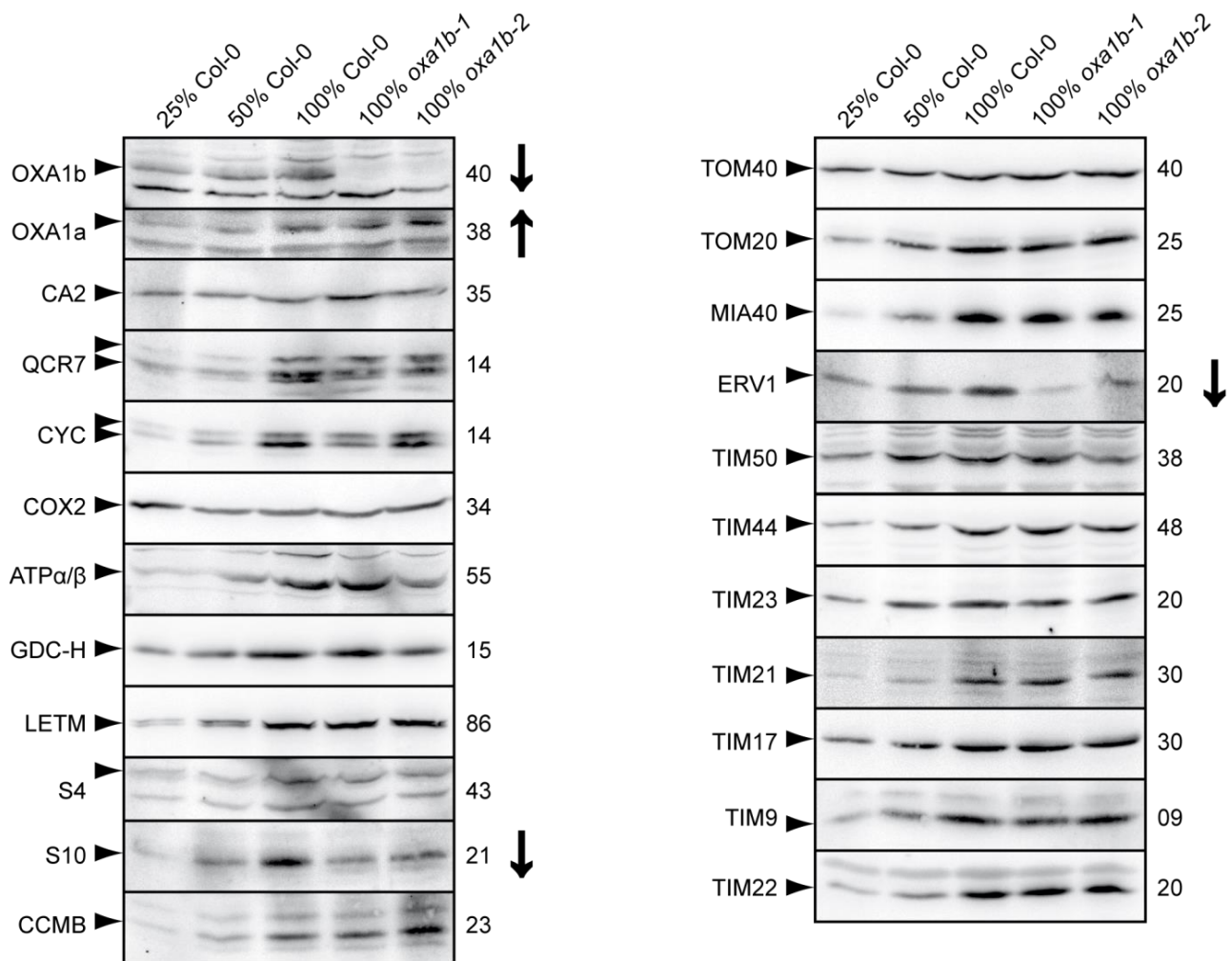


Figure 26. Mitochondrial proteins of *oxa1b* plants. Immunoblot analysis of a selection of proteins in isolated mitochondria as indicated on the left. The apparent molecular weight of the protein is located on the right in kD. The correct band is indicated with an arrow head next to the protein name. In some cases, more than one isoform were detected. Bands not indicated are non-specific reactions of the antibody. 100% corresponds to 40 μ g mitochondrial protein. Where protein abundance is notably different, it is indicated on the right side by either an up or a down arrow for representing more or less abundance respectively of that protein in both the *oxa1b* lines.

7.4.4. TIM22 appears to assemble faster in *oxa1b* mitochondria

In order to check whether mitochondrial protein import and complex assembly are affected in *oxa1b* plants, radiolabelled substrate proteins were imported into the isolated mitochondria. The *in-vitro* import efficiencies of F_AD and AOX, which are substrates of the presequence translocase as well as P_iC and TIM23, which are substrates of the carrier translocase, into *oxa1b* mitochondria remained correspondingly similar to the efficiencies observed with wild-type mitochondria (Figure 27A). Following the import of the radioactive TIM22, its assembly into TIM22 complex was analyzed by resolving the mitochondrial import reaction by BN-PAGE. Interestingly, TIM22 assembly into the

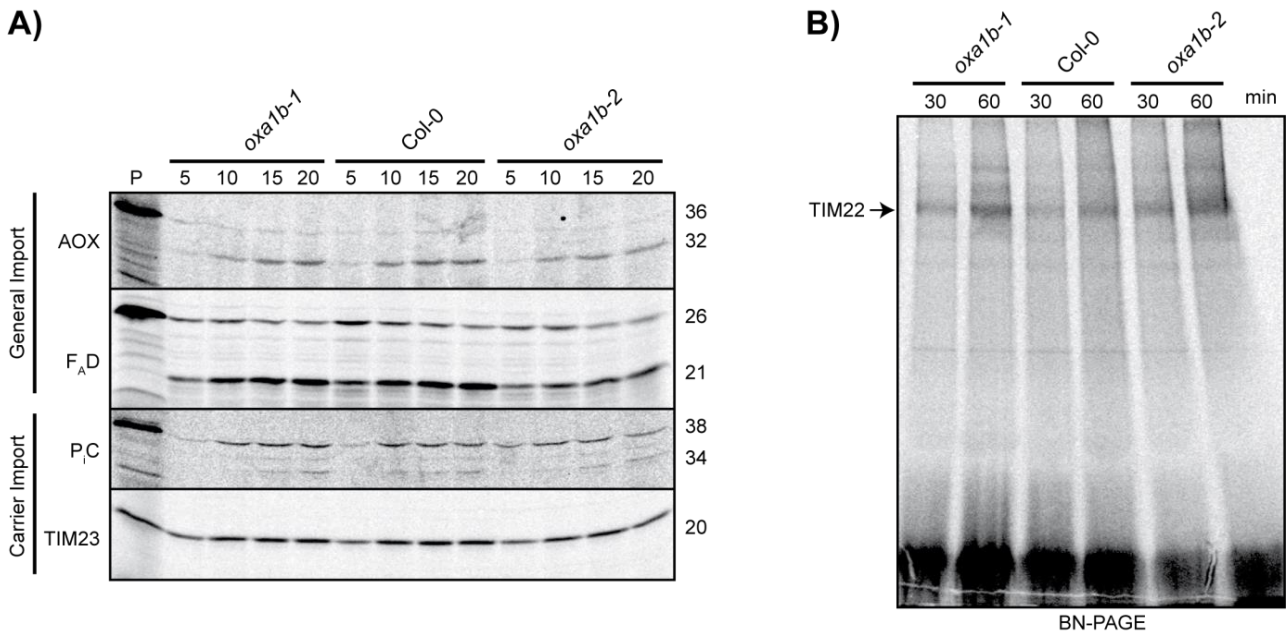


Figure 27. Protein import into *oxa1b* plant mitochondria. A) Autoradiogram of the indicated proteins imported via the general import pathway or the carrier pathway into the mitochondria isolated from the plants mentioned on top. The import reaction incubation time in minutes is stated on the top and the molecular weight of the protein bands in kD is specified on the right. 'P' stands for the precursor protein alone, which represents 10% of the amount used in the import reactions. AOX: alternative oxidase; F_AD: a subunit of mitochondrial ATP synthase; P_iC: inorganic phosphate carrier. B) Autoradiogram of the TIM22 complex that assembled after the indicated time points of importing TIM22 protein into the isolated mitochondria. 60% more TIM22 complex assembled in the *oxa1b* mitochondria as compared to that in the Col-0 mitochondria.

complex was faster in *oxa1b* mitochondria than in the wild-type mitochondria (Figure 27B). About 60% more TIM22 complex accumulated in *oxa1b* mitochondria after 60 min of incubation in the import buffer. This positive effect could be due to higher levels of OXA1a in *oxa1b* plants, in which case, TIM22 is a potential substrate of OXA1a (Figure 26).

7.4.5. RNA silencing of *OXA1a* does not alter the plant phenotype

Since OXA1a is essential for embryogenesis, RNA silencing was used as one of the approaches to generate viable mutants and study its roles in postembryonic older plants. For this, RNA interference using a dexamethasone-inducible pOpOff2 vector as well as a constitutive pK7GWIWG2 vector was performed. A gene-specific sequence was inserted into the vectors and the constructs were transformed into wild-type Arabidopsis plants. Single-locus homozygous insertion lines selected in the T3 generation were propagated for further analyses. Dexamethasone induction and RT-qPCR analysis of the three selected *OXA1a-RNAi* lines revealed that all the three lines exhibited a significant transcript

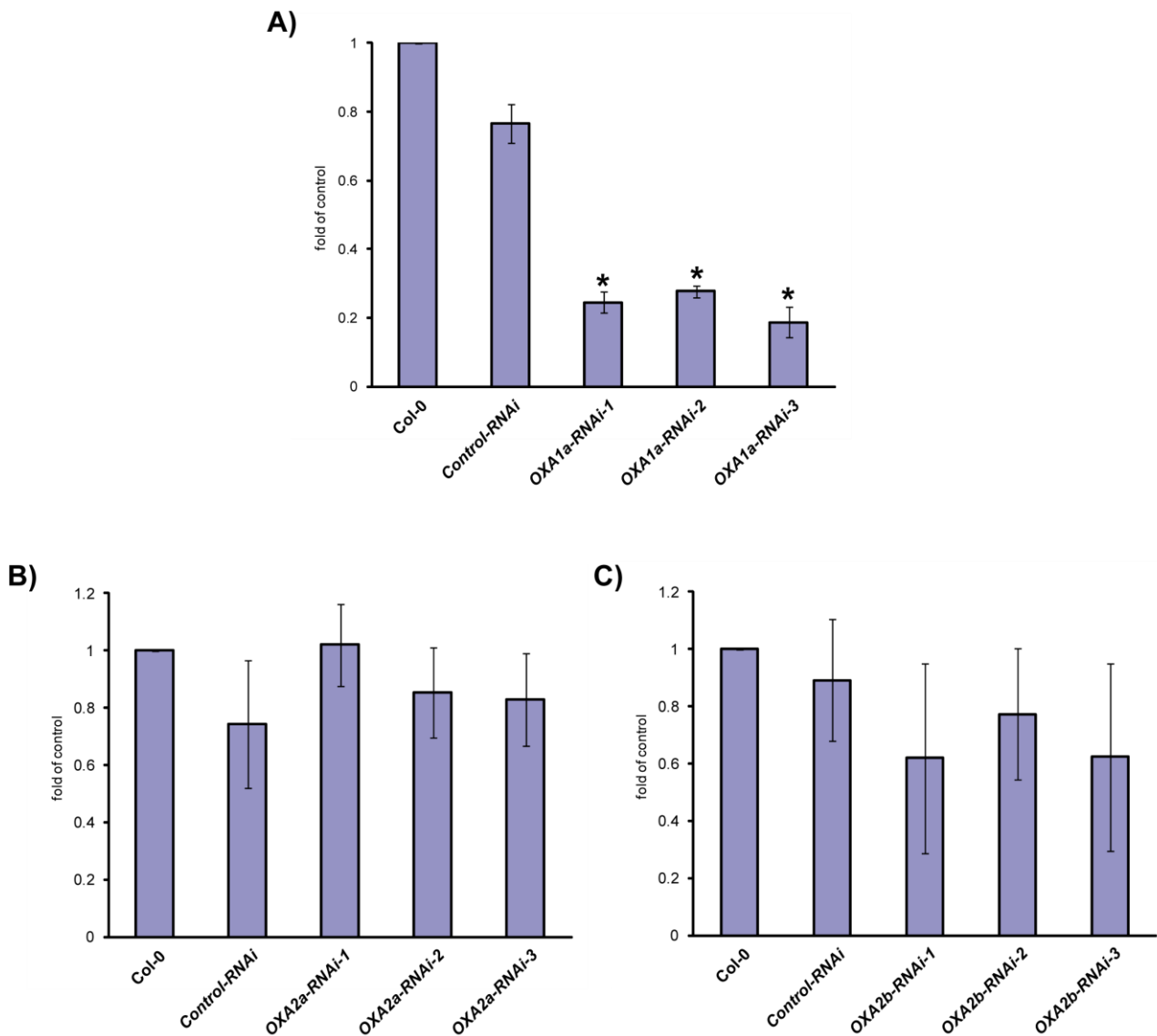


Figure 28. Verification of *OXA1a*-RNAi lines. The transcript abundances of *OXA1a* (A), *OXA2a*, (B) and *OXA2b* (C) with reference to OEP24 transcript abundance were analysed by RT-qPCR in the corresponding RNAi lines after induction with dexamethasone. Control-RNAi was targeted to Luciferase. Data are presented as averages \pm SD of two independent biological replicates and two technical replicates. Statistical significance with a p value < 0.05 based on Student's t test with reference to Col-0 is indicated by *.

reduction of approximately 24% of the wild-type level whereas the transcript level of a control-RNAi line was similar to the wild-type level (Figure 28A).

RNAi approach was employed to produce viable mutants of the other two embryo-lethal plant OXAs, *OXA2a* and *OXA2b* as well. However, the level of transcript reduction was insignificant in both these cases (Figures 28B and 28C). This indicates that *OXA2a* and *OXA2b* could be so important during the growth stages beyond embryogenesis, that

severe transcript reduction was possibly lethal. Hence similar result was assumed with the plants transformed with the constitutive RNAi construct and the corresponding single-locus homozygous insertion lines were not analysed further.

Two of the *OXA1a-RNAi* lines were used for phenotypic and biochemical analyses. Although no major change in the overall plant phenotype was observed, growth on vertical MS plates showed that the roots of *OXA1a-RNAi* plants grew significantly slower in comparison to the roots of wild-type plants (122). Slower root growth has been observed in other *Arabidopsis* mutants with altered mitochondrial biogenesis (123, 124). However, no change in the mitochondrial respiratory complexes or proteins was found (122). This indicates that the remaining level of OXA1a in *OXA1a-RNAi* is possibly sufficient after embryogenesis and/or the other OXAs could be compensating its reduction. OXA1a appears to be essential for plant development beyond embryogenesis as no homozygous line could be isolated by the partial complementation strategy using the *ABI3* promoter (122).

7.4.6. Generation of *OXA1a-RNAi oxa1b* double mutants

The experimental results of *OXA1a-RNAi* and *oxa1b* mutants indicated at least some level of overlapping functionality between the two OXA1 proteins. Hence, double mutants were generated by crossing *OXA1A-RNAi* lines with *oxa1b*. As kanamycin resistance of the T-DNA insert was lost in the *oxa1b* line, the progeny of the crossed plants would derive kanamycin resistance the RNAi construct only. To serve as a control double mutant, the *control-RNAi* was also crossed with *oxa1b*. During selection of the T3 generation, the double mutants already displayed a phenotype even without dexamethasone induction. This might be due to leaky expression from the RNAi construct. The *OXA1a-RNAi oxa1b* double mutant seedlings appeared smaller with elongated cotyledon petioles whereas the *control-RNAi oxa1b* double mutant seedlings appeared similar to the wild-type seedlings (Figure 29).

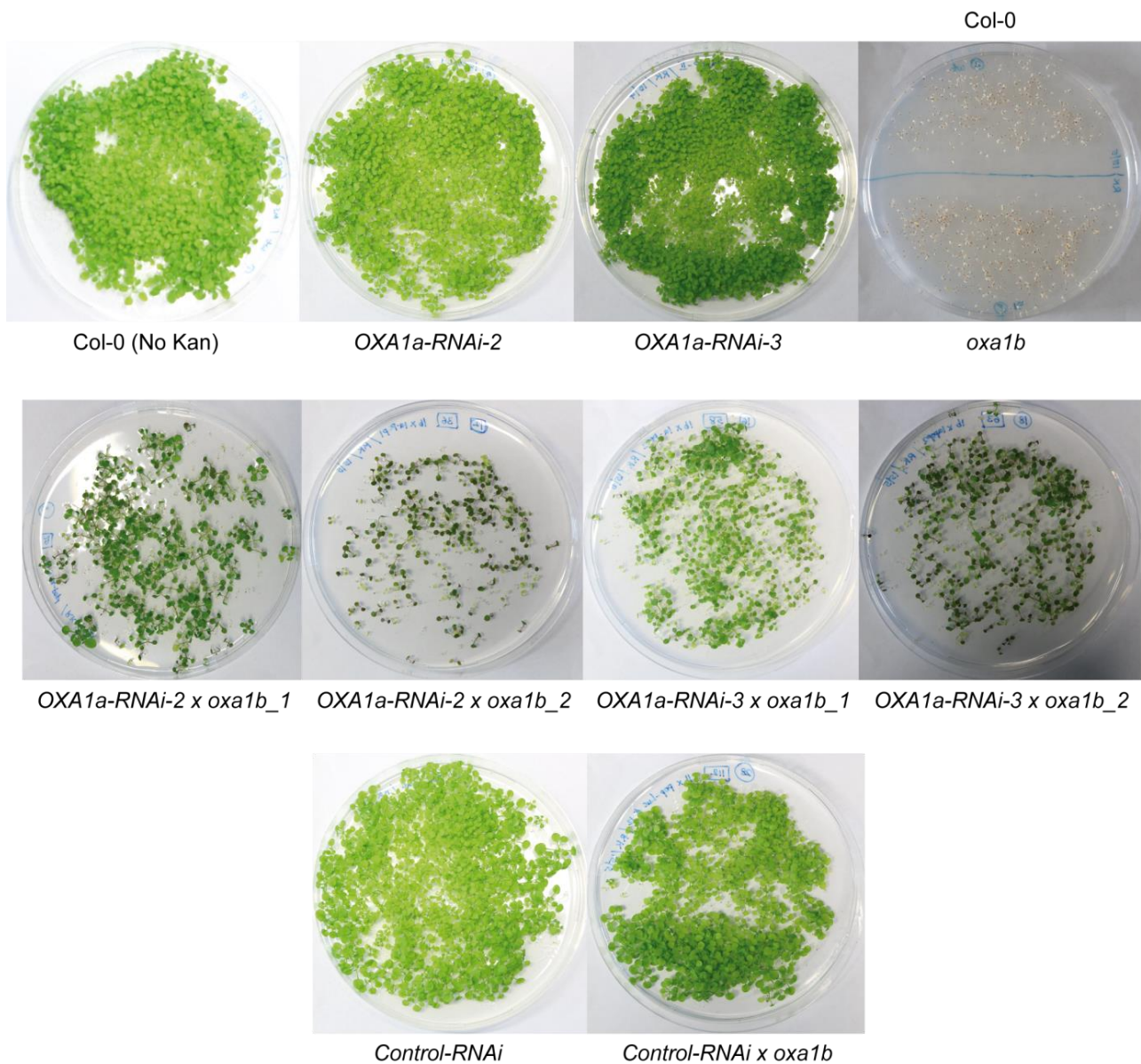


Figure 29. Seedlings of *OXA1a-RNAi oxa1b* double mutants. The T3 generation seeds of the double mutant lines were grown on Kanamycin selection plates before their transfer to soil and genotyping for homozygosity of the T-DNA insert and for the presence of the RNAi construct. For reference, the Col-0 wild-type seeds were grown without the antibiotic. The *OXA1a-RNAi oxa1b* double mutant seedlings displayed a phenotype of smaller size with elongated cotyledon petioles without Dexamethasone induction.

Upon dexamethasone induction, only a fraction of seedlings on plates displayed varying phenotypes such as no germination, growth-arrest at cotyledon stage, smaller darker leaves, etc while the remaining seedlings appeared normal. This was due to non-homogenous population of the seeds. Therefore, further selection and screening was performed to isolate the mutants homozygous for both the *OXA1a/control* RNAi construct and the *OXA1b* T-DNA. The T5 generation double mutant lines homozygous for *OXA1b* T-DNA insert and containing the corresponding RNAi construct were isolated. After

verifying homozygosity of the RNAi construct as well, characterization of the *OXA1a-RNAi oxa1b* double mutants can potentially reveal the substrates and interaction partners of OXA1a and OXA1b in future. Moreover, investigation of the plant lines generated in this study to express the GUS reporter gene under the control of each OXA promoter will provide information regarding the expression levels of the different OXAs at different developmental stages and tissues.

8. Discussion

Members of the Oxa1 protein superfamily are involved in membrane insertion, folding and complex assembly of substrate proteins in bacteria, mitochondria, chloroplasts and the endoplasmic reticulum (69, 71). Mitochondria of fungi and animals contain two members of the Oxa1 superfamily, Oxa1 and Cox18, which have been well-characterized. Oxa1 plays a major role in the cotranslational insertion of mitochondrial-encoded membrane proteins and also in the posttranslational insertion of nuclear-encoded membrane proteins (68, 146). In contrast to Oxa1, Cox18 has been demonstrated to have only one substrate protein, Cox2 (29, 61). However, plant mitochondria contain four Oxa homologs: OXA1a, OXA1b, OXA2a, and OXA2b whose exact functions were previously unknown. This study identified the roles of the OXA2 proteins and laid groundwork for identifying the roles of the OXA1 proteins in Arabidopsis mitochondria.

8.1. OXA2b is required for complex IV biogenesis

The essential role of OXA2b in Arabidopsis mitochondria was studied by rescuing the lethal phenotype of homozygous T-DNA insertion lines via expression of a truncated version of the protein which lacks the C-terminus containing the plant-specific TPR domain. The mutant plants displayed severe growth defects that could be attributed to a lack of complex IV from the respiratory chain, indicating that OXA2b is required for complex IV biogenesis. It was demonstrated that the three mitochondrial-encoded complex IV proteins were still translated, although at a reduced rate. Therefore, the biogenesis defect was not due to a translational defect. It was also shown that the absence of complex IV was due to the failure of COX2 to reach its proper topology with both N- and C-termini facing the IMS. This was further supported by the demonstration that the OXA2b TPR domain specifically binds to newly synthesized COX2, but not to COX1 or COX3.

During complex-IV biogenesis in both yeast and humans, membrane insertion of the Cox2 subunit requires both Oxa1 and Cox18, due to its unique structure (147). Cox2 contains

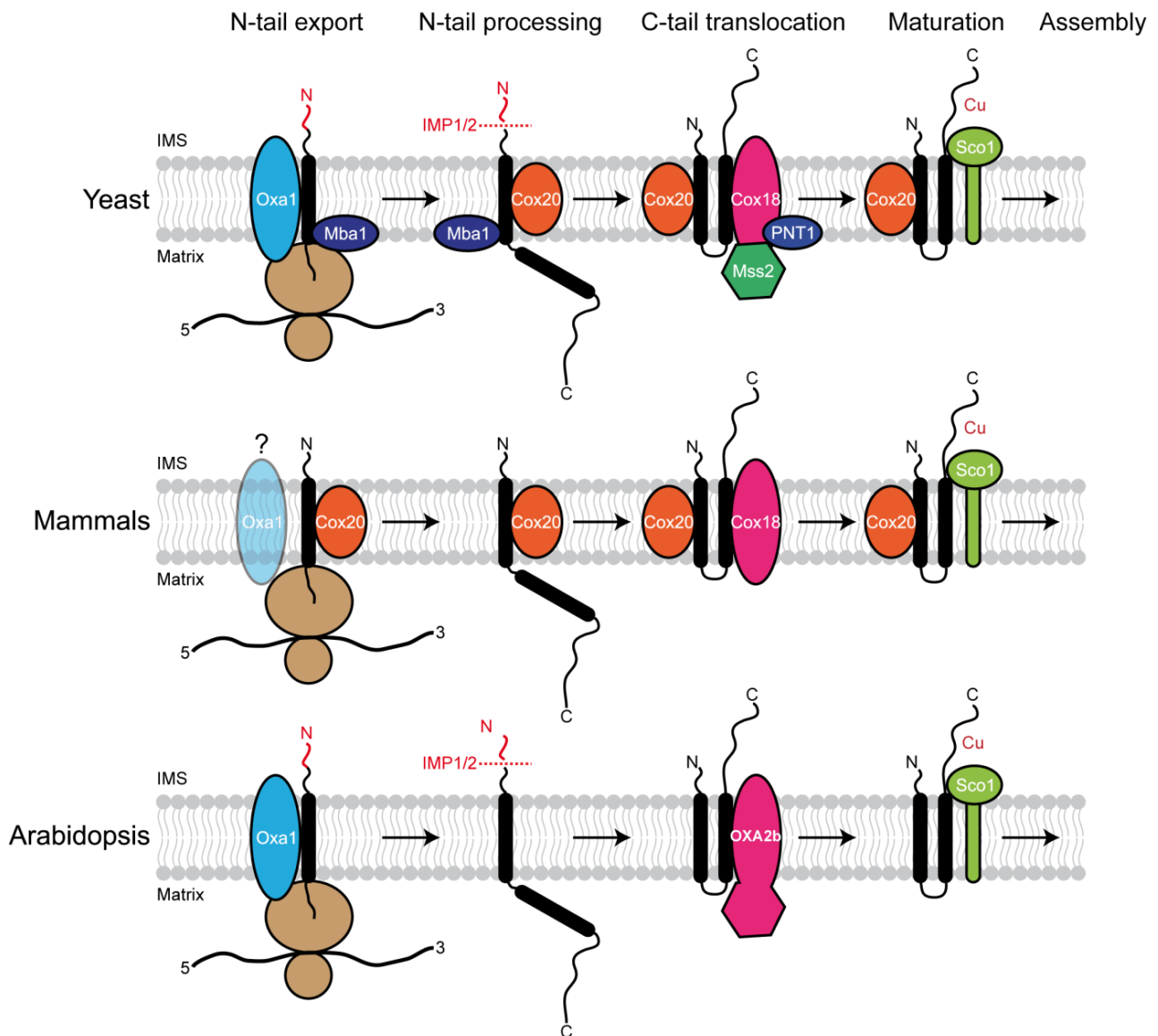


Figure 30. Cox2 biogenesis in different organisms. Current understanding of how Cox2 is inserted into the mitochondrial IM in yeast (*Saccharomyces cerevisiae*), mammals and plants (*Arabidopsis thaliana*). The different steps of the membrane insertion process are followed by maturation by copper insertion and assembly into complex IV as indicated on the top. Cox2 is depicted in black, ribosome in brown, mRNA is a strand with 5' and 3' ends and the proteins involved in Cox2 biogenesis are shown in different colors. N and C indicate N- and C-termini respectively. IMP = inner membrane peptidase; Cu = copper; '?' indicates that the involvement of mammalian Oxa1 in the Cox2 biogenesis is not clear.

two TMHs and an extremely long hydrophilic C terminus located in the IMS that holds the dinuclear copper center. Oxa1 cotranslationally inserts the first TMH of Cox2 into the IM (148, 149) (Figure 30). Cox2 is then stabilized by its specific chaperone, Cox20 (30, 150). After Cox18 inserts the second TMH with the concomitant export of the C terminus into the IMS (29, 61), Cox2 gets metallated and proceeds to complex IV assembly. It is most likely that the second insertion step is impaired in the OXA2b TPR deletion plants based on the phylogenetic analysis, topology studies, and interaction experiments. OXA2b is

most likely performing the same function as Cox18. However, it is possible that plant OXA2b by itself can both stabilize and translocate the COX2 C terminus due to the presence of a TPR domain at its C terminus, while yeast Cox18, which does not have a notable C-terminal extension, requires the participation of Mss2 for stabilization before translocation (151) (Figure 30). This is supported by the *in vitro* interaction of the OXA2b TPR domain with the COX2 C-terminus. Thus, it is highly likely that the OXA2b TPR domain enhances the efficiency of COX2 membrane insertion by stabilizing the COX2 C-terminus.

Cox18 in both yeast and humans is a very low abundance protein due to its controlled synthesis and tight regulation (152). Similarly, the steady-state level of OXA2b in wild-type plants appears to be very low. As for the TPR deletion plants, although the corresponding transcript levels are clearly evident, it could not be demonstrated that the truncated protein was stable within mitochondria. Hence it cannot be ruled out that the phenotypes of the OXA2b Δ 235-complemented plants are not just the result of a TPR deletion, but may be more akin to knockdown mutants, because knockout mutants are lethal. Thus, definite functions of the TPR domain and the insertase domain of OXA2b cannot be separated based on the available data. Mitochondrial Hsp70 is well-known for its role in protein folding and as a central component of the protein import motor (35, 153) and has already been implicated in the assembly of complex IV in yeast (154-156). It was recently found that HSP70 is required for COX assembly in Arabidopsis as well (157). As HSP70 was up-regulated in the OXA2b TPR deletion plant mitochondria, it could be a compensatory mechanism to overcome the defect in COX assembly. Further investigations on the exact role of mitochondrial HSP70 in complex IV assembly in plants are worth following up.

OXA2b may have further interaction partners such as other assembly factors. As no Cox20 homolog has been identified in plants till date, a plant-specific factor playing the role of Cox20 in plants could be a potential interaction partner of OXA2b. Moreover, similar to Oxa1-Ribosome complexes coordinating complex IV assembly, it is plausible that OXA2b could be additionally involved in further steps of complex IV biogenesis beyond COX2

membrane insertion such as metallation and/or assembly (55). Considering that the OXA2b TPR deletion has restored plant viability, substrates other than COX2, which do not require the TPR domain, may also be inserted by OXA2b. However, it is quite likely that OXA2b is only required for COX2 insertion and/or assembly based on the data presented here and previous findings on Cox18 (29, 61).

Apart from some studies on transcript maturation of COX1 and COX2 (23, 124, 127, 158-161), not much is known about the early steps of complex IV biogenesis in plants. This work studies the membrane insertion step of COX2 during complex IV biogenesis in plants. Further investigation on the unknown complex intermediate detected in the *in organello* translation analyses will be worthwhile. Since it is missing in the OXA2b TPR deletion plants, it is very likely to be a complex IV assembly intermediate. This complex runs at about the same migrating distance on the BN gel where OXA2b was identified in a complexome map of Arabidopsis mitochondria (25). Thus, it could be an assembly intermediate containing COX2 and OXA2b. However, further work is required to determine the exact composition of this potential complex IV assembly intermediate. The generation of more viable complex IV-deficient mutants of both nuclear- and mitochondrial-encoded subunits could benefit such studies in Arabidopsis.

8.2. OXA2a appears to be involved in cytochrome *c* maturation

With the majority of plants only containing one OXA2-like protein, OXA2a and OXA2b most likely arose in the Brassicaceae family due to a gene duplication followed by subfunctionalization. The essential role of OXA2a in Arabidopsis mitochondria was studied by rescuing the lethal phenotype of homozygous T-DNA insertion lines via partial complementation using the developmentally regulated *ABI3* promoter. However, even the residual *ABI3* promoter activity beyond germination was sufficient to provide about 60% of the normal OXA2a transcript level in *ABI3p:OXA2a* plants. Whereas OXA2b was at least detectable by using excess amounts of mitochondria for immunoblotting, OXA2a could not be detected at all. Thus, the abundance of OXA2a appears to be even lower than that of OXA2b. This is in line with the low abundance values of OXA2a and OXA2b detected with

transcriptomic and proteomic studies (162-165). Yeast and human Cox18 are also expressed at low levels and appear to be tightly regulated (152, 166).

When the respiratory chain of *ABI3p:OXA2a* plants was examined, complex III and CYC were reduced and AOX was increased, whereas complexes I, IV and V remained unaffected. *In organello* radiolabelling showed that all the three mitochondrial-encoded complex IV subunits, COX1, COX2 and COX3 were being synthesised and assembled normally. Therefore, the reduction in COX3 is probably due to its instability or increased turnover. Very low amounts of CYC resulted in reduced levels and activity of Complex IV in addition to increased AOX expression and delayed development in a previous study (167). In this study, in spite of reduced CYC steady state protein levels, complex IV activity, abundance and rate of assembly all appear unaffected. This could be because CYC levels in *ABI3p:OXA2a* plants are not as low as those in CYC deficient plants of (167).

The process of complex III assembly in plants has not been studied so far. In this study, a putative assembly intermediate of complex III containing COB and QCR7 was identified. Moreover, the steady state levels of COB, QCR7 and MPP α remained unchanged while those of CYC1 and RISP decreased. Assuming that the process of complex III assembly in plants is similar to the linear assembly model in yeast and humans, the formation of the assembly intermediate I containing COB and the assembly intermediate II containing COB, QCR7 and QCR8 is plausibly normal (19). The accumulation of assembly intermediate II in *ABI3p:OXA2a* plants indicates that the formation of the assembly intermediate III with the addition of QCR6, MPP α , MPP β and CYC1 might have been affected. Although CYC1 looked like a suitable candidate to be a substrate of OXA2a due to its N-out C-in topology, it does not appear to be the case since *in vitro* imported CYC1 topology in *ABI3p:OXA2a* plants did not display any deviation from that of wild-type plants. Moreover, plant CYC1 is structurally similar to yeast CYC1 which does not require Cox18 or any other Oxa protein for its membrane topology (147, 168, 169).

The reduction in steady state levels of both the mitochondrial *c*-type cytochromes, CYC and CYC1 in addition to the accumulation of the putative intermediate II prompted us to hypothesize that the process of CCM might be affected in *ABI3p:OXA2a* plants. The CCM process occurs via system III in yeast and human mitochondria whereas in plant mitochondria via system I. System III is very simple consisting of a single component called HCCS. Since HCCS in yeast and humans is a peripheral membrane protein found on the IMS side of the IM (170), there is no need of a special insertase for its biogenesis. But System I is complicated and involves several components, CCMA, CCMB, CCMC, CCME, CCMF_{N1}, CCMF_{N2}, CCMF_C and CCMH in Arabidopsis mitochondria (13) (Figure 22A). Their proposed functions are: CCMA and CCMB acting as ABC transporter, CCMC and CCME in heme delivery, the three CCMF proteins together functioning as heme lyase and CCMH for reducing apocytochrome *c* (13). All the components except CCMA are integral membrane proteins. Hence plants might require a special insertase such as OXA2a for the biogenesis of at least one of the CCM components. *ABI3p:OXA2a* plants had increased abundances of CCMA, CCMB and CCME, but the steady state levels of CCMF_{N1}, CCMF_{N2} and CCMH were normal (Figure 22B). This suggests that the heme delivery process might be affected. Due to lack of an antibody against CCMC, its levels could not be investigated. Bacterial CcmC directly interacts with heme before incorporating it into CcmE for transferring to apocytochrome *c* (171). Plant CCMC is structurally similar to its bacterial homolog and might act as a CCME-specific heme-lyase (13).

In this study, an unknown complex identified upon heme staining was reduced in *ABI3p:OXA2a* plants. Bacterial CcmC, CcmE, and CcmF are involved in heme trafficking, before it reaches apocytochrome *c* (136). Their heme-binding abilities are all detectable by heme staining (137, 172, 173). Since the membrane topologies of CCME, CCMF_{N1} and CCMF_{N2} appeared normal in *ABI3p:OXA2a* plants, there might have been a problem in the membrane insertion, folding and/or heme binding event of CCMC, which is supposed to traffic heme to CCME. CCMC might require the assistance of a special membrane insertase like OXA2a for attaining the correct membrane topology (Figure 22B). Alternatively, it might aid in the heme binding of CCMC. In either case, it would explain the changes in steady-state levels of only specific CCM components in *ABI3p:OXA2a* plants. Higher protein levels of CCMA, CCMB and apoCCME as well as CCMA-containing and CCMH-

containing complexes appear to be compensating for CCMC defect. Thus, CCMC is plausibly the substrate of OXA2a in Arabidopsis. Reduced efficiency of heme transfer from CCMC to CCME might have caused the reduction in CYC1 and CYC, accumulation of intermediate II and the reduction of complex III in *ABI3p:OXA2a* plants. The requirement of OXA2a function is obsolete in yeast and mammalian mitochondria as they have a much simpler system III for CCM.

Higher steady state levels of certain import components (HSP70, TIM17, TIM50 and TIM22) as well as the ribosomal subunit, L16 and mitochondrial TAT proteins were observed in *ABI3p:OXA2a* plants. In yeast mitochondria, Hsp70 is not only involved in protein folding and import, but also in complex IV assembly (154-156). Moreover, its role in Fe-S cluster biogenesis is conserved in yeast, humans and plants (174-176). The plant mitochondrial TAT pathway is predicted to be required for the membrane insertion of folded proteins especially the RISP subunit of complex III (14). Hence, higher steady state levels of the above mentioned proteins in *ABI3p:OXA2a* plants most likely indicate an increase in mitochondrial biogenesis resulting from complex III reduction. A similar pattern of increased mitochondrial biogenesis resulting from complex IV reduction was also observed in *35Sp:OXA2b235* plants as mentioned above. Both these studies exemplify the pivotal correlation between mitochondrial function and mitochondrial biogenesis.

As phenotypic and biochemical analyses of *35Sp:OXA2aΔ245* plants did not result in any deviation from wild-type plants, the TPR domain of OXA2a does not appear to be essential for its functionality. This is in contrast to a very important role played by the TPR domain of OXA2b during biogenesis of COX2 subunit of complex IV

8.3. Roles of OXA1a and OXA1b

Among the two Arabidopsis OXA1 proteins, OXA1a is essential for embryogenesis, but not OXA1b (87). OXA1a could functionally complement a yeast *oxa1* mutant (88). Yeast Oxa1 plays a major role in mediating the insertion and assembly of lots of crucial proteins

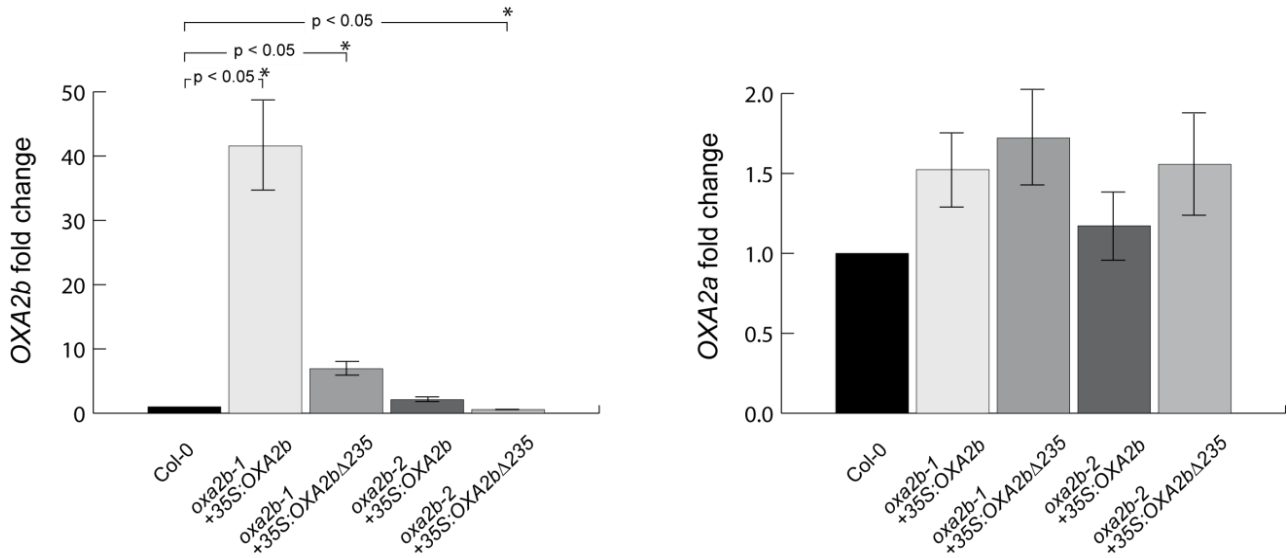
into the IM, irrespective of them being encoded in the mitochondrial or the nuclear genome (55, 56, 59, 177-179). Hence it is likely that OXA1a might serve as the general insertase in plants, similar to yeast Oxa1.

The abundance of mitochondrial respiratory complexes and most of the various protein abundances tested were not affected in *oxa1b* plants. However, more OXA1a and less S10 and ERV1 were detected in these mutant plants. Upregulation of OXA1a in *oxa1b* plants implies OXA1a compensating for the loss of OXA1b. This indicates overlapping functionality between the two OXA1 proteins. Along these lines, faster germination and larger leaf surface area observed in *oxa1b* plants could most likely be due to the increased abundance of OXA1a. S10 is a subunit of the small subunits of mitoribosome and is encoded in the nuclear genome. Its silencing affected the efficiency of translation such that the mitochondrial encoded ribosomal proteins increased whereas and the mitochondrial encoded OXPHOS subunits decreased (143). Reduction of S10 in *oxa1b* plants is possibly due to a regulatory mechanism in relation to the translation of hypothetical OXA1b-specific substrates (Figure 4). Alternatively, OXA1b might aid in the assembly of S10 during mitoribosome formation. Another protein that was found to be reduced in *oxa1b* plants is ERV1. In yeast, the sulfhydryl oxidase, Erv1 generates disulfide bonds and passes them on to the oxidoreductase, Mia40 which then oxidizes substrate proteins in the IMS (180-182). However, Arabidopsis ERV1 appears to promote protein import and oxidative protein folding of proteins in the IMS independently of MIA40 (145, 183). Its downregulation in *oxa1b* plants is very interesting, but further investigations are required to analyze the link between the mitochondrial insertase, OXA1b and the IMS protein, ERV1.

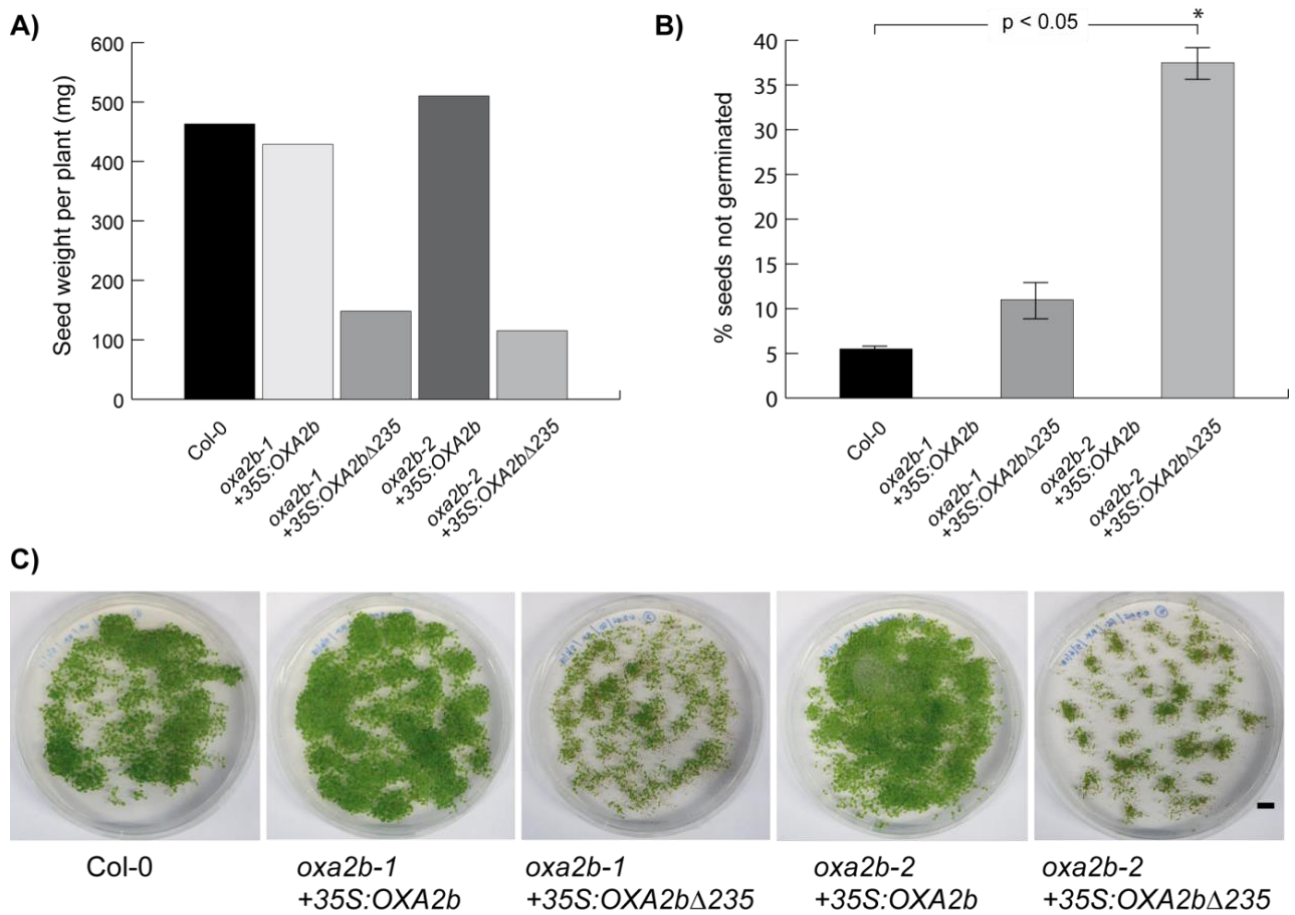
In yeast, Oxa1 is required not only for the biogenesis of the several proteins imported via the general presequence pathway involving the TIM23 complex, but also for that of numerous metabolite carriers via the carrier pathway involving the TIM22 complex (68, 179). The import of substrate proteins via the general import pathway as well as via the carrier import pathway appeared normal in *oxa1b* plant mitochondria. However, following the import and assembly of TIM22 revealed that its assembly into the carrier translocase

complex is faster in *oxa1b* plants. Since more OXA1a was detected in *oxa1b* plants, faster assembly of TIM22 provides an exciting clue that OXA1a could be involved in the assembly of TIM22. This statement is strengthened by an earlier report that yeast Oxa1 promotes the assembly of Tim18-Sdh3 module of the TIM22 complex (179). The yeast TIM22 complex is made up of the membrane-embedded core consisting of Tim22 channel protein, Tim54 receptor and the Tim18-Sdh3 module together with the Tim9-Tim10-Tim12 peripheral chaperone complex (184-186). In plants, the composition and mechanism of TIM22 complex is poorly understood. Orthologs of Tim12, Tim18 and Tim54 could not be found in plants (33, 187, 188). Moreover, it is not certain whether plant SDH3 plays a dual function in complex II as well as TIM22 similar to yeast (185).

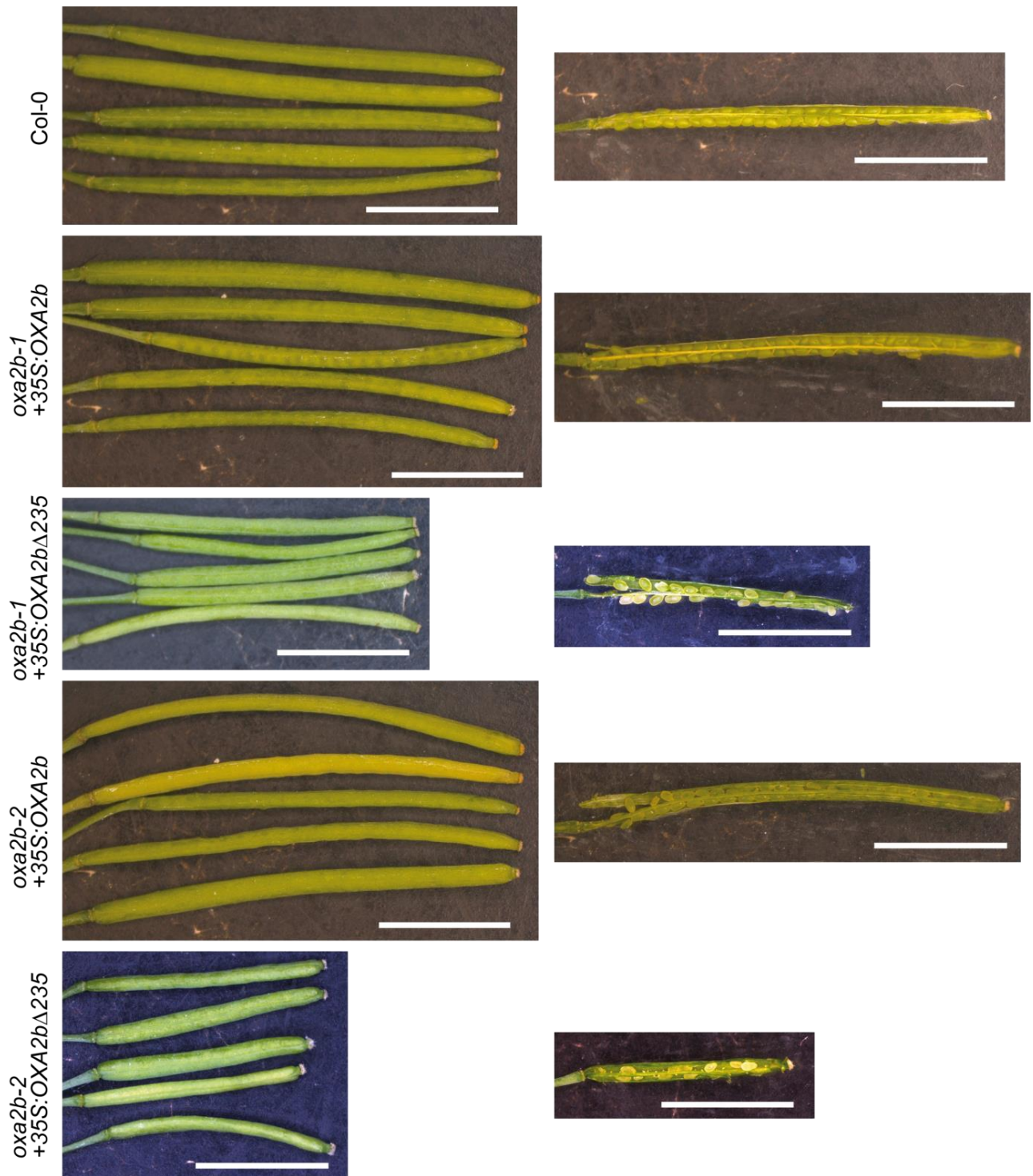
9. Supplemental Figures



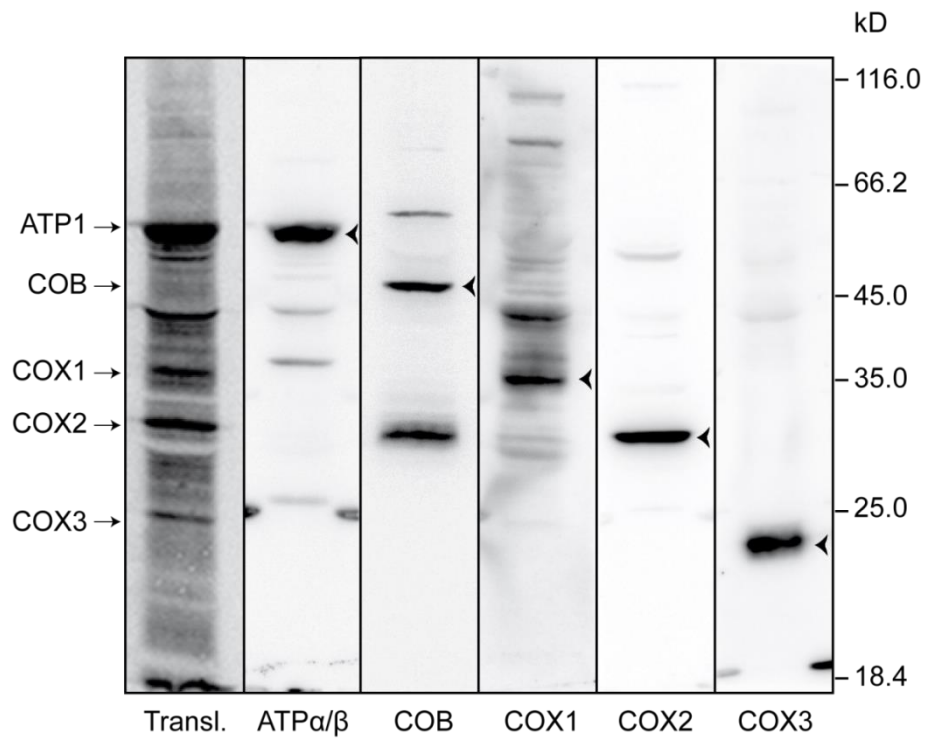
Supplemental Figure 1. RT-qPCR analysis of *OXA2b* and *OXA2a* transcripts. RT-qPCR analysis was carried out on all the *oxa2b* complementation plants with primers specific for *OXA2a* and *OXA2b*. Results are based on four independent biological replicates. Data are presented as averages \pm SE. Statistical significance based on Student's *t* test is indicated by * with a specified *p* value.



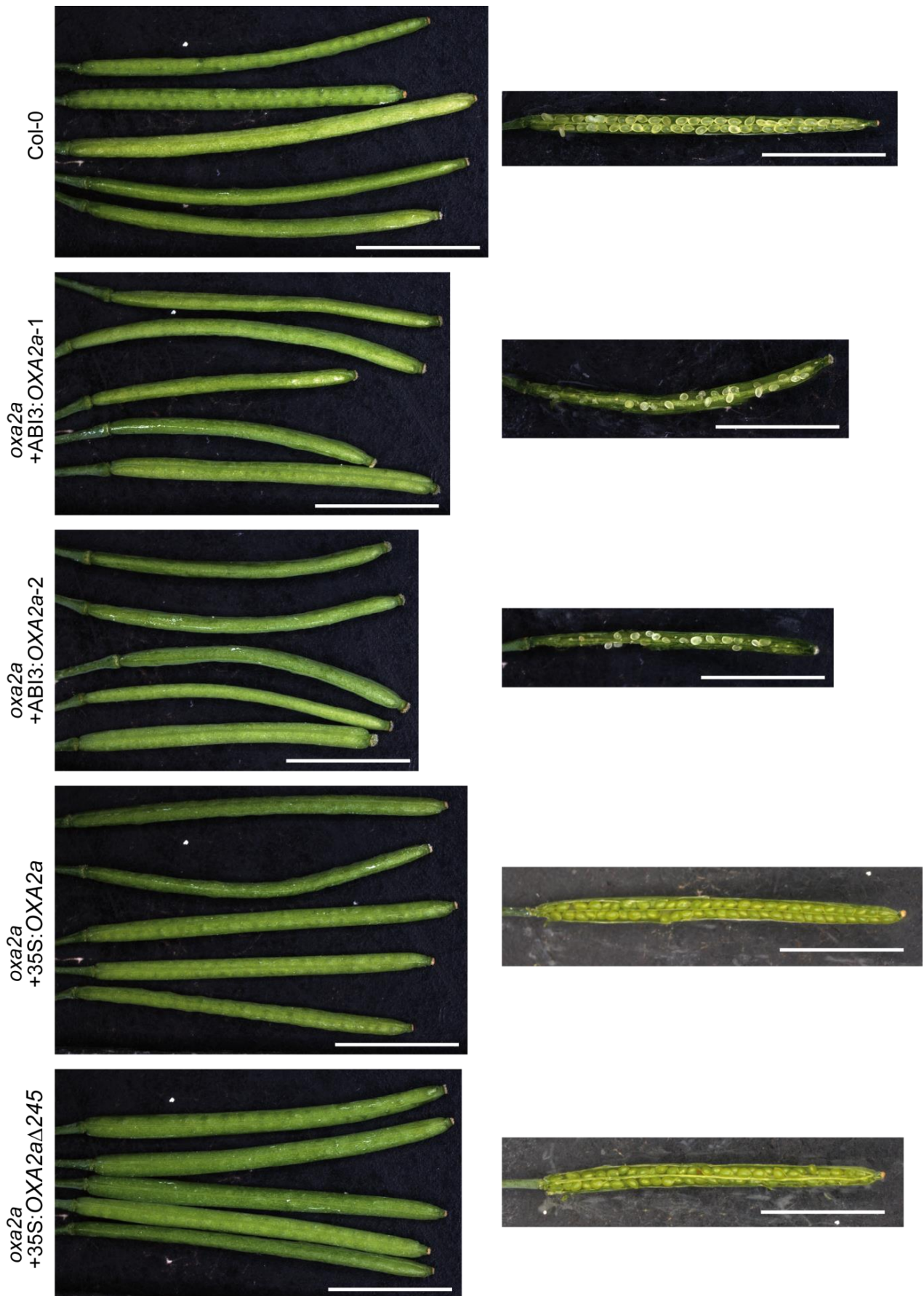
Supplemental Figure 2. Seed weight and germination rates of all the *oxa2b* complementation plants. A) The average weights of seeds collected from a single plant of each genotype are plotted. B) Percentage of seeds not germinated on plates used for phenotyping and root growth analysis are plotted for all genotypes. Data are presented as averages \pm SE. Statistical significance based on Student's *t* test is indicated by * with a specified *p* value. C) Pictures of 1-week-old seedlings germinated on MS plates of all genotypes. The scale bar corresponds to 1 cm.



Supplemental Figure 3. Silique phenotypes of all the *oxa2b* complementation plants. Pictures of five different siliques from each genotype are shown on the left side. One dissected silique from the corresponding genotype is shown on the right side. The scale bar corresponds to 5 mm.



Supplemental Figure 4. Identification of Arabidopsis mitochondrial translation products. A 60 minute *in organello* mitochondrial translation reaction and five samples of unlabelled mitochondria of Arabidopsis wild type were separated by SDS-PAGE on the same gel and used for immuno-blot analysis with antibodies indicated below. The correct protein bands are marked with an arrow head based on their apparent molecular weight. The labelled protein bands identified based on alignment are indicated on the left. This figure was used as a reference for labelling the *in organello* translation products in Figure 9.



Supplemental Figure 5. Silique phenotypes of all the *oxa2a* complementation plants. Pictures of five different siliques from each genotype are shown on the left side. One dissected silique from the corresponding genotype is shown on the right side. The scale bar corresponds to 5 mm.

10. Supplemental Tables

Supplemental Table 1. Primers used in this study

Primer	Sequence
LP1 (<i>OXA2b</i>)	AAGAAGAAAATGGTGCAACCC
RP1 (<i>OXA2b</i>)	TCACTGATCCATCCTCGAAAG
LB1 (<i>OXA2b</i>)	ATTTTGCCGATTTCCGAAC
LP2 (<i>OXA2b</i>)	AATCAATCCTTAACCATCCCG
RP2 (<i>OXA2b</i>)	TGCTTCCTCTCCTTCCTTC
LB2 (<i>OXA2b</i>)	CCCATTGGACGTGAATGTAGACAC
F (<i>OXA2b</i>)	ATGGCATTTCGTAGGGTTTTACTCT
R (<i>OXA2b</i>)	TGAAGTTTTGCTGGTAGAAT
RΔ235	CTGAGCAATGCTGAATGACA
Oxa2b CDS Fw	GGGGACAAGTTTGTACAAAAAAGCAGGCTTCGAAGGAGATAGAACCATG GCATTTTCGTAGGGTT
Oxa2b CDS Rv	GGGGACCACTTTGTACAAGAAAGCTGGGTCTCCACCTCCGGATCATGAAG TTTTGCTGGTAGA
Oxa2b ΔCterm Rv	GGGGACCACTTTGTACAAGAAAGCTGGGTCTCCACCTCCGGATCACTGAG CAATGCTGAATGA
LP1 (<i>OXA2a</i>)	TTGGCTATGCTATTCCACAGG
RP1 (<i>OXA2a</i>)	CCGAAAATTCTAACCTTGGAG
LB1 (<i>OXA2a</i>)	ATTTTGCCGATTTCCGAAC
LP2 (<i>OXA2a</i>)	CGACTGACTGTGAGTCGTCTG
RP2 (<i>OXA2a</i>)	AGTTTGCACAACCATAGAGCG
LB2 (<i>OXA2a</i>)	CCCATTGGACGTGAATGTAGACAC
ApF (<i>OXA2a</i>)	CTTTTTCCTTGCCCTCCTTACTC
2aR (<i>OXA2a</i>)	GAAATGATCCTTTCTGCG
F (<i>OXA2a</i>)	CTCCTCTCGTCACCGTTTATC
R (<i>OXA2a</i>)	TTGTACGCCGGATTGTGATCC
RΔ245	CCTGTGGAATAGCATAGCCAAC
Tim23 F	GGGGACAAGTTTGTACAAAAAAGCAGGCTTCGAAGGAGATAGAACCATG GCGGCTAATAACAGA
Tim23 R	GGGGACCACTTTGTACAAGAAAGCTGGGTCTCCACCTCCGGATCAAATGG GCACATAACCGCTT
Oxa1a F	GGGGACAAGTTTGTACAAAAAAGCAGGCTTCGAAGGAGATAGAACCATG GCTTTCAGGCAAACCT
Oxa1a R	GGGGACCACTTTGTACAAGAAAGCTGGGTCTCCACCTCCGGATCACTTCTT CTTGCTGCTATT
Oxa1b F	GGGGACAAGTTTGTACAAAAAAGCAGGCTTCGAAGGAGATAGAACCATG GCTACTTGCTTGCGT
Oxa1b R	GGGGACCACTTTGTACAAGAAAGCTGGGTCTCCACCTCCGGATCACTTCTT GATCTTTCGGTC
Oxa2a F	GGGGACAAGTTTGTACAAAAAAGCAGGCTTCGAAGGAGATAGAACCATG GCAGTGIGGAGGAGT
Oxa2a R	GGGGACCACTTTGTACAAGAAAGCTGGGTCTCCACCTCCGGATCAGAAAT GATCCITTCIGCG
Oxa2a ΔCterm R	GGGGACCACTTTGTACAAGAAAGCTGGGTCTCCACCTCCGGATCAGACAA GACTTCCCTGTGGAAT
Tim22 F	GGGGACAAGTTTGTACAAAAAAGCAGGCTTCGAAGGAGATAGAACCATG GCTGATTCGAGTGCTGCTGA

Tim22 R	GGGGACCACTTTGTACAAGAAAGCTGGGTCTCCACCTCCGGATCATGTATG CCTATCAAAGAA
Oxa1b LP1	TATCCAGAAGGCATTTTCACG
Oxa1b RP1	TGCAGTTTTGATTTCAATCCC
Oxa1b LB	ATTTTGCCGATTTCCGGAAC
Oxa1b LP2	TATCCAGAAGGCATTTTCACG
Oxa1b RP2	TGCAGTTTTGATTTCAATCCC
Oxa1a RNAi F	GGGGACAAGTTTGTACAAAAAAGCAGGCTGATAAAGCGTCCTCAAGT
Oxa1a RNAi R	GGGGACCACTTTGTACAAGAAAGCTGGGTACTAACAGGACTCAGCG
Oxa2a RNAi F	GGGGACAAGTTTGTACAAAAAAGCAGGCTAATTATCTCTCAAGCACC
Oxa2a RNAi R	GGGGACCACTTTGTACAAGAAAGCTGGGTCTGGTGTTAGAGTCTGTA
Oxa2b RNAi F	GGGGACAAGTTTGTACAAAAAAGCAGGCTAGGGTTTTACTCTCTCAC
Oxa2b RNAi R	GGGGACCACTTTGTACAAGAAAGCTGGGTAAGGCAATCCAGTGATGT
Oxa1a RT F	ATGCAAAAACAAGGGAATGGA
Oxa1a RT R	TGGGGTGAATGGAGTGAC
Oxa2a RT F	TAGATGGTCACCCCTGGCTT
Oxa2a RT R	AGCCACCAGGAAGATCACTC
Oxa2b RT F	TCGTTTTTGTGGGTTCTG
Oxa2b RT R	CCGAATCAAATCCAGGATGA
OEP24 RT F	CAACTCTAAATCAACTGGATCTTTCA
OEP24 RT R	GTCAGTTTTGGCGGCTTC
ACT2,8 RT F	GGTAACATTGTGCTCAGTGGTGG
ACT2,8 RT R	AACGACCTTAATCTTCATGCTGC
Oxa1a RNAi SeqF	CTCAACTTTTATCTTCTTCGTCTTACAC
Oxa1a RNAi OCSR	TTAGGTTTGACCGGTTCTGCC
OXA1A pro A-C F1	ATGAAGACTTTACGGGTCTCAGCGG GCTTCTTGGGATCTCTCAATG
OXA1A pro A-C R1	TAGAAGACAAGAAAAAGACGGTGATGGTGACG
OXA1A pro A-C F2	TAGAAGACAATTTCTTCCATTGACAGGTTTCA
OXA1A pro A-C R2	ATGAAGACTTCAGAGGTCTCAGGTGCC TGCAGAATCTAAACAAGATCCTAC
OXA1B pro A-C F1	ATGAAGACTTTACGGGTCTCAGCGGGCTCAATTCTTTATTAGGTATCAG
OXA1B pro A-C R1	TAGAAGACAAAGACGACTTGGGCATCAGGCCT
OXA1B pro A-C F2	TAGAAGACAAGTCTCGAGTTGGCGGCTA
OXA1B pro A-C R2	ATGAAGACTTCAGAGGTCTCAGGTGCCAACTAAGATCCTGCTAACAAAAA G
OXA2A pro A-C F1	ATGAAGACTTTACGGGTCTCAGCGGAGCGTACCACGGTTCAAT CATCTTATAAACAATTCAAGAAGGCTAAAAAAT
OXA2A pro A-C R1	TAGAAGACAAAACAAGACCTCAGCTGCATTAG
OXA2A pro A-C F2	TAGAAGACAATGTTAAGGAGATTCTGCT
OXA2A pro A-C R2	ATGAAGACTTCAGAGGTCTCAGGTGCCTCCAG TTTTTTTCTTTTGCCTAAAAC
OXA2B pro A-C F1	ATGAAGACTTTACGGGTCTCAGCGG CGGCGATATAAACGATGCAG
OXA2B pro A-C R1	ATGAAGACTTCAGAGGTCTCAGGTGCC TTCCGGTGAAGAAAACGTAC
GUS C-D F	ATGAAGACTTTACGGGTCTCACACC ATGGTACGTCCTGTAGAAACC
GUS C-D R	ATGAAGACTTCAGAGGTCTCACCTT TCATTGTTIGCCTCCCTGCTGCG
T7	AATACGACTCACTATAG
T7terminator	GCTAGTTATTGCTCAGCGG
DNR5	CTGGCAGTCCCTACTCTCG

Seq1B	GTAACATCAGAGATTTTGAGACAC
T35S Rev	TATGCTCAACACATGAGCGAAAC
Intron For	ATTGAATTTGATGGCCATAGGGG
Intron Rev	AATTTTACCCACTAAGCGTGACC
P35S For	TTCATTTGGAGAGGACTGCAGG
pOpOff INT seq Fw	TGAGCTTTGATCTTTCTTTAAACTG
pOpOff2 seq rev	GGGTTCGAAATCGATAAGCTTGCGC
pOpOff INT seq rev	TGTTAGAAATTCCAATCTGCTTGTA
pOpOff2 seq fw	CTCAACTTTTATCTTCTTCGCTTACAC
Oxa2bCtermF	GGGGACAAGTTTGTACAAAAAAGCAGGCTTCGAAGGAGATAGAACCCAA TCAATCCTTAACCATCCCG
Oxa2bCtermR	GGGGACCACCTTTGTACAAGAAAGCTGGGTCTCCACCTCCGGATCATTATGA AGTTTTGCTGGT
Oxa1aLoopF	GGGGACAAGTTTGTACAAAAAAGCAGGCTTCGAAGGAGATAGAACCAAA CAAATGAAAGACACA
Oxa1aLoopR	GGGGACCACCTTTGTACAAGAAAGCTGGGTCTCCACCTCCGGATCATTATGG GGTGAATGGAGT
Oxa1bLoopF	GGGGACAAGTTTGTACAAAAAAGCAGGCTTCGAAGGAGATAGAACCAAT CAACTAAAGGCTACT
Oxa1bLoopR	GGGGACCACCTTTGTACAAGAAAGCTGGGTCTCCACCTCCGGATCATTAAA ATGGAGTTACTCC
Oxa2aLoopF	GGGGACAAGTTTGTACAAAAAAGCAGGCTTCGAAGGAGATAGAACCTTAT TGCCTTTACTCATA
Oxa2aLoopR	GGGGACCACCTTTGTACAAGAAAGCTGGGTCTCCACCTCCGGATCACTAGA AGAACCACAAAAA
Oxa2bLoopF	GGGGACAAGTTTGTACAAAAAAGCAGGCTTCGAAGGAGATAGAACCTTG TTCCTATACTGATT
Oxa2bLoopR	GGGGACCACCTTTGTACAAGAAAGCTGGGTCTCCACCTCCGGATCATCAAG GAACCACAAAAA
Oxa2b pGEX F	ATGCGAATTCCAATCAATCCTTAACCATCCCG
Oxa2b pGEX R	ATGCGCGGCCGCTTATGAAGTTTGCTGGTAG
GSTfor	CCACGTTTGGTGGTGGCG
GSTback	CACCGAAACGCGCGAGGC

Supplemental Table 2. Antibodies used this study

S/N	Antibody Name	Detected Protein(s)	Source
1	CA2	Carbonic Anhydrase subunit 2	(11)
2	SDH4	Succinate DeHydrogenase subunit 4	PhytoAB - PHY0562S
3	RISP	Rieske Iron-Sulfur Protein	(183)
4	COB	CytochrOme B	(189)
5	QCR7	ubiQuinol-cytochrome C oxidoReductase subunit 7	Prof. James Whelan
6	MPP α	Mitochondrial Processing Peptidase - α subunit	Phytoab - PHY0573S
7	CYC1	Cytochrome c_1	abcam - ab167568; Phytoab - PHY0566S
8	CYC	Cytochrome c	Agrisera - AS08 343A
9	COX1	Cytochrome c Oxidase subunit 1	(189)
10	COX2	Cytochrome c Oxidase subunit 2	Agrisera - AS04 053A
11	COX3	Cytochrome c Oxidase subunit 3	abcam - ab110259
12	ATP α/β	ATP synthase subunit α /subunit β	(190)
13	AOX	Alternative Oxidase	Agrisera - AS04 054
14	TOM20	20 kD subunit of TOM complex	(191)
15	TOM40	40 kD subunit of TOM complex	(183)
16	MIA40	Mitochondrial intermembrane space Import and Assembly 40 kD subunit	(183)
17	ERV1	Essential for Respiration and Viability 1	(183)
18	TIM9	9 kD subunit of TIM complex	(126)
19	TIM21-3	21 kD subunit of TIM complex	(126)
20	TIM50	50 kD subunit of TIM complex	(126)
21	TIM17-2	17 kD subunit of TIM complex	(192)
22	TIM23-2	23 kD subunit of TIM complex	(183)
23	TIM44	44 kD subunit of TIM complex	(126)
24	TIM22	22 kD subunit of TIM complex	(126)
25	HSP70	Heat Shock Protein 70 kD	Agrisera - AS08 347
26	GDC-H	Glycine Decarboxylase Complex - H subunit	Agrisera - AS05 074
27	S4	Mitochondrial ribosomal small subunit protein S4	Agrisera - AS15 3068
28	S10	Mitochondrial ribosomal small subunit protein S10	Agrisera - AS15 3067
29	L16	Mitochondrial ribosomal large subunit protein L16	Agrisera - AS15 3069
30	VDAC	Voltage-Dependent Anion-selective Channel protein	(193)
31	CCMB	Cytochrome C Maturation subunit B	This study
32	LETM1	Leucine Zipper And EF-Hand Containing Transmembrane Protein 1	(194)
33	MIC60	Mitochondrial contact site and Cristae organizing system 60 kD subunit	(195)
34	UCP	UnCoupling Protein	Agrisera -AS12 1850
35	TATB	Twin-Arginine Translocase subunit B	(14)
36	TATC	Twin-Arginine Translocase subunit C	(14)
37	CCMA	Cytochrome c Maturation subunit A	(134)
38	CCMB	Cytochrome c Maturation subunit B	(196)
39	CCME	Cytochrome c Maturation subunit E	(197)
40	CCMF _{N1}	Cytochrome c Maturation subunit F _{N1}	(135)
41	CCMF _{N2}	Cytochrome c Maturation subunit F _{N2}	(135)

42	CCMF _C	Cytochrome <i>c</i> Maturation subunit F _C	(135)
43	OXA1a	cytochrome <i>c</i> OXidase Assembly factor 1a	This study
44	OXA1b	cytochrome <i>c</i> OXidase Assembly factor 1b	This study
45	OXA2b	cytochrome <i>c</i> OXidase Assembly factor 2b	This study

Supplemental Table 3. Organisms included in a phylogenetic analysis (Figure 4)

S/N	Organism Name	S/N	Organism Name
1	<i>Aquilegia coerulea</i>	43	<i>Malus domestica</i>
2	<i>Ananas comosus</i>	44	<i>Manihot esculenta</i>
3	<i>Anopheles gambiae</i>	45	<i>Mimulus guttatus</i>
4	<i>Arabidopsis halleri</i>	46	<i>Mus musculus</i>
5	<i>Amaranthus hypochondriacus</i>	47	<i>Marchantia polymorpha</i>
6	<i>Arabidopsis lyrata</i>	48	<i>Micromona pusilla</i> CCMP1545
7	<i>Arabidopsis thaliana</i>	49	<i>Micromonas</i> sp. RCC299
8	<i>Amborella trichopoda</i>	50	<i>Medicago truncatula</i>
9	<i>Brachypodium distachyon</i>	51	<i>Neurospora crassa</i>
10	<i>Brassica oleracea capitata</i>	52	<i>Ostreococcus lucimarinus</i>
11	<i>Brassica rapa</i> FPsc	53	<i>Oryza sativa</i>
12	<i>Brachypodium stacei</i>	54	<i>Oropetium thomaeum</i>
13	<i>Boechera stricta</i>	55	<i>Panicum hallii</i>
14	<i>Bacillus subtilis</i>	56	<i>Physcomitrella patens</i>
15	<i>Clostridium acetobutlicum</i>	57	<i>Prunus persica</i>
16	<i>Citrus clementina</i>	58	<i>Pseudomonas putida</i>
17	<i>Capsella grandiflora</i>	59	<i>Populus trichocarpa</i>
18	<i>Cyanidioschyzon merolae</i>	60	<i>Panicum virgatum</i>
19	<i>Carica papaya</i>	61	<i>Phaseolus vulgaris</i>
20	<i>Chlamydomonas reinhardtii</i>	62	<i>Ricinus communis</i>
21	<i>Capsella rubella</i>	63	<i>Rattus norvegicus</i>
22	<i>Cucumis sativus</i>	64	<i>Sorghum bicolor</i>
23	<i>Citrus sinensis</i>	65	<i>Saccharomyces cerevisiae</i>
24	<i>Coccomyxa subellipsoidea</i>	66	<i>Sphagnum fallax</i>
25	<i>Daucus carota</i>	67	<i>Setaria italica</i>
26	<i>Drosophila melanogaster</i>	68	<i>Solanum lycopersicum</i>
27	<i>Dunaliella salina</i>	69	<i>Selaginella moellendorffii</i>
28	<i>Escherichia coli</i>	70	<i>Streptococcus mutans</i>
29	<i>Eucalyptus grandis</i>	71	<i>Spirodela polyrhiza</i>
30	<i>Eutrema salsugineum</i>	72	<i>Schizosaccharomyces pombe</i>
31	<i>Fragaria vesca</i>	73	<i>Salix purpurea</i>
32	<i>Glycine max</i>	74	<i>Staphylococcus</i>
33	<i>Gossypium raimondii</i>	75	<i>Solanum tuberosum</i>
34	<i>Haemophilus influenzae</i>	76	<i>Setaria viridis</i>
35	<i>Homo sapiens</i>	77	<i>Theobroma cacao</i>
36	<i>Kalanchoe fedtschenkoi</i>	78	<i>Trifolium pratense</i>
37	<i>Kalanchoe laxiflora</i>	79	<i>Volvox carteri</i>
38	<i>Lactococcus lactis</i>	80	<i>Vibrio cholerae</i>
39	<i>Lactococcus plantarum</i>	81	<i>Vitis vinifera</i>
40	<i>Linum usitatissimum</i>	82	<i>Zostera marina</i>
41	<i>Listeria welshimeri</i>	83	<i>Zea mays</i>
42	<i>Musa acuminata</i>		

Supplemental Table 4. Organisms included in a phylogenetic analysis (Figure 6)

S/N	Organism Name	S/N	Organism Name
1	<i>Aquilegia coerulea</i>	33	<i>Malus domestica</i>
2	<i>Ananas comosus</i>	34	<i>Manihot esculenta</i>
3	<i>Anopheles gambiae</i>	35	<i>Mimulus guttatus</i>
4	<i>Arabidopsis halleri</i>	36	<i>Mus musculus</i>
5	<i>Amaranthus hypochondriacus</i>	37	<i>Marchantia polymorpha</i>
6	<i>Arabidopsis lyrata</i>	38	<i>Micromona pusilla</i> CCMP1545
7	<i>Arabidopsis thaliana</i>	39	<i>Micromonas</i> sp. RCC299
8	<i>Amborella trichopoda</i>	40	<i>Medicago truncatula</i>
9	<i>Brachypodium distachyon</i>	41	<i>Ostreococcus lucimarinus</i>
10	<i>Brassica oleracea capitata</i>	42	<i>Oryza sativa</i>
11	<i>Brassica rapa</i> FPsc	43	<i>Oropetium thomaeum</i>
12	<i>Brachypodium stacei</i>	44	<i>Physcomitrella patens</i>
13	<i>Boechera stricta</i>	45	<i>Prunus persica</i>
14	<i>Citrus clementina</i>	46	<i>Populus trichocarpa</i>
15	<i>Capsella grandiflora</i>	47	<i>Panicum virgatum</i>
16	<i>Chlamydomonas reinhardtii</i>	48	<i>Phaseolus vulgaris</i>
17	<i>Capsella rubella</i>	49	<i>Ricinus communis</i>
18	<i>Citrus sinensis</i>	50	<i>Rattus norvegicus</i>
19	<i>Coccomyxa subellipsoidea</i> C-169	51	<i>Sorghum bicolor</i>
20	<i>Daucus carota</i>	52	<i>Saccharomyces cerevisiae</i>
21	<i>Drosophila melanogaster</i>	53	<i>Sphagnum fallax</i>
22	<i>Dunaliella salina</i>	54	<i>Setaria italica</i>
23	<i>Eucalyptus grandis</i>	55	<i>Solanum lycopersicum</i>
24	<i>Eutrema salsugineum</i>	56	<i>Spirodela polyrhiza</i>
25	<i>Fragaria vesca</i>	57	<i>Schizosaccharomyces pombe</i>
26	<i>Glycine max</i>	58	<i>Salix purpurea</i>
27	<i>Gossypium raimondii</i>	59	<i>Setaria viridis</i>
28	<i>Homo sapiens</i>	60	<i>Theobroma cacao</i>
29	<i>Kalanchoe fedtschenkoi</i>	61	<i>Trifolium pratense</i>
30	<i>Kalanchoe laxiflora</i>	62	<i>Volvox carteri</i>
31	<i>Linum usitatissimum</i>	63	<i>Zostera marina</i>
32	<i>Musa acuminata</i>	64	<i>Zea mays</i> PH207

Supplemental Table 5. Plasmids used in this study

S/N	Construct	Insert	Vector	Source
1	OXA1a_RNAi_Ind	<i>OXA1a</i> RNAi	pOpoff2 (Kan)	This study
2	OXA2a_RNAi_Ind	<i>OXA2a</i> RNAi	pOpoff2 (Kan)	This study
3	OXA2b_RNAi_Ind	<i>OXA2b</i> RNAi	pOpoff2 (Kan)	This study
4	Luc_RNAi_Ind	<i>Luc</i> RNAi	pOpoff2 (Kan)	Prof. Dr. Katrin Philippar, Saarland University
5	OXA1a_RNAi_Con	<i>OXA1a</i> RNAi	pK7GWIWG2	This study
6	OXA2a_RNAi_Con	<i>OXA2a</i> RNAi	pK7GWIWG2	This study
7	OXA2b_RNAi_Con	<i>OXA2b</i> RNAi	pK7GWIWG2	This study
8	OXA1a_Comp	<i>OXA1a</i> cDNA	pH2GW7	This study
9	OXA2a_Comp	<i>OXA2a</i> cDNA	pH2GW7	This study
10	OXA2b_Comp	<i>OXA2b</i> cDNA	pH2GW7	This study
11	OXA1aΔCterm_Comp	<i>OXA1a</i> ΔCterm cDNA	pH2GW7	This study
12	OXA2aΔCterm_Comp	<i>OXA2a</i> ΔCterm cDNA	pH2GW7	This study
13	OXA2bΔCterm_Comp	<i>OXA2b</i> ΔCterm cDNA	pH2GW7	This study
14	ABI3p-OXA1a_Comp	<i>OXA1a</i> cDNA	pHABI3pGW7	Dr. Chris Carrie
15	ABI3p-OXA2a_Comp	<i>OXA2a</i> cDNA	pHABI3pGW7	Dr. Chris Carrie
16	ABI3p-OXA2b_Comp	<i>OXA2b</i> cDNA	pHABI3pGW7	Dr. Chris Carrie
17	OXA1ap-GUS	<i>OXA1a</i> promoter	BB2049	This study
18	OXA1bp-GUS	<i>OXA1b</i> promoter	BB2049	This study
19	OXA2ap-GUS	<i>OXA2a</i> promoter	BB2049	This study
20	OXA2bp-GUS	<i>OXA2b</i> promoter	BB2049	This study
21	OXA1a	<i>OXA1a</i> cDNA	pDEST14	This study
22	OXA1b	<i>OXA1b</i> cDNA	pDEST14	This study
23	OXA2a	<i>OXA2a</i> cDNA	pDEST14	This study
24	OXA2b	<i>OXA2b</i> cDNA	pDEST14	This study
25	TIM23	<i>TIM23</i> cDNA	pDEST14	This study
26	TIM22	<i>TIM22</i> cDNA	pDEST14	This study
27	AOX	<i>AOX</i> cDNA (soybean)	pGem-3Zf(+)	Dr. Chris Carrie
28	F _{Ad}	<i>F_{Ad}</i> cDNA (soybean)	pGem-3Zf(+)	Dr. Chris Carrie
29	P _i C	<i>P_iC</i> cDNA (maize)	pGem-3Zf(+)	Dr. Chris Carrie
30	QCR7	<i>QCR7</i> cDNA	pT _N T	Dr. Chris Carrie
31	CYC1	<i>CYC1</i> cDNA	pT _N T	Dr. Chris Carrie
32	CCMA	<i>CCMA</i> cDNA	pT _N T	Dr. Chris Carrie
33	CCME	<i>CCME</i> cDNA	pT _N T	Dr. Chris Carrie
34	CCMH	<i>CCMH</i> cDNA	pT _N T	Dr. Chris Carrie
35	OXA1aLp	<i>OXA1a</i> loop cDNA	pDEST17	This study
36	OXA1bLp	<i>OXA1b</i> loop cDNA	pDEST17	This study
37	OXA2aLp	<i>OXA2a</i> loop cDNA	pDEST17	This study
38	OXA2bLp	<i>OXA2b</i> loop cDNA	pDEST17	This study
39	GST-OXA2bTPR	<i>OXA2b</i> Cterm cDNA	pGEX-6P-1	This study

Cterm: Cterminus; cDNA: complementary DNA; loop: the first matrix-exposed loop region

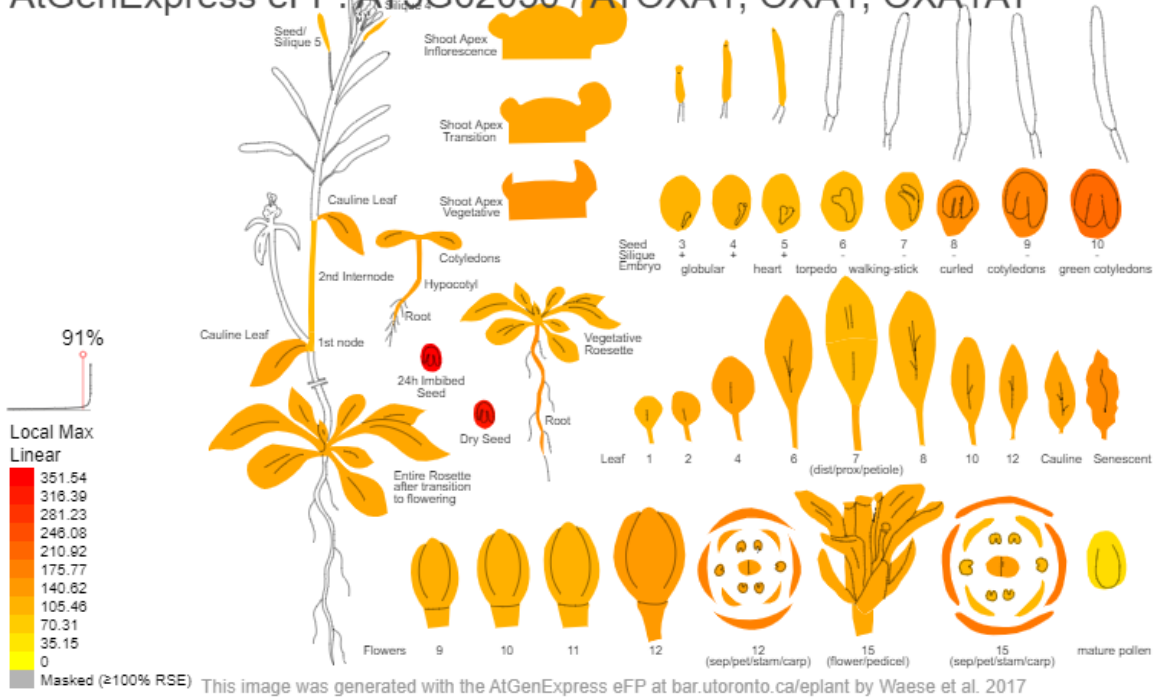
Supplemental Table 6. Gene accession numbers

S/N	Gene Name	Accession Number
1	<i>OXA1a</i>	At5g62050
2	<i>OXA1b</i>	At2g46470
3	<i>OXA2a</i>	At1g65080
4	<i>OXA2b</i>	At3g44370
5	<i>CCMB</i>	Atmg00110
6	<i>TIM23</i>	At1g72750
7	<i>TIM22</i>	At3g10110
8	<i>QCR7</i>	At4g32470
9	<i>CYC1</i>	At3g27240
10	<i>CCMA</i>	At1g63270
11	<i>CCME</i>	At3g51790
12	<i>CCMH</i>	At1g15220

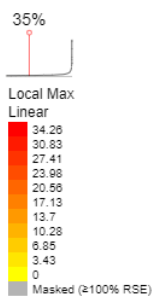
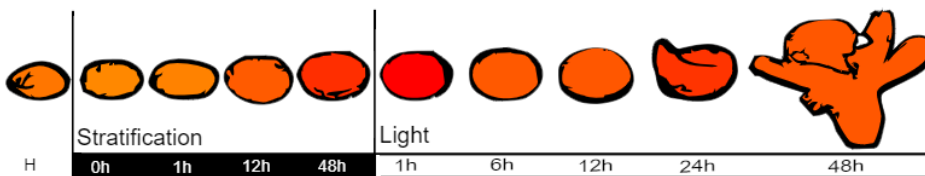
11. Appendix

OXA1a

AtGenExpress eFP: AT5G62050 / ATOXA1, OXA1, OXA1AT



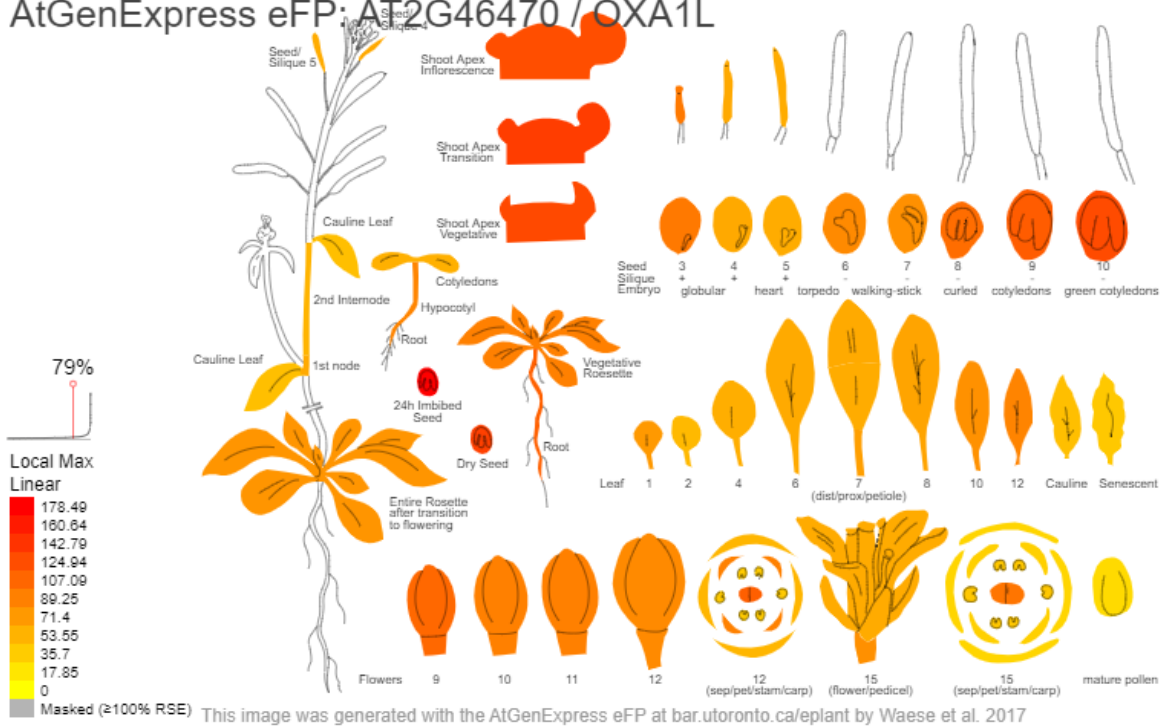
Germination eFP (RNA-Seq data): AT5G62050 / ATOXA1, OXA1, OXA1AT



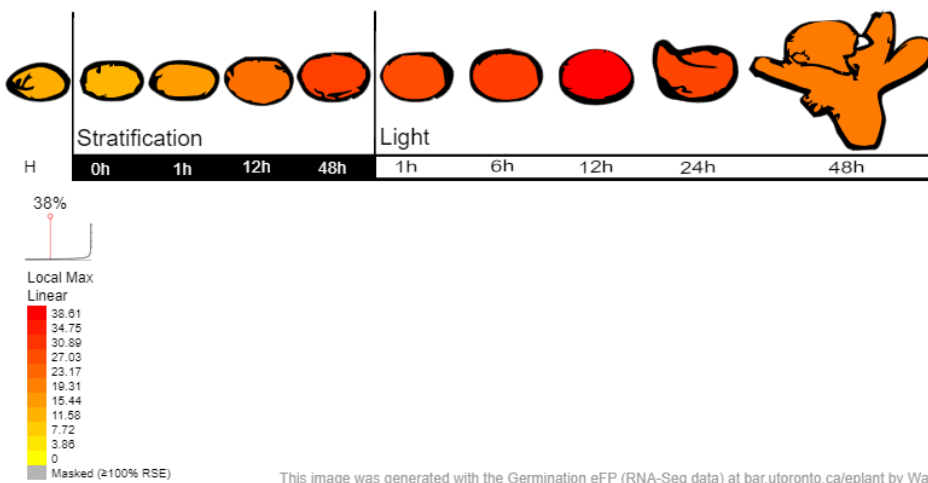
This image was generated with the Germination eFP (RNA-Seq data) at bar.utoronto.ca/eplant by Waese et al. 2017

OXA1b

AtGenExpress eFP: AT2G46470 / OXA1L

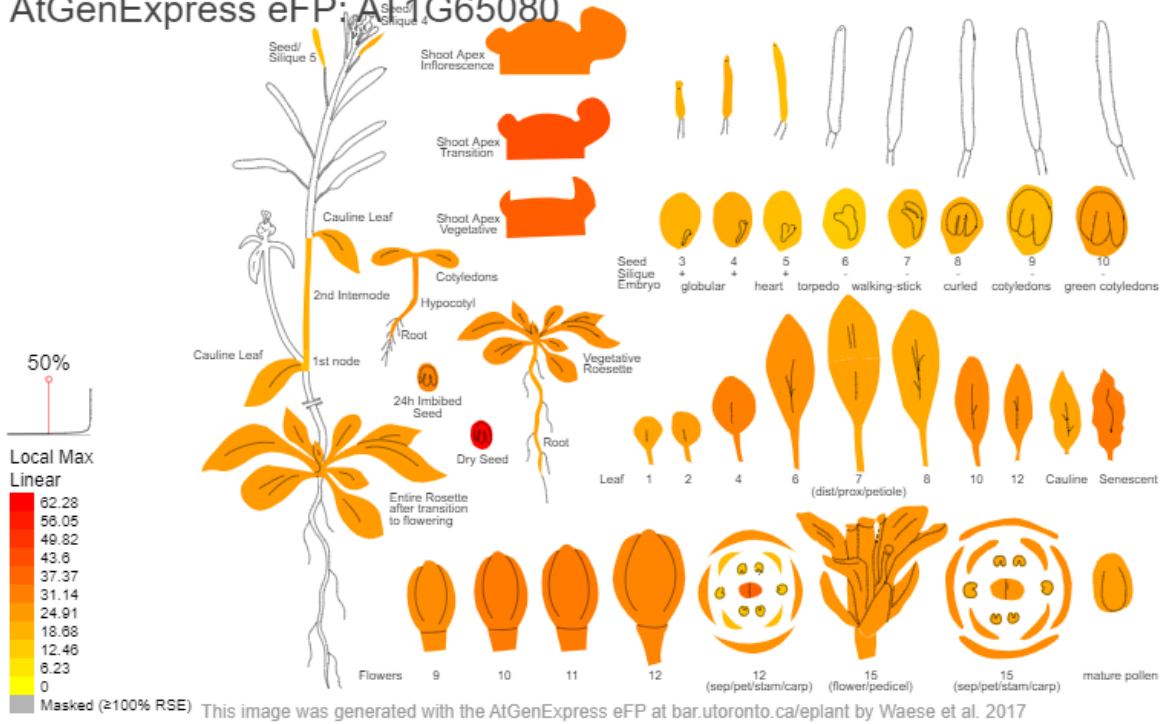


Germination eFP (RNA-Seq data): AT2G46470 / OXA1L

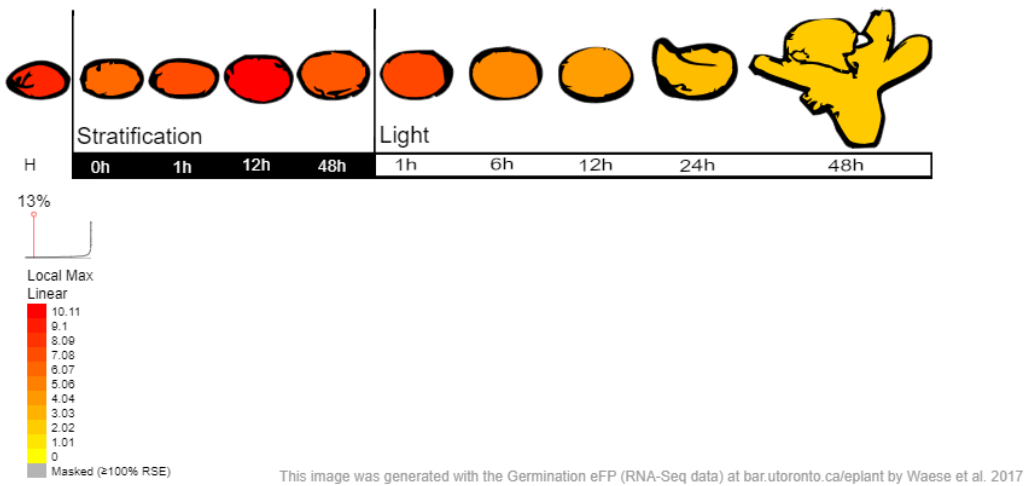


OXA2a

AtGenExpress eFP: AT1G65080

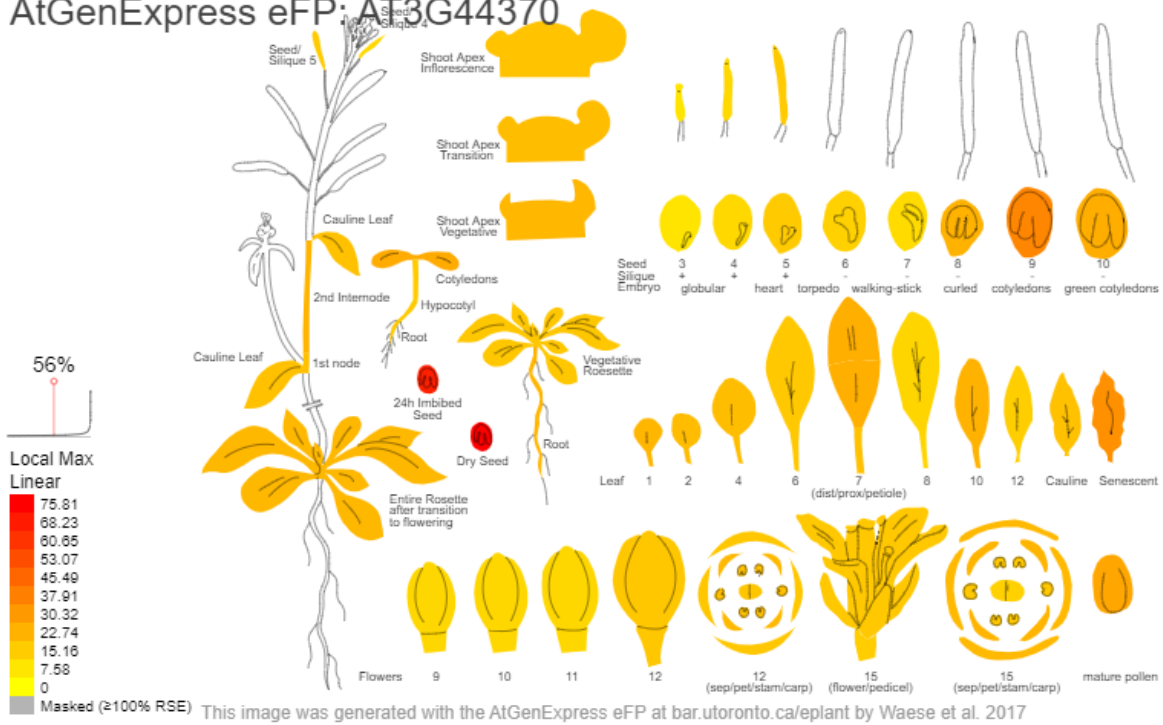


Germination eFP (RNA-Seq data): AT1G65080

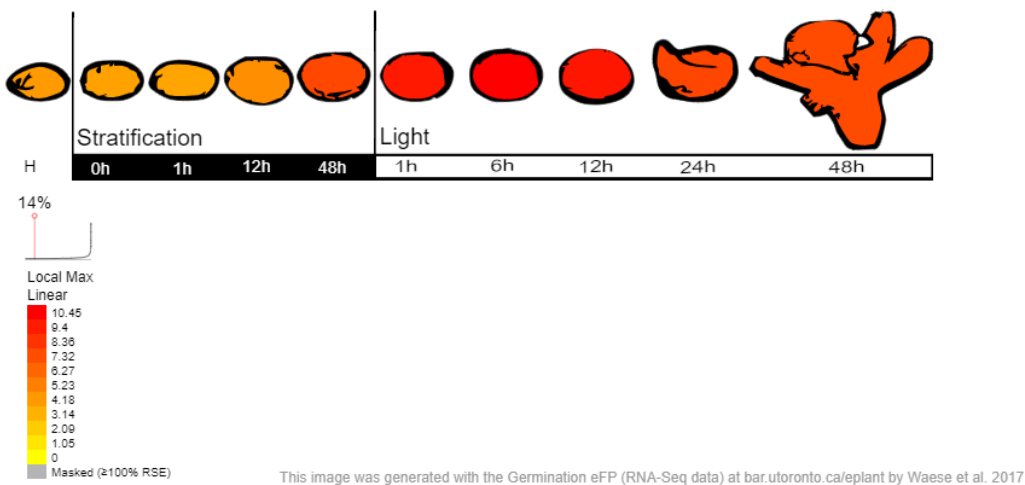


OXA2b

AtGenExpress eFP: AT3G44370

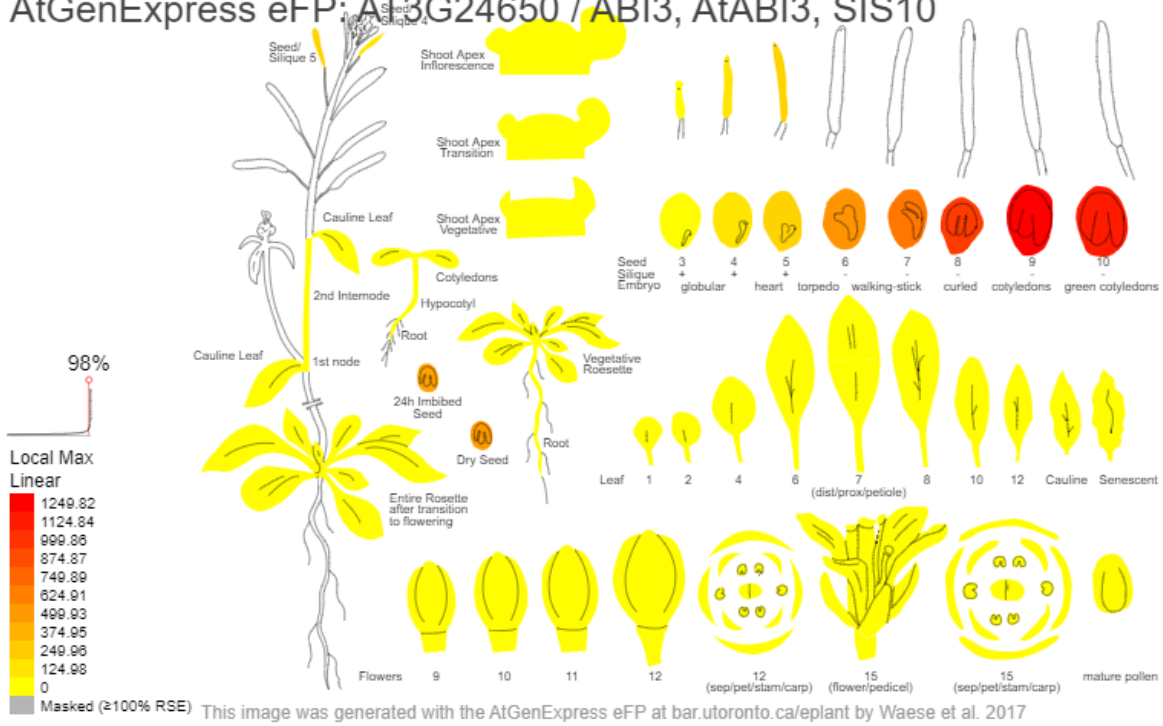


Germination eFP (RNA-Seq data): AT3G44370

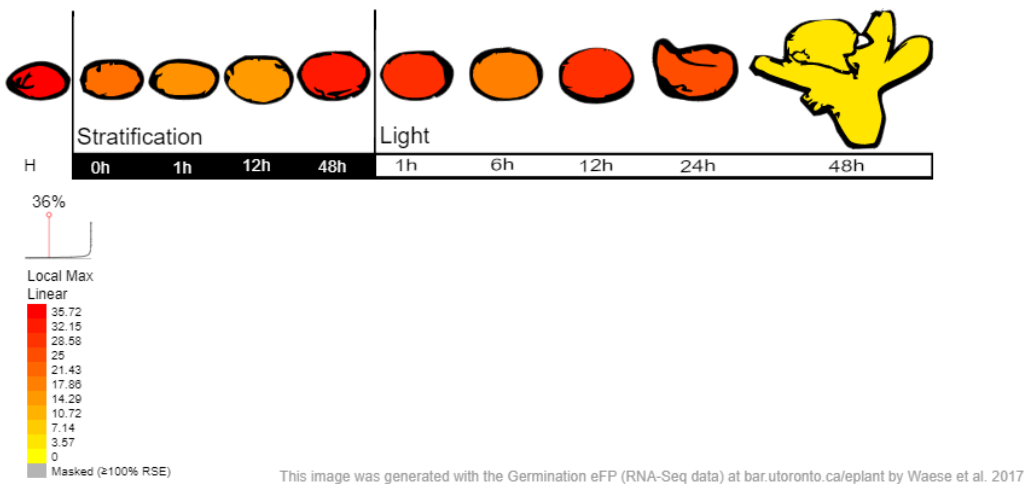


ABI3

AtGenExpress eFP: AT3G24650 / ABI3, AtABI3, SIS10



Germination eFP (RNA-Seq data): AT3G24650 / ABI3, AtABI3, SIS10



12. References

1. Martin WF, Garg S, Zimorski V. Endosymbiotic theories for eukaryote origin. *Philos Trans R Soc Lond B Biol Sci.* 2015;370(1678):20140330.
2. Prasai K. Regulation of mitochondrial structure and function by protein import: A current review. *Pathophysiology.* 2017;24(3):107-22.
3. Gray MW. Mitochondrial evolution. *Cold Spring Harb Perspect Biol.* 2012;4(9):a011403.
4. Palmer JD, Adams KL, Cho Y, Parkinson CL, Qiu YL, Song K. Dynamic evolution of plant mitochondrial genomes: mobile genes and introns and highly variable mutation rates. *Proc Natl Acad Sci U S A.* 2000;97(13):6960-6.
5. Sloan DB, Alverson AJ, Chuckalovcak JP, Wu M, McCauley DE, Palmer JD, et al. Rapid evolution of enormous, multichromosomal genomes in flowering plant mitochondria with exceptionally high mutation rates. *PLoS Biol.* 2012;10(1):e1001241.
6. Hammani K, Giege P. RNA metabolism in plant mitochondria. *Trends Plant Sci.* 2014;19(6):380-9.
7. Binder S, Brennicke A. Gene expression in plant mitochondria: transcriptional and post-transcriptional control. *Philos Trans R Soc Lond B Biol Sci.* 2003;358(1429):181-8; discussion 8-9.
8. Schertl P, Braun HP. Respiratory electron transfer pathways in plant mitochondria. *Front Plant Sci.* 2014;5:163.
9. Liu YJ, Norberg FE, Szilagyi A, De Paepe R, Akerlund HE, Rasmusson AG. The mitochondrial external NADPH dehydrogenase modulates the leaf NADPH/NADP⁺ ratio in transgenic *Nicotiana sylvestris*. *Plant Cell Physiol.* 2008;49(2):251-63.
10. Vanlerberghe GC, Vanlerberghe AE, McIntosh L. Molecular Genetic Evidence of the Ability of Alternative Oxidase to Support Respiratory Carbon Metabolism. *Plant Physiol.* 1997;113(2):657-61.
11. Perales M, Parisi G, Fornasari MS, Colaneri A, Villarreal F, Gonzalez-Schain N, et al. Gamma carbonic anhydrase like complex interact with plant mitochondrial complex I. *Plant Mol Biol.* 2004;56(6):947-57.
12. Sunderhaus S, Dudkina NV, Jansch L, Klodmann J, Heinemeyer J, Perales M, et al. Carbonic anhydrase subunits form a matrix-exposed domain attached to the membrane arm of mitochondrial complex I in plants. *J Biol Chem.* 2006;281(10):6482-8.
13. Giege P, Grienemberger JM, Bonnard G. Cytochrome c biogenesis in mitochondria. *Mitochondrion.* 2008;8(1):61-73.
14. Carrie C, Weissenberger S, Soll J. Plant mitochondria contain the protein translocase subunits TatB and TatC. *J Cell Sci.* 2016;129(20):3935-47.
15. Taiz L, Zeiger E, Møller IM, Murphy AS. *Plant physiology and development.* Sixth edition. ed. Sunderland, Massachusetts: Sinauer Associates, Inc., Publishers; 2015. xxix, 761 pages p.
16. Dudkina NV, Kouril R, Peters K, Braun HP, Boekema EJ. Structure and function of mitochondrial supercomplexes. *Biochim Biophys Acta.* 2010;1797(6-7):664-70.
17. Schagger H, Pfeiffer K. Supercomplexes in the respiratory chains of yeast and mammalian mitochondria. *EMBO J.* 2000;19(8):1777-83.
18. Eubel H, Heinemeyer J, Sunderhaus S, Braun HP. Respiratory chain supercomplexes in plant mitochondria. *Plant Physiol Biochem.* 2004;42(12):937-42.
19. Ndi M, Marin-Buera L, Salvatori R, Singh AP, Ott M. Biogenesis of the bc1 Complex of the Mitochondrial Respiratory Chain. *J Mol Biol.* 2018;430(21):3892-905.
20. Glaser E, Eriksson A, Sjoling S. Bifunctional role of the bc1 complex in plants. Mitochondrial bc1 complex catalyses both electron transport and protein processing. *FEBS Lett.* 1994;346(1):83-7.
21. Carr HS, Winge DR. Assembly of Cytochrome c Oxidase within the Mitochondrion. *Accounts of Chemical Research.* 2003;36(5):309-16.
22. Kolli R, Soll J, Carrie C. Plant Mitochondrial Inner Membrane Protein Insertion. *Int J Mol Sci.* 2018;19(2).
23. Mansilla N, Racca S, Gras DE, Gonzalez DH, Welchen E. The Complexity of Mitochondrial Complex IV: An Update of Cytochrome c Oxidase Biogenesis in Plants. *Int J Mol Sci.* 2018;19(3).
24. Millar AH, Eubel H, Jansch L, Kruff V, Heazlewood JL, Braun HP. Mitochondrial cytochrome c oxidase and succinate dehydrogenase complexes contain plant specific subunits. *Plant Mol Biol.* 2004;56(1):77-90.
25. Senkler J, Senkler M, Eubel H, Hildebrandt T, Lengwenus C, Schertl P, et al. The mitochondrial complexome of *Arabidopsis thaliana*. *Plant J.* 2017;89(6):1079-92.
26. Dennerlein S, Rehling P. Human mitochondrial COX1 assembly into cytochrome c oxidase at a glance. *J Cell Sci.* 2015;128(5):833-7.
27. Ghezzi D, Zeviani M. Assembly factors of human mitochondrial respiratory chain complexes: physiology and pathophysiology. *Adv Exp Med Biol.* 2012;748:65-106.
28. Timon-Gomez A, Nyvltova E, Abriata LA, Vila AJ, Hosler J, Barrientos A. Mitochondrial cytochrome c oxidase biogenesis: Recent developments. *Semin Cell Dev Biol.* 2018;76:163-78.
29. Bourens M, Barrientos A. Human mitochondrial cytochrome c oxidase assembly factor COX18 acts transiently as a membrane insertase within the subunit 2 maturation module. *J Biol Chem.* 2017;292(19):7774-83.

30. Bourens M, Boulet A, Leary SC, Barrientos A. Human COX20 cooperates with SCO1 and SCO2 to mature COX2 and promote the assembly of cytochrome c oxidase. *Hum Mol Genet.* 2014;23(11):2901-13.
31. Timmis JN, Ayliffe MA, Huang CY, Martin W. Endosymbiotic gene transfer: organelle genomes forge eukaryotic chromosomes. *Nat Rev Genet.* 2004;5(2):123-35.
32. Liu Z, Li X, Zhao P, Gui J, Zheng W, Zhang Y. Tracing the evolution of the mitochondrial protein import machinery. *Comput Biol Chem.* 2011;35(6):336-40.
33. Murcha MW, Kmiec B, Kubiszewski-Jakubiak S, Teixeira PF, Glaser E, Whelan J. Protein import into plant mitochondria: signals, machinery, processing, and regulation. *J Exp Bot.* 2014;65(22):6301-35.
34. Abe Y, Shodai T, Muto T, Mihara K, Torii H, Nishikawa S, et al. Structural basis of presequence recognition by the mitochondrial protein import receptor Tom20. *Cell.* 2000;100(5):551-60.
35. Kang PJ, Ostermann J, Shilling J, Neupert W, Craig EA, Pfanner N. Requirement for hsp70 in the mitochondrial matrix for translocation and folding of precursor proteins. *Nature.* 1990;348(6297):137-43.
36. Mokranjac D, Neupert W. The many faces of the mitochondrial TIM23 complex. *Biochim Biophys Acta.* 2010;1797(6-7):1045-54.
37. Truscott KN, Kovermann P, Geissler A, Merlin A, Meijer M, Driessen AJ, et al. A presequence- and voltage-sensitive channel of the mitochondrial preprotein translocase formed by Tim23. *Nat Struct Biol.* 2001;8(12):1074-82.
38. Hawlitschek G, Schneider H, Schmidt B, Tropschug M, Hartl FU, Neupert W. Mitochondrial protein import: identification of processing peptidase and of PEP, a processing enhancing protein. *Cell.* 1988;53(5):795-806.
39. van der Laan M, Meinecke M, Dudek J, Hutu DP, Lind M, Perschil I, et al. Motor-free mitochondrial presequence translocase drives membrane integration of preproteins. *Nat Cell Biol.* 2007;9(10):1152-9.
40. Herrmann JM, Neupert W. Protein insertion into the inner membrane of mitochondria. *IUBMB Life.* 2003;55(4-5):219-25.
41. Sirrenberg C, Bauer MF, Guiard B, Neupert W, Brunner M. Import of carrier proteins into the mitochondrial inner membrane mediated by Tim22. *Nature.* 1996;384(6609):582-5.
42. Laloi M. Plant mitochondrial carriers: an overview. *Cell Mol Life Sci.* 1999;56(11-12):918-44.
43. Murcha MW, Millar AH, Whelan J. The N-terminal cleavable extension of plant carrier proteins is responsible for efficient insertion into the inner mitochondrial membrane. *J Mol Biol.* 2005;351(1):16-25.
44. Murcha MW, Elhafez D, Millar AH, Whelan J. The N-terminal extension of plant mitochondrial carrier proteins is removed by two-step processing: the first cleavage is by the mitochondrial processing peptidase. *J Mol Biol.* 2004;344(2):443-54.
45. Wagener N, Ackermann M, Funes S, Neupert W. A pathway of protein translocation in mitochondria mediated by the AAA-ATPase Bcs1. *Mol Cell.* 2011;44(2):191-202.
46. Wagener N, Neupert W. Bcs1, a AAA protein of the mitochondria with a role in the biogenesis of the respiratory chain. *J Struct Biol.* 2012;179(2):121-5.
47. Folsch H, Guiard B, Neupert W, Stuart RA. Internal targeting signal of the BCS1 protein: a novel mechanism of import into mitochondria. *EMBO J.* 1996;15(3):479-87.
48. Berks BC. The twin-arginine protein translocation pathway. *Annu Rev Biochem.* 2015;84:843-64.
49. Palmer T, Berks BC. The twin-arginine translocation (Tat) protein export pathway. *Nat Rev Microbiol.* 2012;10(7):483-96.
50. Bauer M, Behrens M, Esser K, Michaelis G, Pratje E. PET1402, a nuclear gene required for proteolytic processing of cytochrome oxidase subunit 2 in yeast. *Mol Gen Genet.* 1994;245(3):272-8.
51. Bonnefoy N, Chalvet F, Hamel P, Slonimski PP, Dujardin G. OXA1, a *Saccharomyces cerevisiae* nuclear gene whose sequence is conserved from prokaryotes to eukaryotes controls cytochrome oxidase biogenesis. *J Mol Biol.* 1994;239(2):201-12.
52. Szyrach G, Ott M, Bonnefoy N, Neupert W, Herrmann JM. Ribosome binding to the Oxa1 complex facilitates co-translational protein insertion in mitochondria. *EMBO J.* 2003;22(24):6448-57.
53. Gruschke S, Grone K, Heublein M, Holz S, Israel L, Imhof A, et al. Proteins at the polypeptide tunnel exit of the yeast mitochondrial ribosome. *J Biol Chem.* 2010;285(25):19022-8.
54. Ott M, Herrmann JM. Co-translational membrane insertion of mitochondrially encoded proteins. *Biochim Biophys Acta.* 2010;1803(6):767-75.
55. Keil M, Bareth B, Woellhaf MW, Peleh V, Prestele M, Rehling P, et al. Oxa1-ribosome complexes coordinate the assembly of cytochrome C oxidase in mitochondria. *J Biol Chem.* 2012;287(41):34484-93.
56. Jia L, Dienhart MK, Stuart RA. Oxa1 directly interacts with Atp9 and mediates its assembly into the mitochondrial F1Fo-ATP synthase complex. *Mol Biol Cell.* 2007;18(5):1897-908.
57. Hell K, Neupert W, Stuart RA. Oxa1p acts as a general membrane insertion machinery for proteins encoded by mitochondrial DNA. *EMBO J.* 2001;20(6):1281-8.
58. Stiburek L, Fornuskova D, Wenchich L, Pejznochova M, Hansikova H, Zeman J. Knockdown of human Oxa1l impairs the biogenesis of F1Fo-ATP synthase and NADH:ubiquinone oxidoreductase. *J Mol Biol.* 2007;374(2):506-16.
59. Stuart R. Insertion of proteins into the inner membrane of mitochondria: the role of the Oxa1 complex. *Biochim Biophys Acta.* 2002;1592(1):79-87.

60. Nargang FE, Preuss M, Neupert W, Herrmann JM. The Oxa1 protein forms a homooligomeric complex and is an essential part of the mitochondrial export translocase in *Neurospora crassa*. *J Biol Chem*. 2002;277(15):12846-53.
61. Saracco SA, Fox TD. Cox18p is required for export of the mitochondrially encoded *Saccharomyces cerevisiae* Cox2p C-tail and interacts with Pnt1p and Mss2p in the inner membrane. *Mol Biol Cell*. 2002;13(4):1122-31.
62. Bohnert M, Rehling P, Guiard B, Herrmann JM, Pfanner N, van der Laan M. Cooperation of stop-transfer and conservative sorting mechanisms in mitochondrial protein transport. *Curr Biol*. 2010;20(13):1227-32.
63. Hartl FU, Schmidt B, Wachter E, Weiss H, Neupert W. Transport into mitochondria and intramitochondrial sorting of the Fe/S protein of ubiquinol-cytochrome c reductase. *Cell*. 1986;47(6):939-51.
64. Rojo EE, Stuart RA, Neupert W. Conservative sorting of F0-ATPase subunit 9: export from matrix requires delta pH across inner membrane and matrix ATP. *EMBO J*. 1995;14(14):3445-51.
65. Reif S, Randelj O, Domanska G, Dian EA, Krimmer T, Motz C, et al. Conserved mechanism of Oxa1 insertion into the mitochondrial inner membrane. *J Mol Biol*. 2005;354(3):520-8.
66. Webb CT, Lithgow T. Mitochondrial biogenesis: sorting mechanisms cooperate in ABC transporter assembly. *Curr Biol*. 2010;20(13):R564-7.
67. Park K, Botelho SC, Hong J, Osterberg M, Kim H. Dissecting stop transfer versus conservative sorting pathways for mitochondrial inner membrane proteins in vivo. *J Biol Chem*. 2013;288(3):1521-32.
68. Hildenbeutel M, Theis M, Geier M, Haferkamp I, Neuhaus HE, Herrmann JM, et al. The membrane insertase Oxa1 is required for efficient import of carrier proteins into mitochondria. *J Mol Biol*. 2012;423(4):590-9.
69. Hennon SW, Soman R, Zhu L, Dalbey RE. YidC/Alb3/Oxa1 Family of Insertases. *J Biol Chem*. 2015;290(24):14866-74.
70. Wang P, Dalbey RE. Inserting membrane proteins: the YidC/Oxa1/Alb3 machinery in bacteria, mitochondria, and chloroplasts. *Biochim Biophys Acta*. 2011;1808(3):866-75.
71. Anghel SA, McGilvray PT, Hegde RS, Keenan RJ. Identification of Oxa1 Homologs Operating in the Eukaryotic Endoplasmic Reticulum. *Cell Rep*. 2017;21(13):3708-16.
72. Saller MJ, Wu ZC, de Keyser J, Driessen AJ. The YidC/Oxa1/Alb3 protein family: common principles and distinct features. *Biol Chem*. 2012;393(11):1279-90.
73. Kohler R, Boehringer D, Greber B, Bingel-Erlenmeyer R, Collinson I, Schaffitzel C, et al. YidC and Oxa1 form dimeric insertion pores on the translating ribosome. *Mol Cell*. 2009;34(3):344-53.
74. Falk S, Ravaud S, Koch J, Sinning I. The C terminus of the Alb3 membrane insertase recruits cpSRP43 to the thylakoid membrane. *J Biol Chem*. 2010;285(8):5954-62.
75. Saaf A, Monne M, de Gier JW, von Heijne G. Membrane topology of the 60-kDa Oxa1p homologue from *Escherichia coli*. *J Biol Chem*. 1998;273(46):30415-8.
76. Wu ZC, de Keyser J, Berrelkamp-Lahpor GA, Driessen AJ. Interaction of *Streptococcus mutans* YidC1 and YidC2 with translating and nontranslating ribosomes. *J Bacteriol*. 2013;195(19):4545-51.
77. Nagamori S, Smirnova IN, Kaback HR. Role of YidC in folding of polytopic membrane proteins. *J Cell Biol*. 2004;165(1):53-62.
78. Wagner S, Pop OI, Haan GJ, Baars L, Koningstein G, Klepsch MM, et al. Biogenesis of MalF and the MalFGK(2) maltose transport complex in *Escherichia coli* requires YidC. *J Biol Chem*. 2008;283(26):17881-90.
79. Sachelaru I, Petriman NA, Kudva R, Kuhn P, Welte T, Knapp B, et al. YidC occupies the lateral gate of the SecYEG translocon and is sequentially displaced by a nascent membrane protein. *J Biol Chem*. 2013;288(23):16295-307.
80. Kumazaki K, Chiba S, Takemoto M, Furukawa A, Nishiyama K, Sugano Y, et al. Structural basis of Sec-independent membrane protein insertion by YidC. *Nature*. 2014;509(7501):516-20.
81. Kumazaki K, Kishimoto T, Furukawa A, Mori H, Tanaka Y, Dohmae N, et al. Crystal structure of *Escherichia coli* YidC, a membrane protein chaperone and insertase. *Sci Rep*. 2014;4:7299.
82. Sachelaru I, Winter L, Knyazev DG, Zimmermann M, Vogt A, Kuttner R, et al. YidC and SecYEG form a heterotetrameric protein translocation channel. *Sci Rep*. 2017;7(1):101.
83. Klostermann E, Droste Gen Helling I, Carde JP, Schunemann D. The thylakoid membrane protein ALB3 associates with the cpSecY-translocase in *Arabidopsis thaliana*. *Biochem J*. 2002;368(Pt 3):777-81.
84. Moore M, Harrison MS, Peterson EC, Henry R. Chloroplast Oxa1p homolog albino3 is required for post-translational integration of the light harvesting chlorophyll-binding protein into thylakoid membranes. *J Biol Chem*. 2000;275(3):1529-32.
85. Benz M, Bals T, Gugel IL, Piotrowski M, Kuhn A, Schunemann D, et al. Alb4 of *Arabidopsis* promotes assembly and stabilization of a non chlorophyll-binding photosynthetic complex, the CF1CF0-ATP synthase. *Mol Plant*. 2009;2(6):1410-24.
86. Gerdes L, Bals T, Klostermann E, Karl M, Philippar K, Hunken M, et al. A second thylakoid membrane-localized Alb3/Oxa1/YidC homologue is involved in proper chloroplast biogenesis in *Arabidopsis thaliana*. *J Biol Chem*. 2006;281(24):16632-42.
87. Benz M, Soll J, Ankele E. *Arabidopsis thaliana* Oxa proteins locate to mitochondria and fulfill essential roles during embryo development. *Planta*. 2013;237(2):573-88.
88. Hamel P, Sakamoto W, Wintz H, Dujardin G. Functional complementation of an oxa1- yeast mutation identifies an *Arabidopsis thaliana* cDNA involved in the assembly of respiratory complexes. *Plant J*. 1997;12(6):1319-27.

89. Zhang YJ, Tian HF, Wen JF. The evolution of YidC/Oxa/Alb3 family in the three domains of life: a phylogenomic analysis. *BMC Evol Biol.* 2009;9:137.
90. Fan AC, Young JC. Function of cytosolic chaperones in Tom70-mediated mitochondrial import. *Protein Pept Lett.* 2011;18(2):122-31.
91. Waese J, Fan J, Pasha A, Yu H, Fucile G, Shi R, et al. ePlant: Visualizing and Exploring Multiple Levels of Data for Hypothesis Generation in Plant Biology. *Plant Cell.* 2017;29(8):1806-21.
92. Law SR, Narsai R, Taylor NL, Delannoy E, Carrie C, Giraud E, et al. Nucleotide and RNA metabolism prime translational initiation in the earliest events of mitochondrial biogenesis during Arabidopsis germination. *Plant Physiol.* 2012;158(4):1610-27.
93. Law SR, Narsai R, Whelan J. Mitochondrial biogenesis in plants during seed germination. *Mitochondrion.* 2014;19 Pt B:214-21.
94. Narsai R, Law SR, Carrie C, Xu L, Whelan J. In-depth temporal transcriptome profiling reveals a crucial developmental switch with roles for RNA processing and organelle metabolism that are essential for germination in Arabidopsis. *Plant Physiol.* 2011;157(3):1342-62.
95. Koncz C, Schell J. The promoter of TL-DNA gene 5 controls the tissue-specific expression of chimaeric genes carried by a novel type of Agrobacterium binary vector. *Molecular and General Genetics MGG.* 1986;204(3):383-96.
96. Karpenahalli MR, Lupas AN, Soding J. TPRpred: a tool for prediction of TPR-, PPR- and SEL1-like repeats from protein sequences. *BMC Bioinformatics.* 2007;8:2.
97. Crowe ML, Serizet C, Thareau V, Aubourg S, Rouze P, Hilson P, et al. CATMA: a complete Arabidopsis GST database. *Nucleic Acids Res.* 2003;31(1):156-8.
98. Klodmann J, Senkler M, Rode C, Braun HP. Defining the protein complex proteome of plant mitochondria. *Plant Physiol.* 2011;157(2):587-98.
99. Schneider CA, Rasband WS, Eliceiri KW. NIH Image to ImageJ: 25 years of image analysis. *Nat Methods.* 2012;9(7):671-5.
100. Sambrook J, Fritsch EF, Maniatis T. *Molecular cloning: a laboratory manual*: Cold spring harbor laboratory press; 1989.
101. Whelan J, Murcha MW. *Plant Mitochondria: Methods and Protocols*: Springer; 2015.
102. Hanahan D, Glover D. DNA cloning: a practical approach. *DNA cloning: a practical approach.* 1985;1:109-35.
103. Saiki RK, Gelfand DH, Stoffel S, Scharf SJ, Higuchi R, Horn GT, et al. Primer-directed enzymatic amplification of DNA with a thermostable DNA polymerase. *Science.* 1988;239(4839):487-91.
104. Binder A, Lambert J, Morbitzer R, Popp C, Ott T, Lahaye T, et al. A modular plasmid assembly kit for multigene expression, gene silencing and silencing rescue in plants. *PLoS One.* 2014;9(2):e88218.
105. Chiasson D, Gimenez-Oya V, Bircheneder M, Bachmaier S, Studtrucker T, Ryan J, et al. A unified multi-kingdom Golden Gate cloning platform. *Sci Rep.* 2019;9(1):10131.
106. Altschul SF, Gish W, Miller W, Myers EW, Lipman DJ. Basic local alignment search tool. *J Mol Biol.* 1990;215(3):403-10.
107. Goodstein DM, Shu S, Howson R, Neupane R, Hayes RD, Fazo J, et al. Phytozome: a comparative platform for green plant genomics. *Nucleic Acids Res.* 2012;40(Database issue):D1178-86.
108. Li W, Cowley A, Uludag M, Gur T, McWilliam H, Squizzato S, et al. The EMBL-EBI bioinformatics web and programmatic tools framework. *Nucleic Acids Res.* 2015;43(W1):W580-4.
109. Capella-Gutierrez S, Silla-Martinez JM, Gabaldon T. trimAl: a tool for automated alignment trimming in large-scale phylogenetic analyses. *Bioinformatics.* 2009;25(15):1972-3.
110. Nguyen LT, Schmidt HA, von Haeseler A, Minh BQ. IQ-TREE: a fast and effective stochastic algorithm for estimating maximum-likelihood phylogenies. *Mol Biol Evol.* 2015;32(1):268-74.
111. Clough SJ, Bent AF. Floral dip: a simplified method for Agrobacterium-mediated transformation of Arabidopsis thaliana. *Plant J.* 1998;16(6):735-43.
112. Wielopolska A, Townley H, Moore I, Waterhouse P, Helliwell C. A high-throughput inducible RNAi vector for plants. *Plant Biotechnol J.* 2005;3(6):583-90.
113. Harrison SJ, Mott EK, Parsley K, Aspinall S, Gray JC, Cottage A. A rapid and robust method of identifying transformed Arabidopsis thaliana seedlings following floral dip transformation. *Plant Methods.* 2006;2:19.
114. Boyes DC, Zayed AM, Ascenzi R, McCaskill AJ, Hoffman NE, Davis KR, et al. Growth stage-based phenotypic analysis of Arabidopsis: a model for high throughput functional genomics in plants. *Plant Cell.* 2001;13(7):1499-510.
115. Eubel H, Millar AH. Systematic monitoring of protein complex composition and abundance by blue-native PAGE. *Cold Spring Harb Protoc.* 2009;2009(5):pdb prot5221.
116. Keech O, Dizengremel P, Gardeström P. Preparation of leaf mitochondria from Arabidopsis thaliana. *Physiologia Plantarum.* 2005;124(4):403-9.
117. Murcha MW, Whelan J. Isolation of Intact Mitochondria from the Model Plant Species Arabidopsis thaliana and Oryza sativa. *Methods Mol Biol.* 2015;1305:1-12.
118. Schertl P, Braun HP. Activity measurements of mitochondrial enzymes in native gels. *Methods Mol Biol.* 2015;1305:131-8.

119. Smet J, De Paepe B, Seneca S, Lissens W, Kotarsky H, De Meirleir L, et al. Complex III staining in blue native polyacrylamide gels. *J Inher Metab Dis*. 2011;34(3):741-7.
120. Sabar M, Balk J, Leaver CJ. Histochemical staining and quantification of plant mitochondrial respiratory chain complexes using blue-native polyacrylamide gel electrophoresis. *Plant J*. 2005;44(5):893-901.
121. Feissner R, Xiang Y, Kranz RG. Chemiluminescent-based methods to detect subpicomole levels of c-type cytochromes. *Anal Biochem*. 2003;315(1):90-4.
122. Akbaş Ş. Protein Sorting in Mitochondria [Master's Thesis]. Munich: Ludwig Maximilians University of Munich; 2017.
123. Hsieh WY, Liao JC, Hsieh MH. Dysfunctional mitochondria regulate the size of root apical meristem and leaf development in Arabidopsis. *Plant Signal Behav*. 2015;10(10):e1071002.
124. Radin I, Mansilla N, Rodel G, Steinebrunner I. The Arabidopsis COX11 Homolog is Essential for Cytochrome c Oxidase Activity. *Front Plant Sci*. 2015;6:1091.
125. Kuhn K, Yin G, Duncan O, Law SR, Kubiszewski-Jakubiak S, Kaur P, et al. Decreasing electron flux through the cytochrome and/or alternative respiratory pathways triggers common and distinct cellular responses dependent on growth conditions. *Plant Physiol*. 2015;167(1):228-50.
126. Wang Y, Carrie C, Giraud E, Elhafez D, Narsai R, Duncan O, et al. Dual location of the mitochondrial preprotein transporters B14.7 and Tim23-2 in complex I and the TIM17:23 complex in Arabidopsis links mitochondrial activity and biogenesis. *Plant Cell*. 2012;24(6):2675-95.
127. Kuhn K, Richter U, Meyer EH, Delannoy E, de Longevialle AF, O'Toole N, et al. Phage-type RNA polymerase RPOTmp performs gene-specific transcription in mitochondria of Arabidopsis thaliana. *Plant Cell*. 2009;21(9):2762-79.
128. Despres B, Delseny M, Devic M. Partial complementation of embryo defective mutations: a general strategy to elucidate gene function. *Plant J*. 2001;27(2):149-59.
129. Steinebrunner I, Gey U, Andres M, Garcia L, Gonzalez DH. Divergent functions of the Arabidopsis mitochondrial SCO proteins: HCC1 is essential for COX activity while HCC2 is involved in the UV-B stress response. *Front Plant Sci*. 2014;5:87.
130. Zara V, Conte L, Trumpower BL. Biogenesis of the yeast cytochrome bc1 complex. *Biochim Biophys Acta*. 2009;1793(1):89-96.
131. Davies KM, Blum TB, Kuhlbrandt W. Conserved in situ arrangement of complex I and III2 in mitochondrial respiratory chain supercomplexes of mammals, yeast, and plants. *Proc Natl Acad Sci U S A*. 2018;115(12):3024-9.
132. Lapuente-Brun E, Moreno-Loshuertos R, Acin-Perez R, Latorre-Pellicer A, Colas C, Balsa E, et al. Supercomplex assembly determines electron flux in the mitochondrial electron transport chain. *Science*. 2013;340(6140):1567-70.
133. Lenaz G, Genova ML. Supramolecular organisation of the mitochondrial respiratory chain: a new challenge for the mechanism and control of oxidative phosphorylation. *Adv Exp Med Biol*. 2012;748:107-44.
134. Rayapuram N, Hagenmuller J, Grienemberger JM, Giege P, Bonnard G. AtCCMA interacts with AtCcmB to form a novel mitochondrial ABC transporter involved in cytochrome c maturation in Arabidopsis. *J Biol Chem*. 2007;282(29):21015-23.
135. Rayapuram N, Hagenmuller J, Grienemberger JM, Bonnard G, Giege P. The three mitochondrial encoded CcmF proteins form a complex that interacts with CCMH and c-type apocytochromes in Arabidopsis. *J Biol Chem*. 2008;283(37):25200-8.
136. Richard-Fogal CL, Frawley ER, Bonner ER, Zhu H, San Francisco B, Kranz RG. A conserved haem redox and trafficking pathway for cofactor attachment. *EMBO J*. 2009;28(16):2349-59.
137. Sutherland MC, Jarodsky JM, Ovchinnikov S, Baker D, Kranz RG. Structurally Mapping Endogenous Heme in the CcmCDE Membrane Complex for Cytochrome c Biogenesis. *J Mol Biol*. 2018;430(8):1065-80.
138. Afshar T, Dass N, Lau C, Lee A. The effect of temperature on the germination of Arabidopsis thaliana seeds. *The Expedition*. 2017;6.
139. Kamani N, Kim J, MacLean J. Effect of temperature on the germination and growth rate of Thale Cress (Arabidopsis thaliana). *The Expedition*. 2012;1.
140. Finkelstein R, Reeves W, Ariizumi T, Steber C. Molecular aspects of seed dormancy. *Annu Rev Plant Biol*. 2008;59:387-415.
141. Shu K, Zhou W, Chen F, Luo X, Yang W. Abscisic Acid and Gibberellins Antagonistically Mediate Plant Development and Abiotic Stress Responses. *Front Plant Sci*. 2018;9:416.
142. Hilhorst H, Karssen C. Seed dormancy and germination: the role of abscisic acid and gibberellins and the importance of hormone mutants. *Plant growth regulation*. 1992;11(3):225-38.
143. Kwasniak M, Majewski P, Skibior R, Adamowicz A, Czarna M, Sliwinska E, et al. Silencing of the nuclear RPS10 gene encoding mitochondrial ribosomal protein alters translation in Arabidopsis mitochondria. *Plant Cell*. 2013;25(5):1855-67.
144. Farver O, Vitu E, Wherland S, Fass D, Pecht I. Electron transfer reactivity of the Arabidopsis thaliana sulfhydryl oxidase AtErv1. *J Biol Chem*. 2009;284(4):2098-105.
145. Peleh V, Zannini F, Backes S, Rouhier N, Herrmann JM. Erv1 of Arabidopsis thaliana can directly oxidize mitochondrial intermembrane space proteins in the absence of redox-active Mia40. *BMC Biol*. 2017;15(1):106.
146. Thompson K, Mai N, Olahova M, Scialo F, Formosa LE, Stroud DA, et al. OXA1L mutations cause mitochondrial encephalopathy and a combined oxidative phosphorylation defect. *EMBO Mol Med*. 2018;10(11).

147. Bonnefoy N, Fiumera HL, Dujardin G, Fox TD. Roles of Oxa1-related inner-membrane translocases in assembly of respiratory chain complexes. *Biochim Biophys Acta*. 2009;1793(1):60-70.
148. Hell K, Herrmann J, Pratje E, Neupert W, Stuart RA. Oxa1p mediates the export of the N- and C-termini of pCoxII from the mitochondrial matrix to the intermembrane space. *FEBS Lett*. 1997;418(3):367-70.
149. Hell K, Herrmann JM, Pratje E, Neupert W, Stuart RA. Oxa1p, an essential component of the N-tail protein export machinery in mitochondria. *Proc Natl Acad Sci U S A*. 1998;95(5):2250-5.
150. Elliott LE, Saracco SA, Fox TD. Multiple roles of the Cox20 chaperone in assembly of *Saccharomyces cerevisiae* cytochrome c oxidase. *Genetics*. 2012;190(2):559-67.
151. Broadley SA, Demlow CM, Fox TD. Peripheral mitochondrial inner membrane protein, Mss2p, required for export of the mitochondrially coded Cox2p C tail in *Saccharomyces cerevisiae*. *Mol Cell Biol*. 2001;21(22):7663-72.
152. Gaisne M, Bonnefoy N. The COX18 gene, involved in mitochondrial biogenesis, is functionally conserved and tightly regulated in humans and fission yeast. *FEMS Yeast Res*. 2006;6(6):869-82.
153. van der Laan M, Hutu DP, Rehling P. On the mechanism of preprotein import by the mitochondrial presequence translocase. *Biochim Biophys Acta*. 2010;1803(6):732-9.
154. Bottinger L, Guiard B, Oeljeklaus S, Kulawiak B, Zufall N, Wiedemann N, et al. A complex of Cox4 and mitochondrial Hsp70 plays an important role in the assembly of the cytochrome c oxidase. *Mol Biol Cell*. 2013;24(17):2609-19.
155. Bottinger L, Oeljeklaus S, Guiard B, Rospert S, Warscheid B, Becker T. Mitochondrial heat shock protein (Hsp) 70 and Hsp10 cooperate in the formation of Hsp60 complexes. *J Biol Chem*. 2015;290(18):11611-22.
156. Fontanesi F, Soto IC, Horn D, Barrientos A. Mss51 and Ssc1 facilitate translational regulation of cytochrome c oxidase biogenesis. *Mol Cell Biol*. 2010;30(1):245-59.
157. Wei SS, Niu WT, Zhai XT, Liang WQ, Xu M, Fan X, et al. Arabidopsis mtHSC70-1 plays important roles in the establishment of COX-dependent respiration and redox homeostasis. *J Exp Bot*. 2019;70(20):5575-90.
158. Dahan J, Tcherkez G, Macherel D, Benamar A, Belcram K, Quadrado M, et al. Disruption of the CYTOCHROME C OXIDASE DEFICIENT1 gene leads to cytochrome c oxidase depletion and reorchestrated respiratory metabolism in Arabidopsis. *Plant Physiol*. 2014;166(4):1788-802.
159. Ichinose M, Tasaki E, Sugita C, Sugita M. A PPR-DYW protein is required for splicing of a group II intron of cox1 pre-mRNA in *Physcomitrella patens*. *Plant J*. 2012;70(2):271-8.
160. Mansilla N, Garcia L, Gonzalez DH, Welchen E. AtCOX10, a protein involved in haem o synthesis during cytochrome c oxidase biogenesis, is essential for plant embryogenesis and modulates the progression of senescence. *J Exp Bot*. 2015;66(21):6761-75.
161. Steinebrunner I, Landschreiber M, Krause-Buchholz U, Teichmann J, Rodel G. HCC1, the Arabidopsis homologue of the yeast mitochondrial copper chaperone SCO1, is essential for embryonic development. *J Exp Bot*. 2011;62(1):319-30.
162. Baerenfaller K, Hirsch-Hoffmann M, Svozil J, Hull R, Russenberger D, Bischof S, et al. pep2pro: a new tool for comprehensive proteome data analysis to reveal information about organ-specific proteomes in Arabidopsis thaliana. *Integr Biol (Camb)*. 2011;3(3):225-37.
163. Fuchs P, Rugen N, Carrie C, Elsasser M, Finkemeier I, Giese J, et al. Single organelle function and organization as estimated from Arabidopsis mitochondrial proteomics. *Plant J*. 2019.
164. Klepikova AV, Kasianov AS, Gerasimov ES, Logacheva MD, Penin AA. A high resolution map of the Arabidopsis thaliana developmental transcriptome based on RNA-seq profiling. *Plant J*. 2016;88(6):1058-70.
165. Morgenstern M, Stiller SB, Lubbert P, Peikert CD, Dannenmaier S, Drepper F, et al. Definition of a High-Confidence Mitochondrial Proteome at Quantitative Scale. *Cell Rep*. 2017;19(13):2836-52.
166. Souza RL, Green-Willms NS, Fox TD, Tzagoloff A, Nobrega FG. Cloning and characterization of COX18, a *Saccharomyces cerevisiae* PET gene required for the assembly of cytochrome oxidase. *J Biol Chem*. 2000;275(20):14898-902.
167. Welchen E, Hildebrandt TM, Lewejohann D, Gonzalez DH, Braun HP. Lack of cytochrome c in Arabidopsis decreases stability of Complex IV and modifies redox metabolism without affecting Complexes I and III. *Biochim Biophys Acta*. 2012;1817(7):990-1001.
168. Braun HP, Emmermann M, Krufft V, Schmitz UK. Cytochrome c1 from potato: a protein with a presequence for targeting to the mitochondrial intermembrane space. *Mol Gen Genet*. 1992;231(2):217-25.
169. Nicholson DW, Stuart RA, Neupert W. Biogenesis of cytochrome c1. Role of cytochrome c1 heme lyase and of the two proteolytic processing steps during import into mitochondria. *J Biol Chem*. 1989;264(17):10156-68.
170. Babbitt SE, Sutherland MC, San Francisco B, Mendez DL, Kranz RG. Mitochondrial cytochrome c biogenesis: no longer an enigma. *Trends Biochem Sci*. 2015;40(8):446-55.
171. Ren Q, Thony-Meyer L. Physical interaction of CcmC with heme and the heme chaperone CcmE during cytochrome c maturation. *J Biol Chem*. 2001;276(35):32591-6.
172. Richard-Fogal C, Kranz RG. The CcmC:heme:CcmE complex in heme trafficking and cytochrome c biosynthesis. *J Mol Biol*. 2010;401(3):350-62.
173. San Francisco B, Bretsnyder EC, Rodgers KR, Kranz RG. Heme ligand identification and redox properties of the cytochrome c synthetase, CcmF. *Biochemistry*. 2011;50(50):10974-85.
174. Dutkiewicz R, Nowak M, Craig EA, Marszalek J. Fe-S Cluster Hsp70 Chaperones: The ATPase Cycle and Protein Interactions. *Methods Enzymol*. 2017;595:161-84.

175. Leaden L, Busi MV, Gomez-Casati DF. The mitochondrial proteins AtHscB and AtIsc1 involved in Fe-S cluster assembly interact with the Hsp70-type chaperon AtHscA2 and modulate its catalytic activity. *Mitochondrion*. 2014;19 Pt B:375-81.
176. Olive JA, Cowan JA. Role of the HSPA9/HSC20 chaperone pair in promoting directional human iron-sulfur cluster exchange involving monothiol glutaredoxin 5. *J Inorg Biochem*. 2018;184:100-7.
177. Funes S, Hasona A, Bauerschmitt H, Grubbauer C, Kauff F, Collins R, et al. Independent gene duplications of the YidC/Oxa/Alb3 family enabled a specialized cotranslational function. *Proc Natl Acad Sci U S A*. 2009;106(16):6656-61.
178. Jia L, Dienhart M, Schramp M, McCauley M, Hell K, Stuart RA. Yeast Oxa1 interacts with mitochondrial ribosomes: the importance of the C-terminal region of Oxa1. *EMBO J*. 2003;22(24):6438-47.
179. Stiller SB, Hopker J, Oeljeklaus S, Schutze C, Schrempf SG, Vent-Schmidt J, et al. Mitochondrial OXA Translocase Plays a Major Role in Biogenesis of Inner-Membrane Proteins. *Cell Metab*. 2016;23(5):901-8.
180. Ang SK, Lu H. Deciphering structural and functional roles of individual disulfide bonds of the mitochondrial sulfhydryl oxidase Erv1p. *J Biol Chem*. 2009;284(42):28754-61.
181. Tienison HL, Dabir DV, Neal SE, Loo R, Hasson SA, Boontheung P, et al. Reconstitution of the mia40-erv1 oxidative folding pathway for the small tim proteins. *Mol Biol Cell*. 2009;20(15):3481-90.
182. Hell K. The Erv1-Mia40 disulfide relay system in the intermembrane space of mitochondria. *Biochim Biophys Acta*. 2008;1783(4):601-9.
183. Carrie C, Giraud E, Duncan O, Xu L, Wang Y, Huang S, et al. Conserved and novel functions for Arabidopsis thaliana MIA40 in assembly of proteins in mitochondria and peroxisomes. *J Biol Chem*. 2010;285(46):36138-48.
184. Wiedemann N, Pfanner N. Mitochondrial Machineries for Protein Import and Assembly. *Annu Rev Biochem*. 2017;86:685-714.
185. Gebert N, Gebert M, Oeljeklaus S, von der Malsburg K, Stroud DA, Kulawiak B, et al. Dual function of Sdh3 in the respiratory chain and TIM22 protein translocase of the mitochondrial inner membrane. *Mol Cell*. 2011;44(5):811-8.
186. Neupert W, Herrmann JM. Translocation of proteins into mitochondria. *Annu Rev Biochem*. 2007;76:723-49.
187. Murcha MW, Narsai R, Devenish J, Kubiszewski-Jakubiak S, Whelan J. MPIC: a mitochondrial protein import components database for plant and non-plant species. *Plant Cell Physiol*. 2015;56(1):e10.
188. Murcha MW, Wang Y, Narsai R, Whelan J. The plant mitochondrial protein import apparatus - the differences make it interesting. *Biochim Biophys Acta*. 2014;1840(4):1233-45.
189. Meyer EH, Lehmann C, Boivin S, Brings L, De Cauwer I, Bock R, et al. CMS-G from Beta vulgaris ssp. maritima is maintained in natural populations despite containing an atypical cytochrome c oxidase. *Biochem J*. 2018;475(4):759-73.
190. Meurer J, Meierhoff K, Westhoff P. Isolation of high-chlorophyll-fluorescence mutants of Arabidopsis thaliana and their characterisation by spectroscopy, immunoblotting and northern hybridisation. *Planta*. 1996;198(3):385-96.
191. Lister R, Carrie C, Duncan O, Ho LH, Howell KA, Murcha MW, et al. Functional definition of outer membrane proteins involved in preprotein import into mitochondria. *Plant Cell*. 2007;19(11):3739-59.
192. Murcha MW, Elhafez D, Millar AH, Whelan J. The C-terminal region of TIM17 links the outer and inner mitochondrial membranes in Arabidopsis and is essential for protein import. *J Biol Chem*. 2005;280(16):16476-83.
193. Blake JA, Lee KW, Morris TJ, Elthon TE. Effects of turnip crinkle virus infection on the structure and function of mitochondria and expression of stress proteins in turnips. *Physiologia Plantarum*. 2007;129(4):698-706.
194. Zhang B, Carrie C, Ivanova A, Narsai R, Murcha MW, Duncan O, et al. LETM proteins play a role in the accumulation of mitochondrially encoded proteins in Arabidopsis thaliana and AtLETM2 displays parent of origin effects. *J Biol Chem*. 2012;287(50):41757-73.
195. Michaud M, Gros V, Tardif M, Brugiére S, Ferro M, Prinz WA, et al. AtMic60 Is Involved in Plant Mitochondria Lipid Trafficking and Is Part of a Large Complex. *Curr Biol*. 2016;26(5):627-39.
196. Kolli R, Soll J, Carrie C. OXA2b is Crucial for Proper Membrane Insertion of COX2 during Biogenesis of Complex IV in Plant Mitochondria. *Plant Physiol*. 2019;179(2):601-15.
197. Spielewoy N, Schulz H, Grienberger JM, Thony-Meyer L, Bonnard G. CCME, a nuclear-encoded heme-binding protein involved in cytochrome c maturation in plant mitochondria. *J Biol Chem*. 2001;276(8):5491-7.

13. Acknowledgements

I have been in a continuous learning process during my PhD journey over the past 4.3 years; I would like to thank all the people who went out of their way to contribute to my education and impact my life. They will always hold a special place in my heart.

I am very grateful to my doctor-father, Prof. Dr. Jürgen Soll, for giving me the opportunity to perform PhD research work for in his laboratory. I also appreciate his constant support, advice and motivation in various aspects that helped me enhance my scientific abilities, from the start till the end of my doctoral studies. I shall always cherish his friendly nature and kindness. My special thanks goes to the DAAD team for awarding me the doctoral scholarship for four years. If not for DAAD, I would have missed out on all the wonderful experiences I had here in Germany.

I give credit to my supervisor, Dr. Chris Carrie, for developing my passion for mitochondria. His ideas, suggestions and support were of great help to me. I am obliged to LSM graduate school for supporting me to attend several workshops and courses as well as retreats and outings. I would like to thank PD Dr. Kai Hell for his time and advice as a member of my TAC. I thank PD Dr. Serena Schwenkert and PD Dr. Bettina Bölter for their prompt support and valuable suggestions. I appreciate the friendship and cooperation of Karl Meyer, Petra Schuhmann, Kerstin Schäfer, Carina Engstler and all other members of AG Soll.

My deepest gratitude goes to my family, friends and well-wishers for their unflagging and unparalleled love, help and support.

14. Publications

Portions of this thesis have been published or submitted for publication in the following articles.

Research Articles:

1. **Kolli R**, Soll J, Carrie C. OXA2b is Crucial for Proper Membrane Insertion of COX2 during Biogenesis of Complex IV in Plant Mitochondria. *Plant Physiol.* 2019;179(2):601-15.
2. **Kolli R**, Akbaş Ş, Soll J, Carrie C. OXA2a is Required for Cytochrome *c* Maturation in Arabidopsis. *Plant Physiol.* Under Revision.

Review Article:

1. **Kolli R**, Soll J, Carrie C. Plant Mitochondrial Inner Membrane Protein Insertion. *Int J Mol Sci.* 2018;19(2).

The reuse of images or portions of the above-mentioned articles in this dissertation does not affect the copy right of the journal as the journal has granted the authors the permission to reuse images, portions of the article or full article in any academic, non-commercial publication of which the author is the author. The co-authors approve that unless specified, any figures or portions of this dissertation that are identical or similar to those of the above-mentioned articles are the work of the author, Renuka Kolli herself.

Munich, 05/03/2020

.....

(Jürgen Soll)

.....

(Chris Carrie)